ABSTRACT

Polarimetric Fiber Optic Sensor for the Measurement of Strain

by

Wei Ma

In this thesis, development of a Polarimetric Fiber-Optic strain sensor is presented. The sensor uses the phenomenon that strain can deform the probing part of the fiber and hence change the polarization of the transmitted light signal. By counting the resulting fringes, we can measure the exact strain in the material. Calibration of the sensor was achieved by setting up tension tests. Optical fibers were glued on the surface of the specimen. Reference strain gages were used to record the strain in the specimens. Resulting fringes from the fiber optic sensors were then related to the strain measured by the strain gages. As compared to strain gages and the Interferometric sensors, Polarimetric sensors offer many advantages. They are extremely sensitive, easy to install, and most importantly they offer geometric flexibility and embeddment capabilities. They are immune to electrical and electromagnetic interferences, and can be operated from remote locations.

POLARIMETRIC FIBER OPTIC SENSOR FOR THE MEASUREMENT OF STRAIN

by

Wei Ma

A Thesis
Submitted to the Faculty of the
New Jersey Institute of Technology
in Partial Fulfillment of the Requirement for the Degree of
Master of Science in Electrical Engineering

Department of Electrical and Computer Engineering

May 1993

APPROVAL PAGE

Polarimetric Fiber Optic
Sensor for the Measurement of Strain

Wei Ma

Dr. Farhad Ansari, Thesis Advisor — Date
Professor of Civil and Environmental Engineering, NJIT

Dr. Gerald Martin Whitman, Committee Member — Date
Professor of Electrical Engineering, Director of the Center for
Microwave and Lightwave Engineering, NJIT

Dr. Edip Niver, Committee Member — Date
Associate Professor of Electrical Engineering, NJIT

BIOGRAPHICAL SKETCH

Author: Wei Ma

Degree: Master of Science in Electrical Engineering

Date: May, 1993

Undergraduate and Graduate Education:

- Master of Science in Electrical Engineering
  New Jersey Institute of Technology
  Newark, NJ 1993
- Bachelor of Science in Electrical Engineering,
  East China Normal University
  Shanghai, China, 1991

Major: Electrical Engineering

This thesis is dedicated to my parents.

ACKNOWLEDGMENT

The author wishes to express his gratitude and thanks to his thesis advisor, Professor Farhad Ansari, for his selection of the thesis topic, guidance and encouragement at all stages of the work.

Special thanks to Professor Gerald Martin Whitman and Professor Edip Niver for serving as members of the committee.

The author appreciates the timely help and suggestions from the Concrete Laboratory members, including: Rajendra Navalurkar, Been-jyh Yu, and Allyn Luke.

TABLE OF CONTENTS

LIST OF TABLES

LIST OF FIGURES

Figure **Page**

Figure **Page**

Figure **Page**

Figure **Page**

CHAPTER 1

INTRODUCTION

1.1 Background and Objectives

The measurement of strain is an integral part of every material testing program. The definition of strain is as follows: if L_o is the initial length of a specimen and L is the observed length under a given load, the elongation $\Delta L = L - L_o$. The elongation ε per unit of initial gage length is then given as $\varepsilon = \frac{L - L_o}{L_o} = \frac{\Delta L}{L_o}$. This expression defines the average strain. It is a dimensionless quantity, but it is customary to refer to it as having the dimensions of in/in, m/m, or μm/m (micro-strain).

Traditionally, strain gages are employed for the measurement of strain. Since the strains generally encountered are very small, it is possible to employ a highly versatile means for measuring them, using electric resistance strain gages. These are made of very fine wires or foils that are glued to the member being investigated. As the forces are applied to the member, elongation or contraction of the wires or foils takes place concurrently with similar changes in the material. These changes in length alter the electric resistance of the gage, which can be measured and calibrated to indicate the strain taking place.

In addition to the strain gages a number of other highly sophisticated instruments are available for the measurement of deformation. For example , Linear-Variable-Differential-Transformers (LVDT), and clip gage

extensometers are employed for monitoring changes in specimen dimension due to applied loads.

The main reasons for exploring the possibility of using the fiber optic sensors are the following:

(1) They possess geometric flexibility and can be adhered and embedded within materials in any desired shape. Strain gages are not capable of doing so.

(2) Fiber Optic sensors are immune to electromagnetic interferences, and are specifically very useful in hazardous environments.

(3) Being capable for remote operations.

(4) They are light weight and easy to handle.

The main objective of this thesis is to perform simple calibration test for understanding basic properties of the polarimetric type fiber optic sensors. It is desired to examine the repeatability of results under different testing conditions such as velocity of loading. In this thesis, two types of polarization maintaining fibers (Low and High-Birefringence) were employed. In this way the performance of both types of fibers were compared.

1.2 Wave Theory of Light

Electromagnetic radiation is predicted by Maxwell's theory to be a transverse wave motion that propagates with an extremely high velocity. Associated with the wave are oscillating electric and magnetic fields that can be described with electric and magnetic vectors E and H. These vectors are in phase, perpendicular to each other, and at right angles to the direction of propagation. For simplicity and convenience of representation, the wave has been given sinusoidal form which provides the basic information need for the

analysis. The vector used to represent the light wave can be either the electric vector or the magnetic vector. Both exist simultaneously, and either or both can be used to describe the optical effects associated with strain, temperature , pressure, etc. In this thesis, the electric vector has been employed for the representation of the light wave. Since the disturbance producing light can be represented by a transverse wave motion, it is possible to express the magnitude of the light (electric) vector in terms of the solution of the one-dimensional wave equation [9]:

$$E = f(z-ct) + g(z+ct) \tag{1.1}$$

where, E is the magnitude of light vector, z is the position along axis of propagation, t is time and c is the propagating speed of the light. $f(z-ct)$ and $g(z+ct)$ represent the wave motion in positive z direction and negative z direction, respectively. Most optical effects of interest in experimental stress analysis can be described with a simple sinusoidal waveform. Thus, light propagation in the positive z direction away from the source can be represented by:

$$E = f(z-ct) = a\cos\left[\frac{2\pi}{\lambda}(z-ct)\right] \tag{1.2}$$

where, a is the amplitude of the wave, λ is the wavelength. The direction of the electric field determines the polarization of the wave. In many light sources, the polarization of the light varies in a random manner and these sources are said to be randomly polarized. Other sources, such as the output of many lasers, are linearly (plane) polarized. In Equation 1.2, the electric

vector used to describe the light wave is restricted to a single plane. So the light is linearly polarized. When light is linearly polarized, the electric vector maintains a constant orientation in space. Since the light field is a vector, it can be resolved into its components along two perpendicular axes. If the light propagating through a plate with different refractive indexes, there is a time lag between the two components which can be translated into a phase delay, then other forms of polarization are created. In this case, the electric field vector of the wave is the resultant of the two components, and the electric field vector traces out an ellipse in space. For this reason, it is called elliptically polarized light (Figure 1.1). As a special case, if the two components are equal and the phase difference between the two components is 90°, the wave would be circularly polarized. In the case of optical fibers, the polarization of light transmitted through them may be preserved if the polarization maintaining fiber is used.

1.3 Optical Instruments

The polariscope is an optical instrument that utilizes the properties of polarized light in its operation. Two types are frequently employed, the plane polariscope and the circular polariscope. The names follow from the type of polarized light used in their operation.

In practice, plane-polarized light is produced with an optical element known as a plane or linear polarizer. Production of circularly polarized light or the more general elliptically polarized light requires the use of a linear polarizer together with an optical element known as a wave plate. A brief discussion of linear polarizers, wave plates and their series combination follows.

1.3.1 Linear Polarizer

When a light wave strikes a plane polarizer, this optical element resolves the wave into two mutually perpendicular components, as shown in Figure 1.2. The component parallel to the axis of polarization is transmitted while the component perpendicular to the axis of polarization is either absorbed, or suffers total internal reflection.

If the plane polarizer is fixed at some point z_o along the Z axis, the equation for the light vector can be written as:

$$E = \alpha \cos [\frac{2\pi}{\lambda}(z_\circ - ct)] \tag{1.3}$$

Since the initial phase of the wave, z_o is not important in developments that follow, Equation 1.3 can be reduced to:

$$E = \alpha \cos\ 2\pi\ ft = \alpha \cos\ (\omega\ t) \tag{1.4}$$

where, $\omega=2\pi f$ is known as the circular frequency of the wave. The absorbed and transmitted components of the light vector are:

$$E_a = a \cos\ (\omega\ t) \sin \alpha \tag{1.5}$$

$$E_t = a \cos\ (\omega\ t) \cos \alpha \tag{1.6}$$

where, α is the angle between the axis of polarization and light vector.

1.3.2 Wave Plate

A wave plate is defined as an optical element which has the ability to resolve a light vector into two orthogonal components to transmit the components with different velocities. Such a material has been referred to as doubly refracting or birefringent. The doubly refracting plate illustrated in Figure 1.3 has two principal axes labeled 1 and 2. The transmission of light along axis 1 proceeds at velocity c_1 and along axis 2 at velocity c_2. Since c_1 is greater than c_2, axis 1 is called the *fast axis* and axis 2 the *slow axis.*

If this doubly refracting plate is placed in a field of a linearly polarized light so that the light vector E_t makes an angle β with axis 1(the fast axis), then upon entering the plate the light vector is first resolved into two components E_{t1} and E_{t2} along axes 1 and 2, respectively. The magnitudes of the individual components E_{t1} and E_{t2} are given by [9]:

$$E_{t1} = E_t \cos\beta = a\cos(\alpha)\cos(\omega t)\cos\beta = k\cos(\omega t)\cos\beta \qquad (1.7)$$

$$E_{t2} = E_t \sin\beta = a\cos(\alpha)\cos(\omega t)\sin\beta = k\cos(\omega t)\sin\beta \qquad (1.8)$$

where, $k=a\cos\alpha$. The light components E_{t1} and E_{t2} travel through the plate with different velocities c_1 and c_2, respectively. Because of this velocity difference, the two components will emerge from the plate at different times. In other words, one component is retarded in time relative to the other component. This retardation can be handled most effectively by considering the relative phase shift between the two components. The relative angular phase shift Δ between the two components as they emerge from the plate is given by [9]:

$$\Delta = \frac{2h\pi}{\lambda}(n_1 - n_2) \tag{1.9}$$

The relative phase shift Δ produced by a doubly refracting plate is dependent upon its thickness h, the wave length of the light λ, and the properties of the plate as described by n_2-n_1. When the doubly refracting plate is designed to give an angular retardation of $\pi/2$ (which is a quarter of 1 cycle 2π), it is called a quarter-wave plate. Upon emergence from a general wave plate exhibiting a retardation Δ, the two components of light are described by the equations [9]:

$$\begin{aligned} E'_{t1} &= k\cos\beta\ \cos\ \omega\, t \\ E'_{t2} &= k\sin\beta\ \cos\ (\omega\, t - \Delta) \end{aligned} \tag{1.10}$$

With this representation, only the relative phase shift between components has been considered. The magnitude of the light vector which is equivalent to these two components can be expressed as [9]:

$$E't = \sqrt{(E't2)^2 + (E't1)^2} = k\sqrt{\cos^2\beta\cos^2\omega\, t + \sin^2\beta\cos^2(\omega\, t - \Delta)} \tag{1.11}$$

The angle that the emerging light vector makes with axis 1 (the fast axis) is given by [9]:

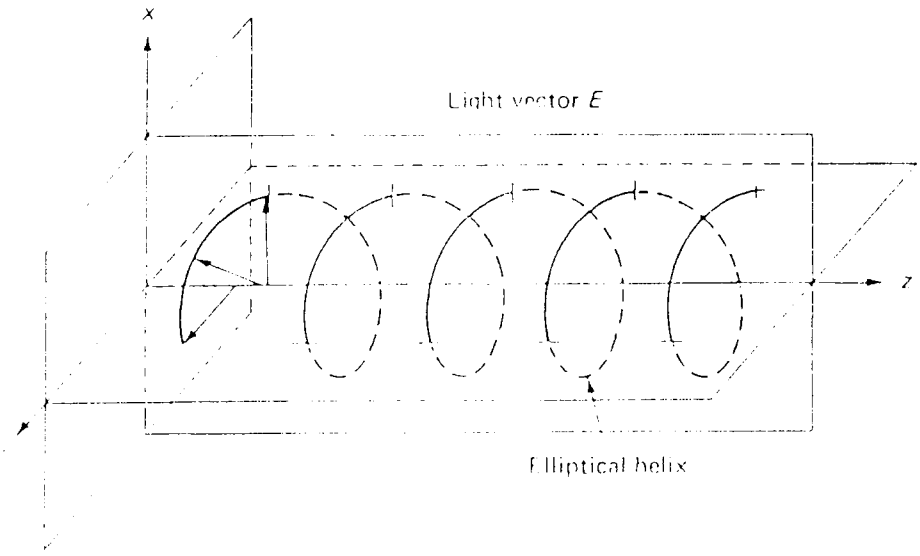

Figure 1.1 The elliptical polarized light vectors along the axis of propagation at a fixed instant of time.

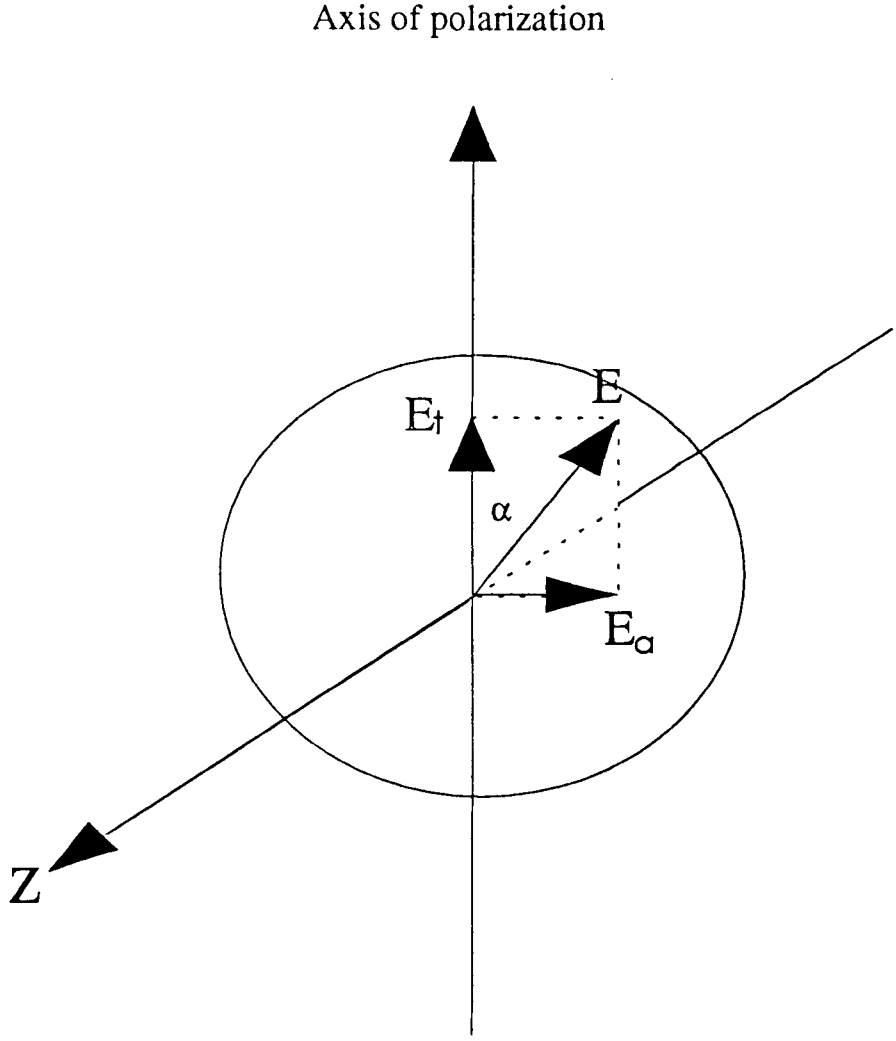

Figure 1.2 Absorbing and transmitting characteristics of a plane polarizer.

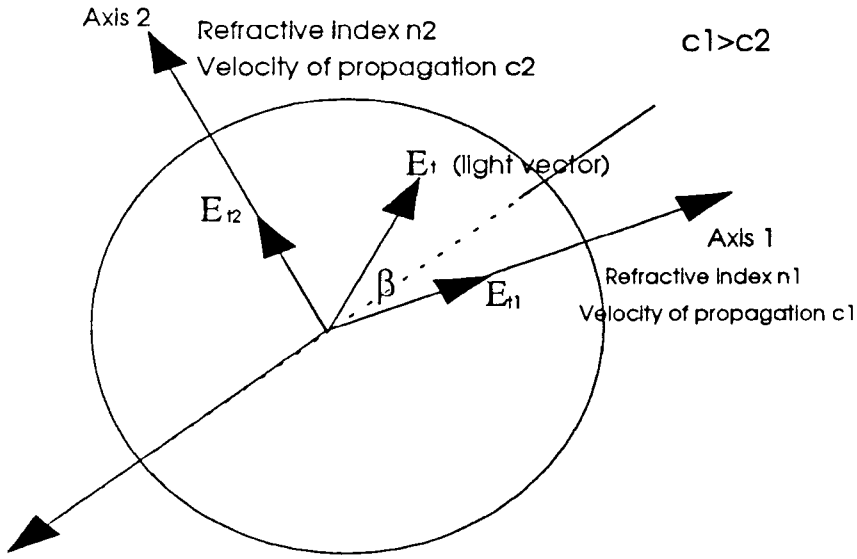

Figure 1.3 A plane-polarized light vector entering a wave plate.

$$\tan\gamma = \frac{E'_{t2}}{E'_{t1}} = \frac{\cos(\omega t - \Delta)}{\cos(\omega t)}\tan\beta \qquad (1.12)$$

Thus, clearly both the amplitude and the rotation of the emerging light vector can be controlled by the wave plate. Controlling factors are the relative phase difference Δ and orientation angle β.

1.3.3 Combination of A Linear Polarizer and A Wave Plate

The light emerging from a series combination of a linear polarizer and a wave plate is always polarized; however, the type of polarization may be plane, circular, or elliptical. In this thesis, the circularly polarized light was employed for the development of the fiber optic sensor.

If a wave plate is selected so that $\Delta=\pi/2$, that is, a quarter-wave plate, and β is set equal to $\pi/4$, the magnitude and direction of the light vector as it emerges from the plate are given by Equation 1.11 and 1.12 as:

$$E'_t = \frac{\sqrt{2}}{2}k\sqrt{\cos^2\omega t + \sin^2\omega t} = \frac{\sqrt{2}}{2}k \qquad (1.13)$$

In Equation 1.13, ωt is substituted for γ. The light vector described by these expressions has a constant magnitude: therefore, the tip of the light vector traces out a circle as it rotates. The vector rotates with a constant angular velocity in a counterclockwise direction when viewed from a distant position along the path of propagation of the beam. Such light is known as circularly polarized light.

1.4 Fiber Optic Sensor

Fiber optical sensing techniques have been associated with precise and non-intrusive measurements. There are many advantages in using fiber optic sensors, such as good electrical isolation, immunity to electromagnetic interference, safety in explosive environments, low signal attenuation, compactness, lightweights, and flexibility. Furthermore, fiber optic sensors exhibit high sensitivity.

The fiber optic sensor used in this system belongs to the fiber optic polarimetric sensor category. The optical fiber used in these sensors is usually birefringent or highly birefringent (Hi-Bi). If anisotropy is introduced in the fiber, then the optical fiber can be constructed with dissimilar refractive indices along the X and Y axes. Hence, the velocities of the components of light transmitted along the two axes will be different and a phase difference is developed. Anisotropy can be achieved by making the core fibers elliptical (e-core fiber) as shown in Figure 1.4, or bow-tie, panda-type elliptical cladding (e-cladding fiber), or two-core fibers as shown in Figure 1.5.

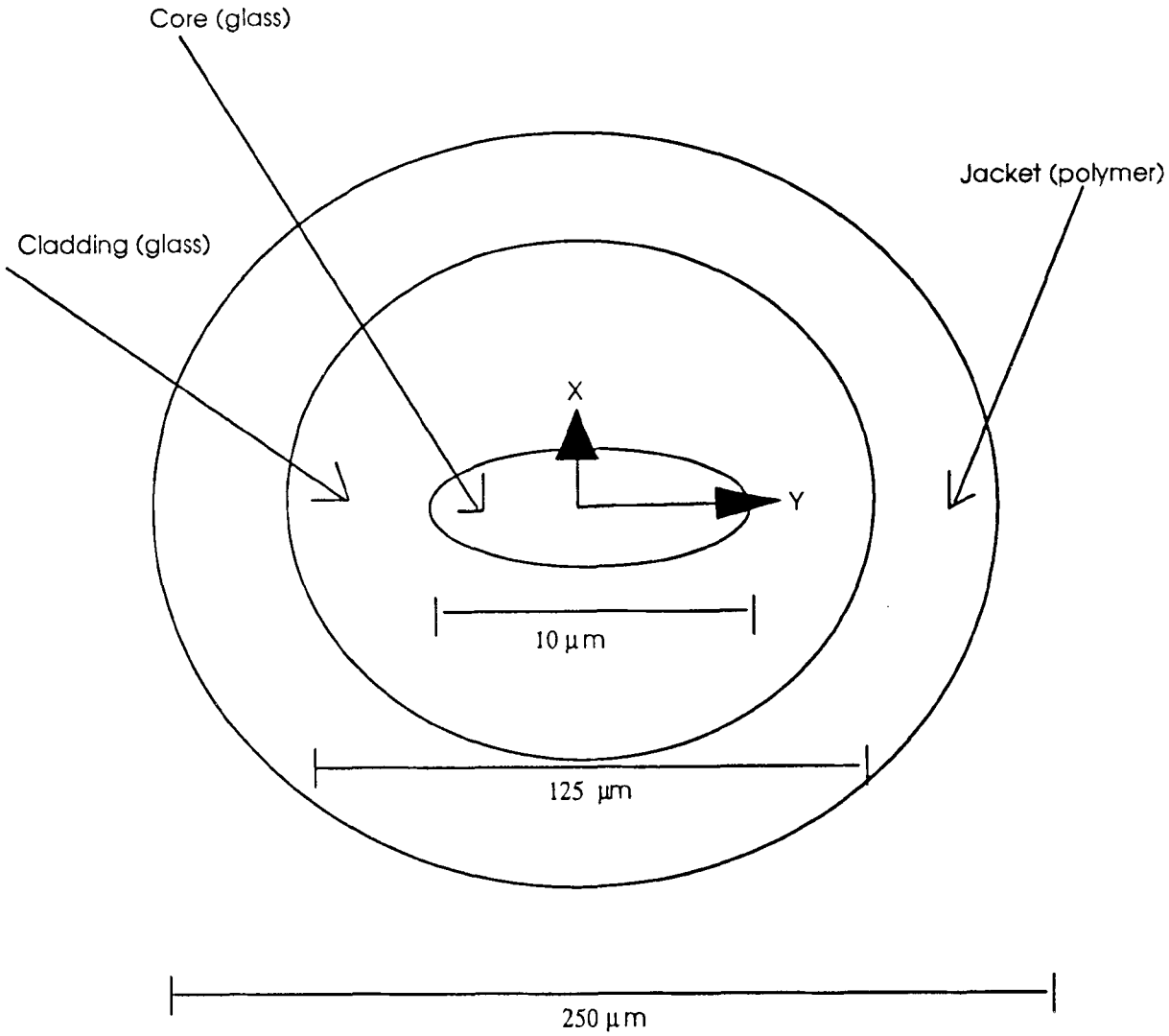

Figure 1.4 Cross section of an elliptical-core fiber.

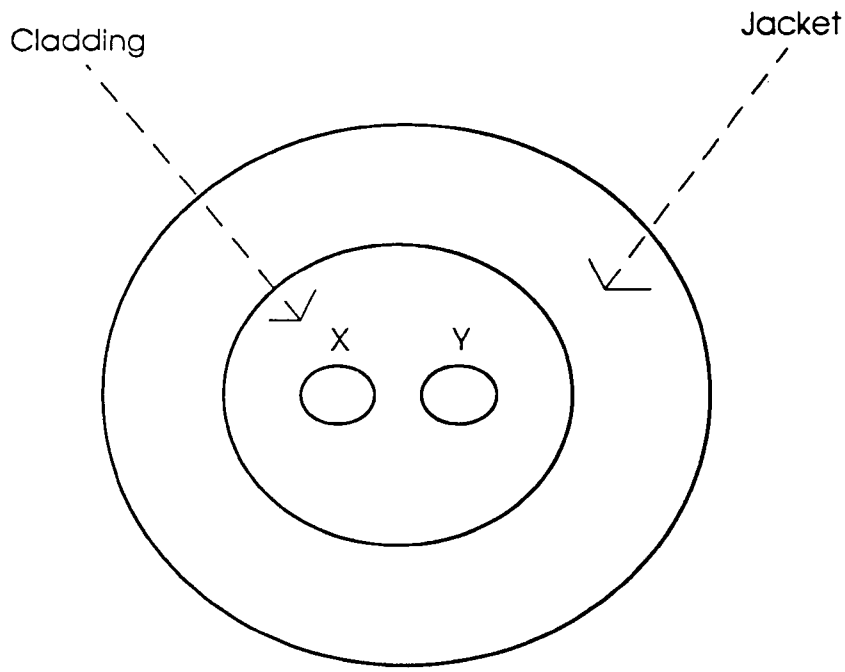

Figure 1.5 Cross section of a two-core fiber.

CHAPTER 2

THEORETICAL BACKGROUND

2.1 Theory of the System

The optical arrangement shown in Figure 2.1 has been employed in this thesis. The light emerging from the He-Ne laser source is 633 nm (wavelength). The plane-polarized light emerging from the first plane-polarizer can be represented by Equation 2.1:

$$E_{py} = k \cos(\omega t) \tag{2.1}$$

where, ω is the angular frequency of the light which is $2.978*10^{15}$ rad/second ($\omega=2\pi c/\lambda$), and k was described earlier in Chapter 1. As the light enters the first quarter-wave plate, it is resolved into components E_f and E_s with vibrations parallel to the fast and slow axes, respectively. Since the axes of the quarter-wave plate are oriented at 45^o with respect to the axis of the polarizer,

$$Ef = Es = \frac{\sqrt{2}}{2} k \cos(\omega t) \tag{2.2}$$

As the components propagate through the plate, they develop a relative angular phase shift $\Delta=\pi/2$: therefore, the components emerging from the plate can be expressed as [9]:

$$E_f^{'} = \frac{\sqrt{2}}{2} k \cos\ (\omega\ t)$$
$$E_s^{'} = \frac{\sqrt{2}}{2} k \cos\ (\omega\ t - \frac{\pi}{2}) = \frac{\sqrt{2}}{2} k \sin\ (\omega\ t) \tag{2.3}$$

It has been previously shown that these two plane-polarized beams represent circularly polarized light with the vector rotating counterclockwise at any point along the axis of propagation of the light.

After leaving the first quarter-wave plate, the components enter the birefringence fiber optic in the manner illustrated in Figure 2.2 [9]. Since the stressed birefringence optical fiber acts as a temporary wave plate, the components E'_f and E'_s are resolved into components E_1 and E_2, which have directions of vibration parallel to the axes of fiber. Thus

$$E1 = E_f^{'} \cos\ (\frac{\pi}{4} - \alpha) + E_s^{'} \sin(\frac{\pi}{4} - \alpha)$$
$$E2 = E_s^{'} \cos\ (\frac{\pi}{4} - \alpha) - E_f^{'} \sin(\frac{\pi}{4} - \alpha) \tag{2.4}$$

where, α is the angle between the fast axis of fiber and the fast axis of first quarter-wave plate. Substituting Equation 2.3 into 2.4 yields [9]

$$E1 = \frac{\sqrt{2}}{2}k\ [\cos\omega\ t\cos\ (\frac{\pi}{4}-\alpha)+\sin\omega\ t\sin(\frac{\pi}{4}-\alpha)] = \frac{\sqrt{2}}{2}k\cos\ (\omega\ t+\alpha-\frac{\pi}{4})$$
$$E2 = \frac{\sqrt{2}}{2}k\ [\sin\omega\ t\cos\ (\frac{\pi}{4}-\alpha)-\cos\omega\ t\sin(\frac{\pi}{4}-\alpha)] = \frac{\sqrt{2}}{2}k\sin(\omega\ t+\alpha-\frac{\pi}{4}) \quad (2.5)$$

The two components E_1 and E_2 propagate through the birefringence fiber with different velocities. The relative retardation Δ which is related to strain, accumulated during passage through the fiber is given by Equation 2.6 as

$$\Delta = \frac{2\pi l}{\lambda}(n_1 - n_2) \quad (2.6)$$

where, l is the length of the probing part of the fiber, λ is the wavelength of the light (633 nano-meter), and n_1 and n_2 are the refractive indices of the birefringence fiber which will change when the fiber is deformed. Thus the wave upon emerging from the first quarter-wave plate can be expressed as Equation 2.7 [9]

$$E_f' = \frac{\sqrt{2}}{2}k\cos\ (\omega\ t+\alpha-\frac{\pi}{4})$$
$$E_s' = \frac{\sqrt{2}}{2}k\sin(\omega\ t+\alpha-\frac{\pi}{4}-\Delta) \quad (2.7)$$

The light emerging from the optical fiber propagates to the second quarter-wave plate and enters it according to the diagram shown in Figure 2.3

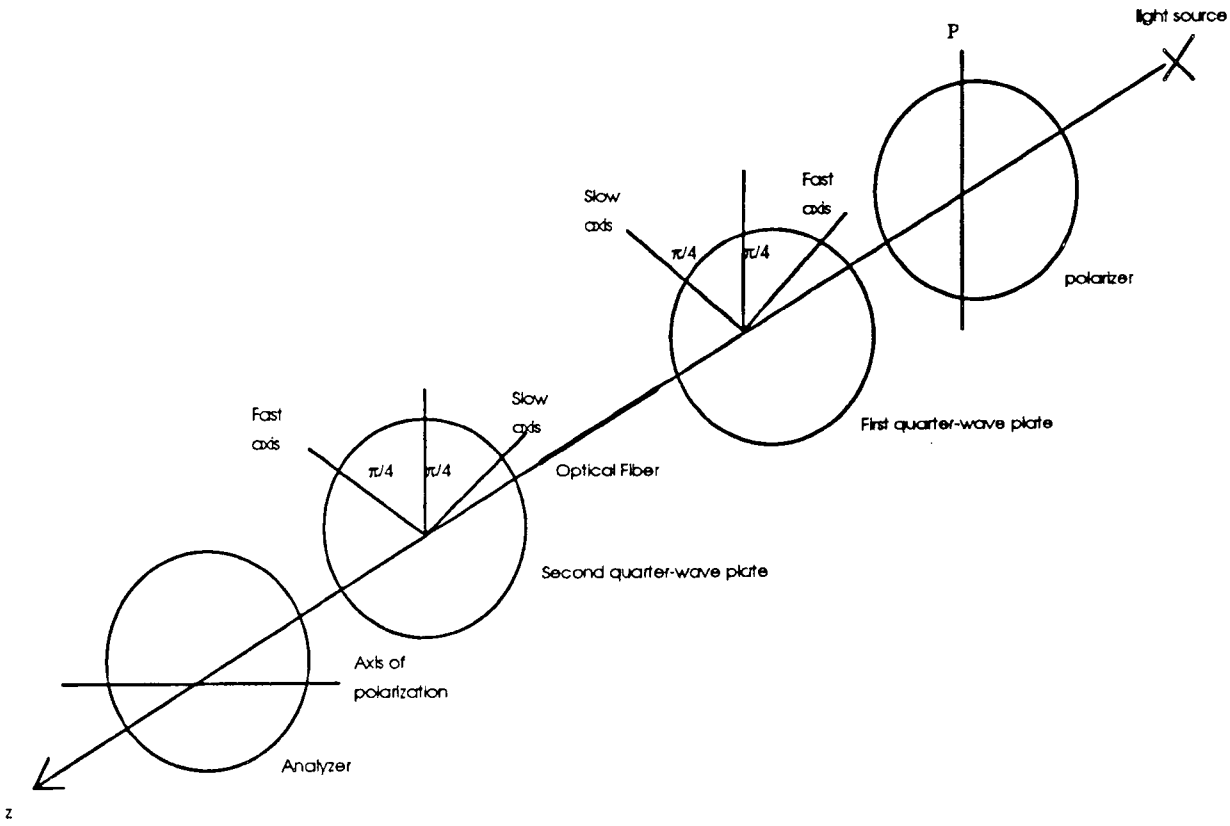

Figure 2.1 Optical arrangement of the system.

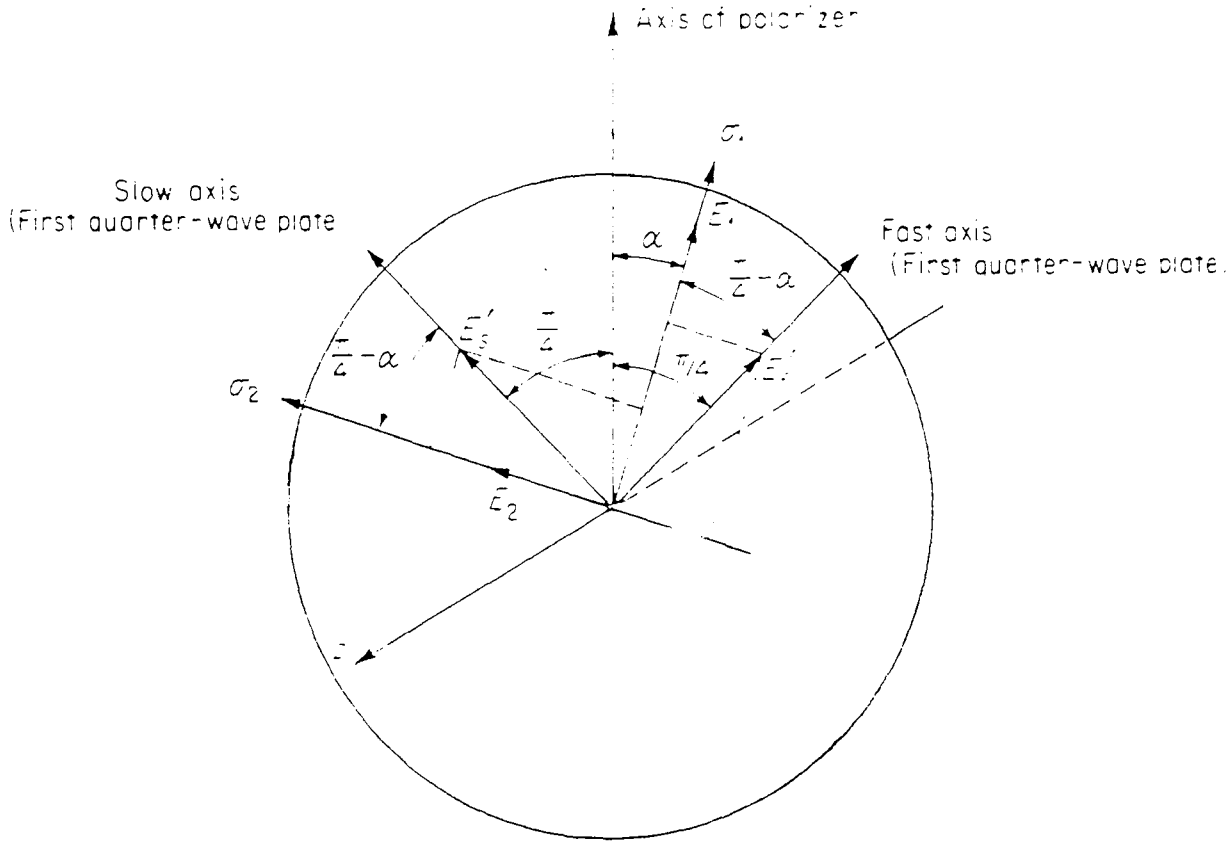

Figure 2.2 Light components at the first end of fiber.

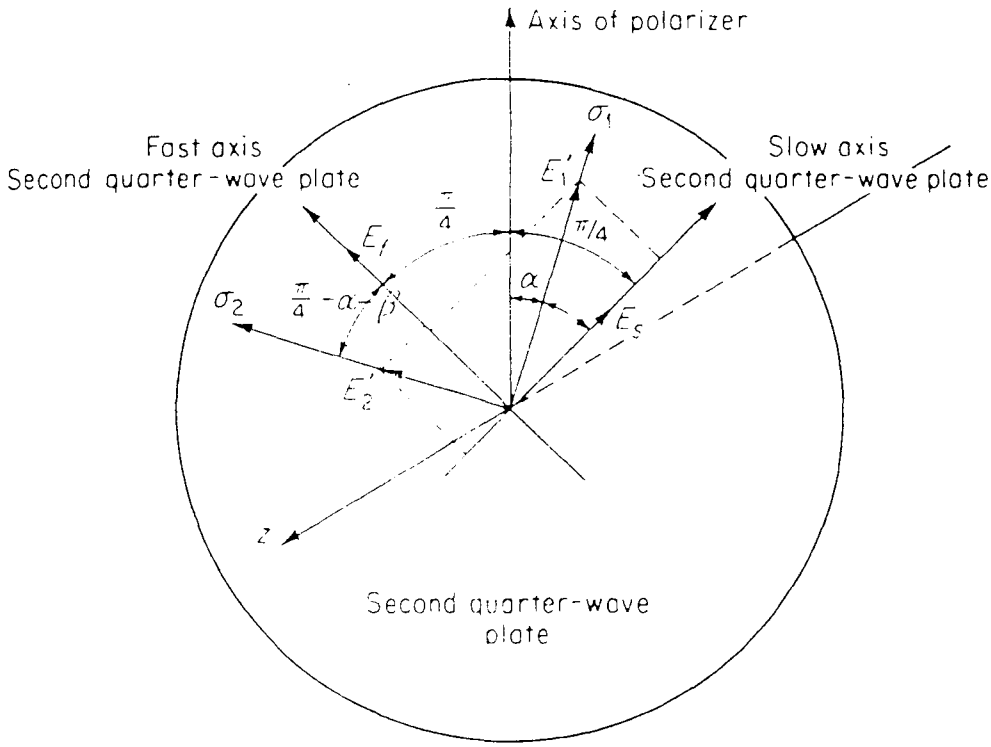

Figure 2.3 Light components at the second quarter-wave plate.

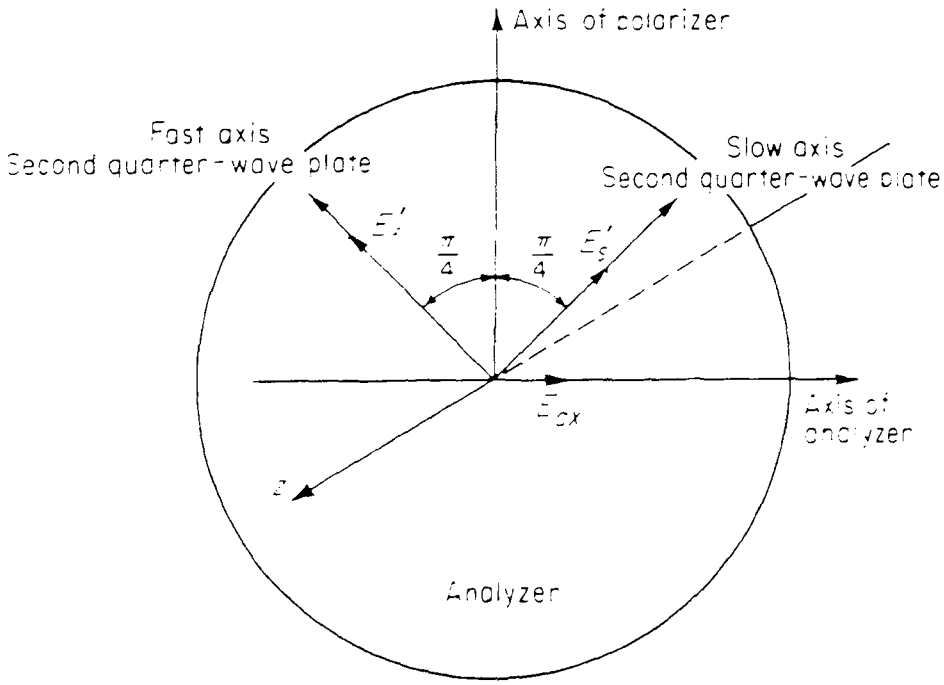

Figure 2.4 Components of the light transmitted through the analyzer.

[9]. The components associated with the fast and slow axes of the second quarter-wave plate are

$$\begin{aligned} Ef &= E'_1 \sin\left(\frac{\pi}{4}-\alpha-\beta\right) + E'_2 \cos\left(\frac{\pi}{4}-\alpha-\beta\right) \\ Es &= E'_1 \cos\left(\frac{\pi}{4}-\alpha-\beta\right) - E'_2 \sin\left(\frac{\pi}{4}-\alpha-\beta\right) \end{aligned} \tag{2.8}$$

where, β is the angle between the fast axis of the fiber and the fast axis of the second quarter-wave plate. Substituting Equation 2.7 into 2.8 yields

$$\begin{aligned} Ef &= \frac{\sqrt{2}}{2}k\left[\cos\left(\omega t+\alpha-\frac{\pi}{4}\right)\sin\left(\frac{\pi}{4}-\alpha-\beta\right)+\sin\left(\omega t+\alpha-\frac{\pi}{4}-\Delta\right)\cos\left(\frac{\pi}{4}-\alpha-\beta\right)\right] \\ Es &= \frac{\sqrt{2}}{2}k\left[\cos\left(\omega t+\alpha-\frac{\pi}{4}\right)\cos\left(\frac{\pi}{4}-\alpha-\beta\right)-\sin\left(\omega t+\alpha-\frac{\pi}{4}-\Delta\right)\sin\left(\frac{\pi}{4}-\alpha-\beta\right)\right] \end{aligned} \tag{2.9}$$

As the light passes through the second quarter-wave plate, a relative phase shift of $\Delta=\pi/2$ develops between the fast and slow components. Thus the waves emerging from the plate can be expressed as

$$\begin{aligned} E'_f &= \frac{\sqrt{2}}{2}k\left[\cos\left(\omega t+\alpha-\frac{\pi}{4}\right)\sin\left(\frac{\pi}{4}-\alpha-\beta\right)+\sin\left(\omega t+\alpha-\frac{\pi}{4}-\Delta\right)\cos\left(\frac{\pi}{4}-\alpha-\beta\right)\right] \\ E'_s &= \frac{\sqrt{2}}{2}k\left[\sin\left(\omega t+\alpha-\frac{\pi}{4}\right)\cos\left(\frac{\pi}{4}-\alpha-\beta\right)+\cos\left(\omega t+\alpha-\frac{\pi}{4}-\Delta\right)\sin\left(\frac{\pi}{4}-\alpha-\beta\right)\right] \end{aligned} \tag{2.10}$$

Finally, the light enters the analyzer, as shown in Figure 2.4 [9]. The vertical components of E'_f and E'_s are absorbed in the analyzer(the second plane-polarizer) while the horizontal components are transmitted to give [9]

$$Eax = \frac{\sqrt{2}}{2}(E'_s - E'_f) \tag{2.11}$$

Substituting Equation 2.10 into 2.11 gives an expression for the light emerging from the analyzer of a circular polariscope. Thus

$$Eax = \frac{k}{2}[\cos(\omega t + \alpha - \frac{\pi}{4})\sin(\frac{\pi}{4} - \alpha - \beta) + \sin(\omega t + \alpha - \frac{\pi}{4} - \Delta)\cos(\frac{\pi}{4} - \alpha - \beta)$$
$$-\sin(\omega t + \alpha - \frac{\pi}{4})\cos(\frac{\pi}{4} - \alpha - \beta) - \cos(\omega t + \alpha - \frac{\pi}{4} - \Delta)\sin(\frac{\pi}{4} - \alpha - \beta)]$$

$$Eax = k\sin(\frac{\Delta}{2})\sin(\omega t + 2\alpha + \beta - \frac{\Delta}{2}) \tag{2.12}$$

Since the intensity of light is proportional to the square of the amplitude of the light wave, the intensity of light emerging from the analyzer of a circular polariscope is given by

$$I = k_I \sin^2\frac{\Delta}{2} \tag{2.13}$$

Inspection of Equation 2.13 indicates that the intensity of light beam emerging from the system is a function only of Δ since the angles α and β do not appear in the amplitude of the wave.

2.2 Relationship Between the Fiber Signal and Strain

The relationship between the light intensity of the optical fiber and the applying strain can be obtained by calibration through tension tests. The sensitivity of the fiber optic sensor is dependent on the modulus of elasticity of the fiber and the probing length. Probing length is the length of the fiber which is being strained. This is the fiber length glued to the specimen. Experimental results indicated that the larger probing lengths yielded more sensitive measurements. As will be shown in the following, this is due to the fact that the output signal is proportional to the accumulated strain along the probing length and not strain at a single point.

The phase term Δ which appeared in Equation 2.13 is directly related to the propagation constants and the probing length of the optic fiber by the expression [12]:

$$\Delta = \beta \Delta L + L \Delta \beta \tag{2.14}$$

where, β can be calculated from a theoretical analysis of the fiber propagation curves which is:

$$\beta = \beta^{X} - \beta^{Y} \tag{2.15}$$

where, β^X and β^Y represent the propagation constants of the x- and y-polarized fundamental modes of single mode fiber, respectively.

The total resulting phase shift due to a change in the strain is:

$$\Delta = [\beta \frac{\partial L}{\partial \varepsilon} + L \frac{\partial \beta}{\partial \varepsilon}] \Delta\varepsilon \qquad (2.16)$$

where, $\Delta\varepsilon$ is the change in the strain and L is the probing length of fiber.

As it will be discussed later in this thesis, the relationship between the change in phase Δ and the induced strain $\Delta\varepsilon$ can be obtained by calibration from a tension test.

CHAPTER 3

EXPERIMENTAL PROGRAM

The complete experimental setup is shown in Figure 3.1. The system consists of four segments: the testing machine, strain gage instrumentation, optical system, and data acquisition.

3.1 Testing Machine

The testing machine employed for the application of load to the specimen is a closed loop servo controlled system manufactured by Test Systems and Simulation, Inc. The control system consists of a 386 AT compatible computer, Analog and Digital Input/Output Interfaces, Signal Conditioning, and the Digital Closed Loop (DCL) Servo Controller Interfaces.

The Control Management System is an interface between the user, parallel and serial communication, analog subsystems, and DCL Servo Controller. The control system enables a user to Easily set-up DCL parameter and request desired commands for force or motion control.

The control software includes programs which assist the user in transducer information, initializing and tuning DCLs, setting up wave forms which command the DCLs, and driving the DCLs with these commands. Axial elongation of the specimens were monitored by a Linear-Variable-

Differential-Transformer (LVDT). As shown in Figure 3.1, the LVDT signal was employed as a feedback signal for the closed loop control.

3.2 Strain Gage Calibration

Strain gages were employed for the calibration of fiber optic sensors. Strain gages were glued on to the surface of the specimens as shown in Figure 3.2. The strain gages were manufactured by the measurements group (CEA-06-125-UN-350) with the gage resistance of 350 ohms. A Wheatstone Bridge and an amplifier was employed for obtaining the voltage output due to change in strain. The output signal was transmitted to the data acquisition board. A microcomputer was employed for providing the command signals for the data acquisition. A correlation was obtained between output voltage and strain by linear regression. The Strain-Voltage correlation is:

$$1\ Volt = 6000\ micro\text{-}strain = 0.6\%\ strain \qquad (3.1)$$

3.3 Optical System

The optical system included a 633 nano-meter He-Ne laser source, two quarter-wave plates, two plane-polarizers, two bare fiber (FC) adapters for connecting the polarization-maintaining optical fiber to the quarter-wave plates, a photo-detector, and the signal amplifier.

The light from He-Ne laser was coupled into the first plane-polarizer and then into the first quarter-wave plate. The axes of the polarizer and the

quarter-wave plate were set at 45° with respect to each other. The polarization-maintaining fiber was connected to the quarter-wave plate via the FC fiber connectors.

Elliptical and two-core fibers, both of which polarization-maintaining were employed in this study. The elliptical core fiber (SMP-A0630B) which operates at a wavelength of 630 nm has a cladding diameter of 125 μm, coating diameter of 250 μm, and a maximum attenuation of 12 dB per km.

At the receive end of the system, the fiber adapter was connected to the second quarter-wave plate and the light output was passed through the analyzer. The axes of the second quarter-wave plate and the analyzer were set at 45° with respect to each other.

The optical signal emerging from the optical system propagates into the photo-detector. The optical signal is converted into the electrical signal at the photo detector stage and then amplified. The photo detector and the amplifier assembly are shown in Figure 3.3. The photo detector (AXGS-R2F) is manufactured by SHARP. Data was then transferred to the data acquisition board via a PC.

3.4 Data Acquisition

The data acquisition board acquired four separate signals during each experiment. Data included the strain gage signal, the fiber optic signal, and the deformation signal from the LVDT, and the load signal from test control system.

DAS-8 interface board manufactured by Keithley-Metrabyte was employed for data acquisition. The data acquisition interface card is an eight

channel data acquisition board. As described above, four channels of data was acquired at the rate of 1 hertz. Data was stored in the computer for later processing.

3.5 Specimen Preparation

Figure 3.2 depicts the geometry of the specimen employed for the calibration tension tests. The test specimen was fabricated from a plexiglass material which exhibited linear-elastic behavior (except at near fracture load). The specimen dimensions are given in Figure 3.2. A longitudinal groove of 0.1 inch depth was machined in the specimen as shown. Epoxy glue was applied in the groove and the optical fiber was embedded within the groove. This operation ensured full transmission of surface strains to the optical fiber. The strain gage was glued to the opposite surface of the specimen. Specimens were prepared at least 24 hours prior to the experiments so as to ensure proper curing period for the epoxied portions of the optical fiber. At this point the input and output ends of the optical fiber were cut flat and ready for being connectorization by the FC type connector (adapter).

3.6 Testing Procedure

(1) Turn on He-Ne laser for at least one hour prior to the experiment for the laser to reach its stabilized power level.

(2) Turn on all the electronic instruments, namely: IBM-AT, testing control system, LeCroy 9314 Oscilloscope, strain gage amplifier, and the photo-

detector circuit twenty minutes prior to the commencement of the experiment (for system warm up).

(3) Set up the specimen in the testing system by way of grips as shown in Figure 3.4.

(4) Connect the strain gage wires to the amplifier and adjust the offset level of the amplifier to 0 volt.

(5) Connect the two ends of the optical fiber to the bare adapters. Adjust the offset level of the photo-detector for the output signal to deviate ± 10 volts.

(6) Adjust the LVDT to the proper position.

(7) Set the Velocity of the testing system to a certain value such as 0.0005 inch/second, the 'SetPoint' to 0.1253 inch, the 'Max Flow' to 100 and the 'Wave Form' to 'RAMP'.

(8) Set the 'Run Mode' to 'Start' in order to commence the experiment and at the same time trigger the data acquisition.

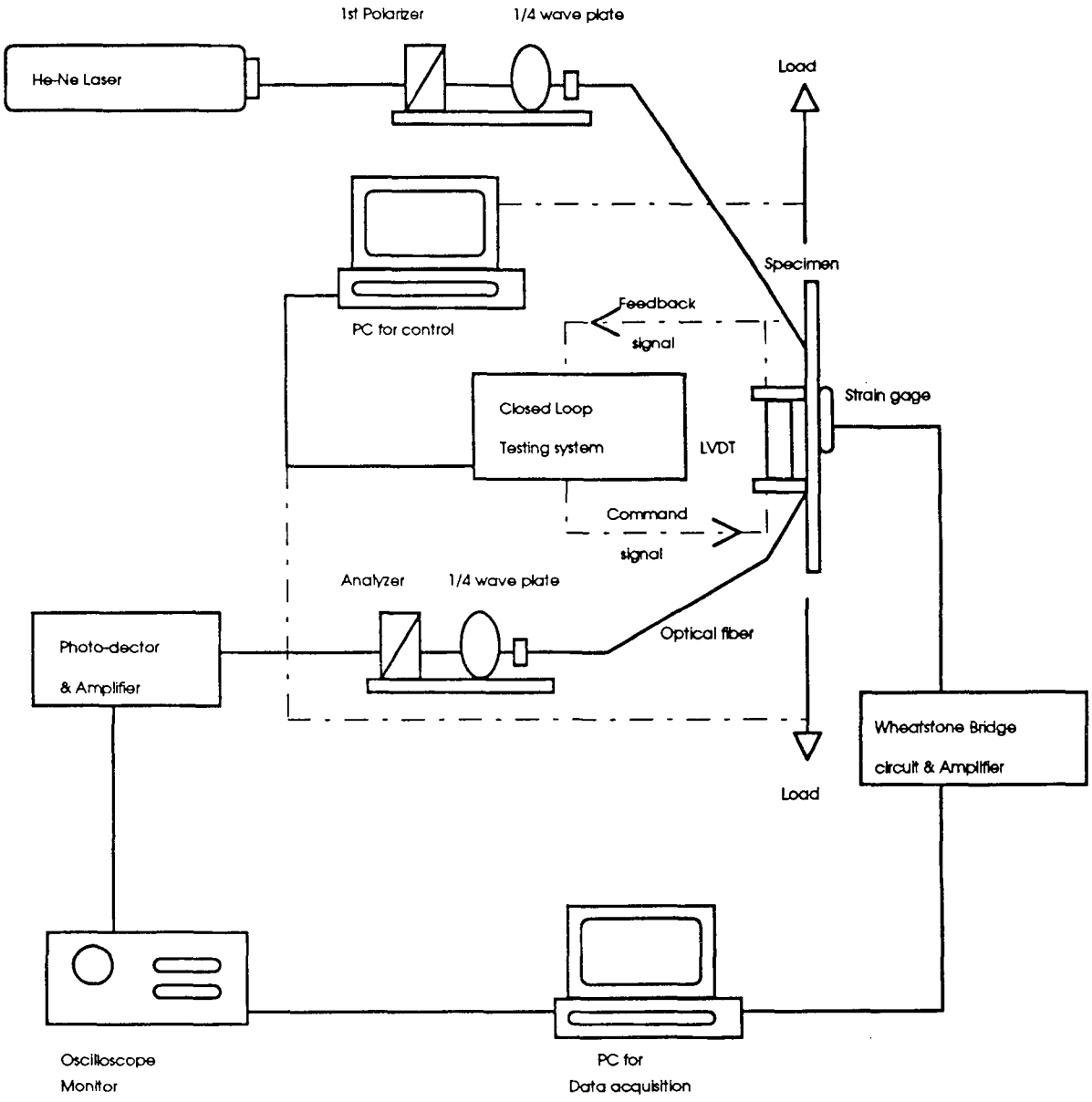

Figure 3.1 Experimental setup.

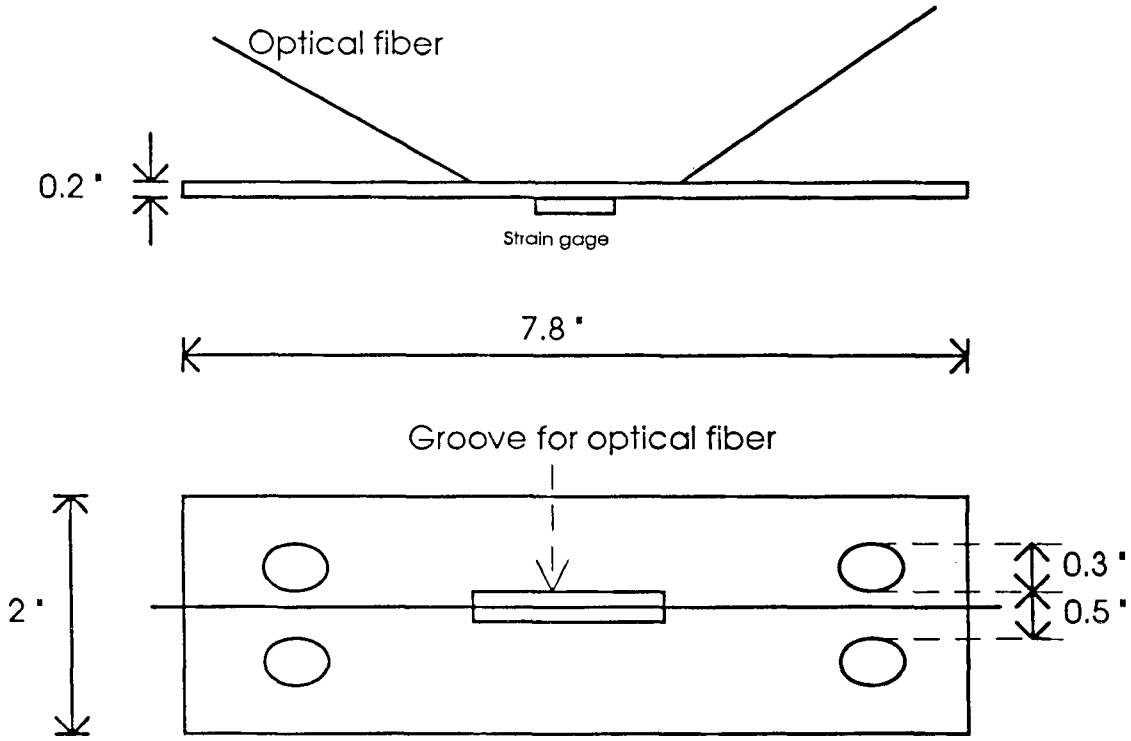

Figure 3.2 Specimen for the tension test.

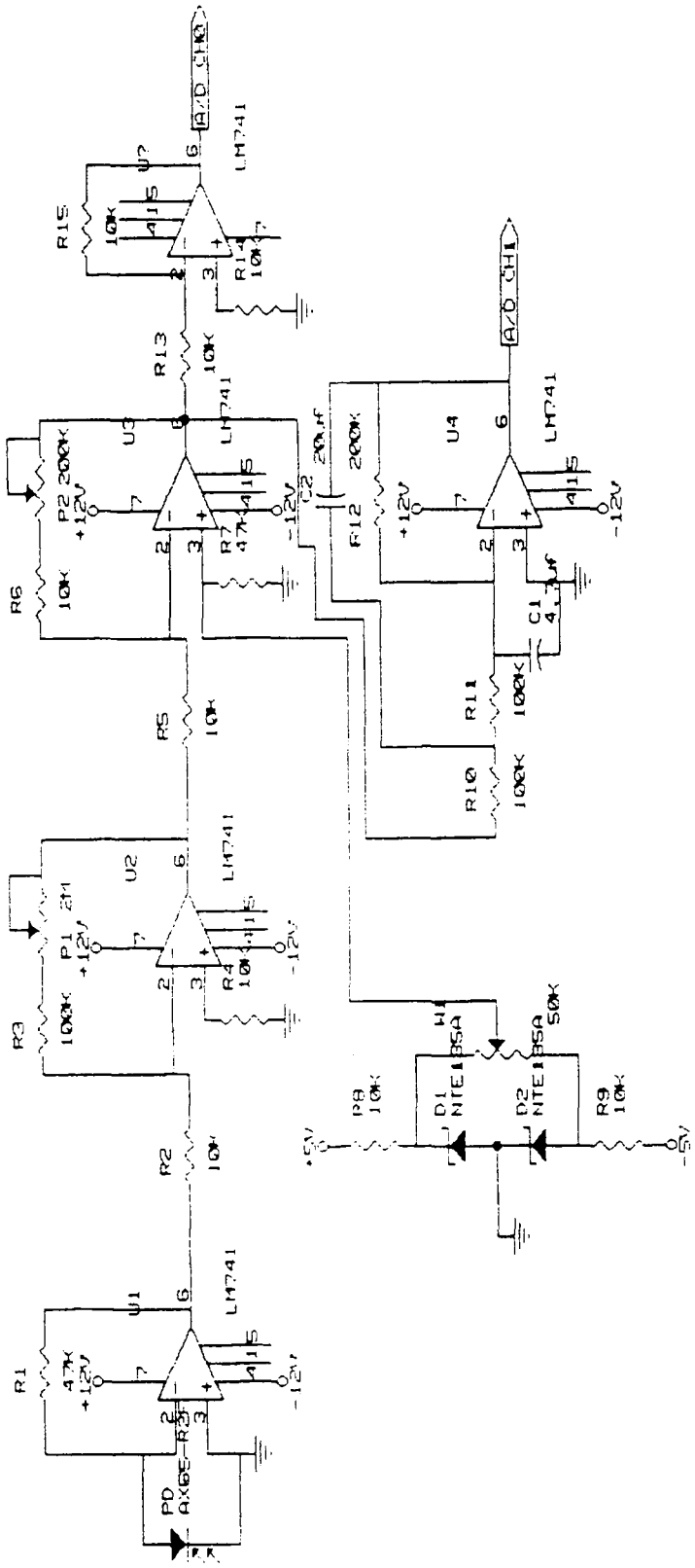

Figure 3.3 Photo detector and amplifier.

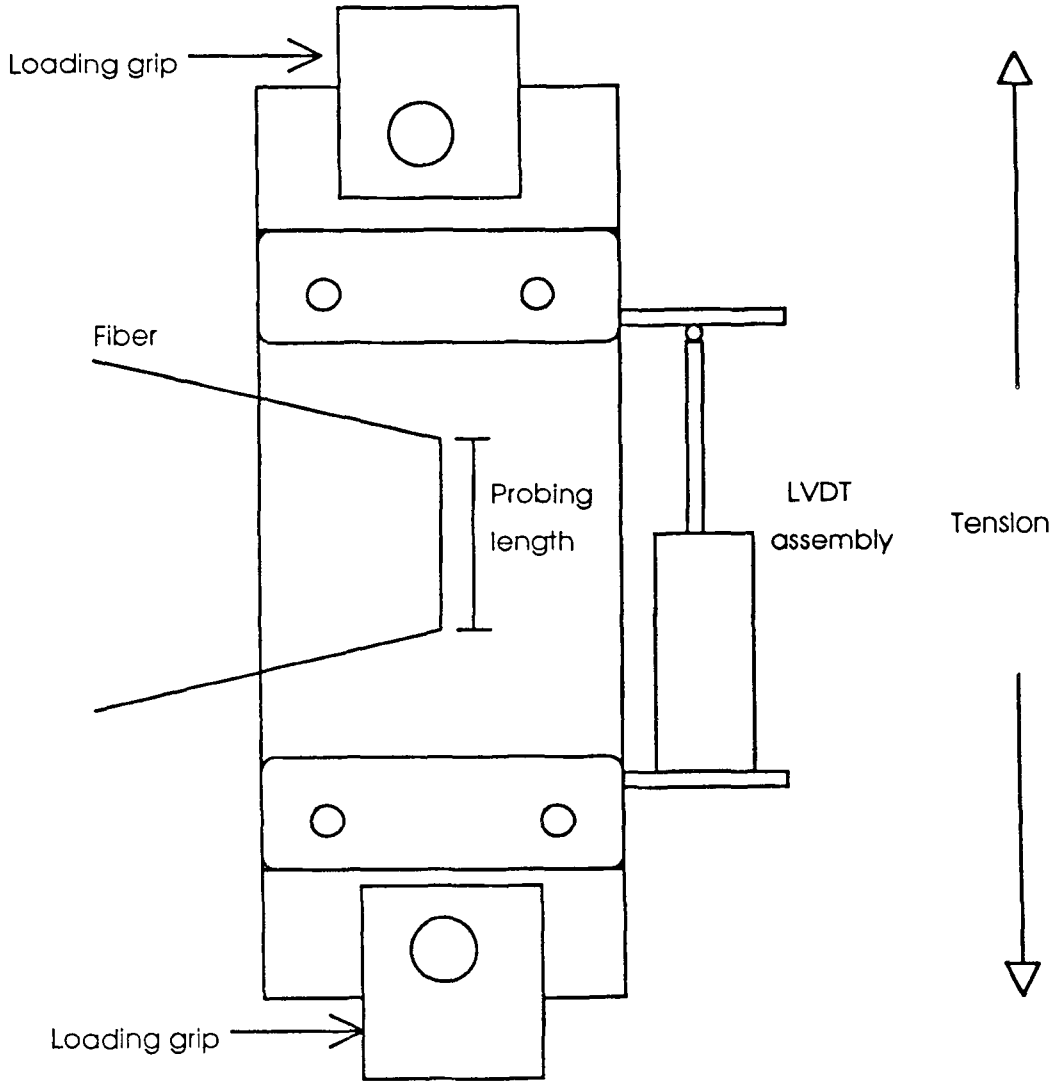

Figure 3.4 Setup of tension test.

CHAPTER 4

RESULTS, ANALYSIS AND DISCUSSION

This chapter presents the experimental results, their analysis and a discussion of the observed trends. Both Low and High-Birefringence optical fibers were employed in the experiments. Tension tests were employed to calibrate the fiber optic sensor. Each specimen was assigned a name. For example, HMAR25A, where 'H' stands for High-Birefringence, 'MAR25' stands for the date, and 'A' to designate the test number on a particular day. For example, if there was another test performed on March 25, then the specimen designation would have been HMAR25B including the second test on that day. In Hi-Birefringence fiber for each probing length two tension tests were employed at different loading velocities. Loading velocities were controlled by the axial rate of deformation imposed by the testing system, namely, 0.0002 and 0.0005 inch/second. Specimen designations for High-Birefringence fiber are given in Tables 4.1 through 4.2 for the different testing velocities.

The raw data for Hi-Birefringence fiber comprising of load-time response, strain-time response, intensity-time response, and axial displacement-time response are given in Figures 4.1 through 4.32. The raw data were recorded by a DAS-8 Data Acquisition and Control Interface Board in the IBM PC. Figures 4.1 through 4.32 depict the raw data obtained from testing the specimens listed in Tables 4.1 through 4.2. Fiber optic intensity output versus tensile strains are given in Figures 4.33 through 4.40. Load versus axial displacement curves are given in Figures 4.41 through 4.48.

Stress-strain curves are given in Figures 4.49 through 4.56. Fiber optic intensity versus tensile stress curves are given in Figures 4.57 through 4.64.

Low-Birefringence fiber was employed in the tension tests. Specimen designations for Low-Birefringence fiber are shown in Table 4.3. The raw data and the corresponding calibration results are shown in Figures 4.74 through 4.76. A specimen fabricated from copper was employed in the tests. The specimen geometry is depicted in Figure 4.73.

4.1 Intensity-Time Response

As explained earlier, a photo detector was employed in changing the light intensity into an electrical signal. The signal was then amplified, converted to digital values and stored in the PC via the acquisition board. The data was observed to have different offset values due to the power level of the amplifier. However, polarimetric measurements do not involve the amplitude of the signal and are only dependent on the variations in the optical phase. In all the experiments, the fiber intensity signals were observed to be sine curves which is in agreement with the theory of the polarimetric fiber sensors explained in Chapter 2.

4.2 Calibration of the Fiber Optic Sensor

The calibration of the fiber optic sensor was employed by relating the fiber intensity signal and the strain in the tension test. Results are shown in the Tables 4.1 through 4.2.. Calibration tests were performed by employing the different probing lengths of the fiber optic ranging from 1 inch to 4 inches.

4.3 Low-Birefringence Optic Fiber

Low-Birefringence optical fiber was employed in order to compare their performance with the Hi-Birefringence fiber optic sensors. As shown in Figures 4.74 through 4.76, the calibration constant for Low-Birefringence optical fiber with probing length of 4 inches is approximately:

$$1 fringe = 7000 micro - strain$$

Low-Birefringence optical fiber sensor exhibits a much lower sensitivity as compared to the High-Birefringence optical fiber. However, they are much more economical to use as they are about 30 percent less expensive than their higher birefringence counter parts.

4.4 Discussion

The relationship between the sensitivity and probing lengths of Hi-Birefringence fiber are shown in Figures 4.71 through 4.72. It shows that for a constant strain, the longer probing lengths provide more sensitive results. Intensity-strain relationships for specimen tested at different velocities are shown in Figures 4.67 through 4.70. These figures include probing lengths form 1 to 4 inches respectively. Results indicate that the calibration constants do not vary much by the testing velocity. The relationship between the number of fringes and probing lengths are shown in Tables 4.1 through 4.2.

Specimen Designation	Probing Length (inches)	Number of Fringes for 3500 micro strain *	Calibration Constant Micro-strain Per Fringe	Calibration Constant PSI Per Fringe
HMAR25A	1	Not Sufficient	Not Sufficient	Not Sufficient
HMAR26A	2	1.40	2500	1200
HAPR01A	3	2.59	1350	600
HAPR08A	4	4.24	825	400

Table 4.1 Tension test results for Hi-Birefringence fiber tested at the axial deformation rate of 0.0002 inch/second.

* Linear range limit of the specimen.

Specimen Designation	Probing Length (inches)	Number of Fringes for 3500 micro strain *	Calibration Constant Micro-strain Per Fringe	Calibration Constant PSI Per Fringe
HMAR25B	1	Not Sufficient	Not Sufficient	Not Sufficient
HMAR26B	2	1.46	2400	1200
HAPR01B	3	2.80	1250	600
HAPR12B	4	5	700	400

Table 4.2 Tension test results for Hi-Birefringence fiber tested at the axial deformation rate of 0.0005 inch/second.

* Linear range limit of the specimen.

Specimen Designation	Probing Length (inch)	Axial Deformation Rate (inch/second)	Calibration Constant (micro-strain per fringe)
LMAR03	4	0.0003	Bad
LMAR10	4	0.0002	7000

Table 4.3 Tension test results for Low-Birefringence fiber.

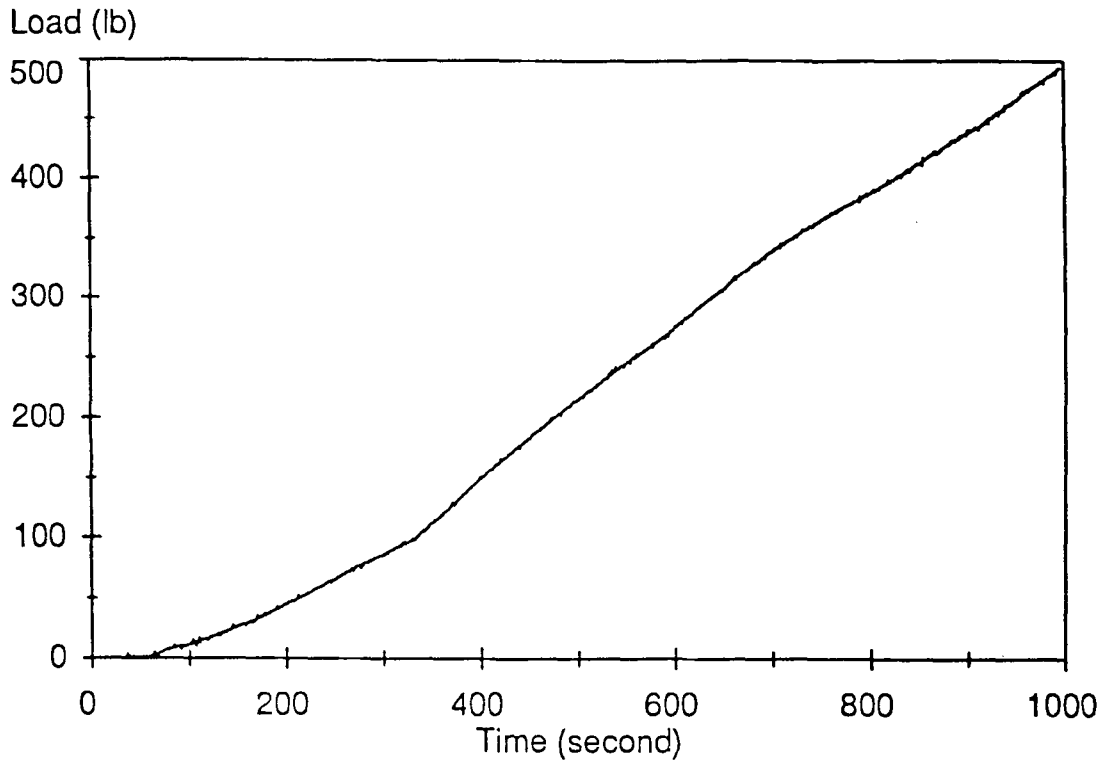

Figure 4.1 Load-time response for HMAR25A .

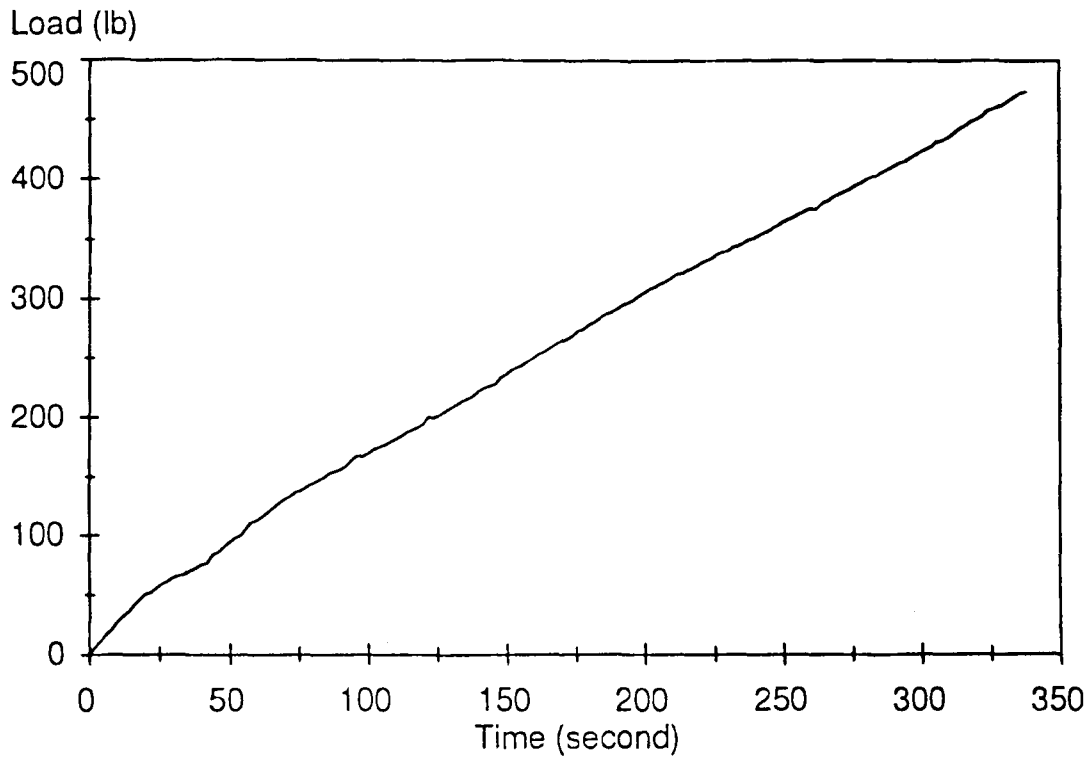

Figure 4.2 Load-time response for HMAR25B.

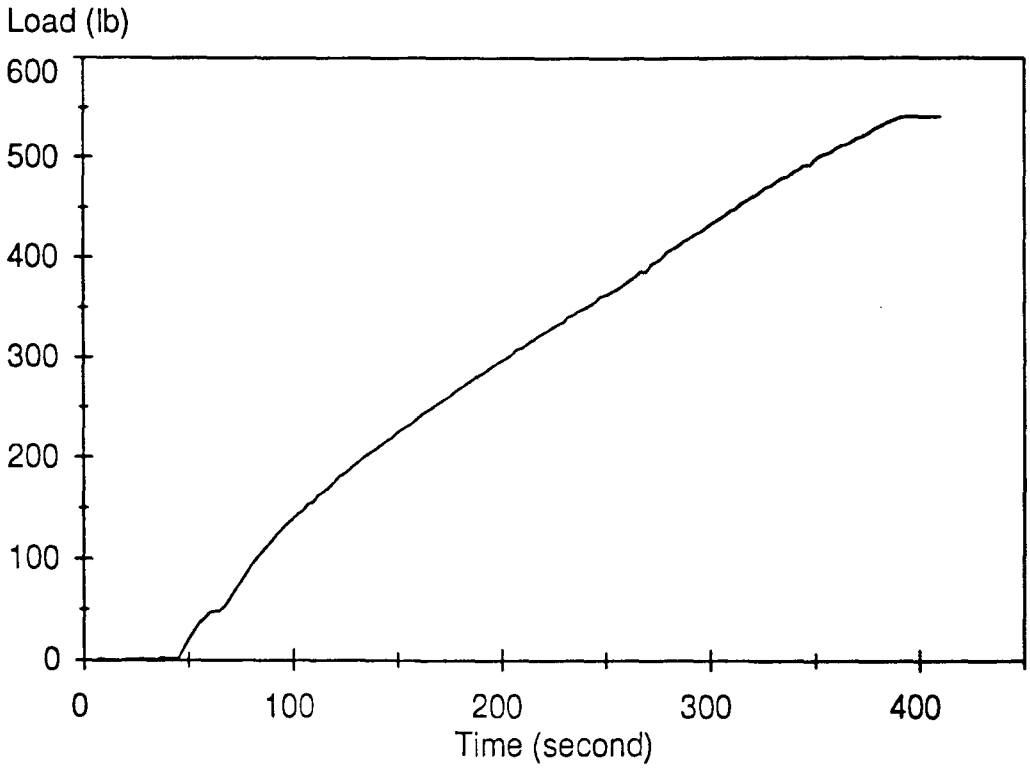

Figure 4.3 Load-time response for HMAR26A.

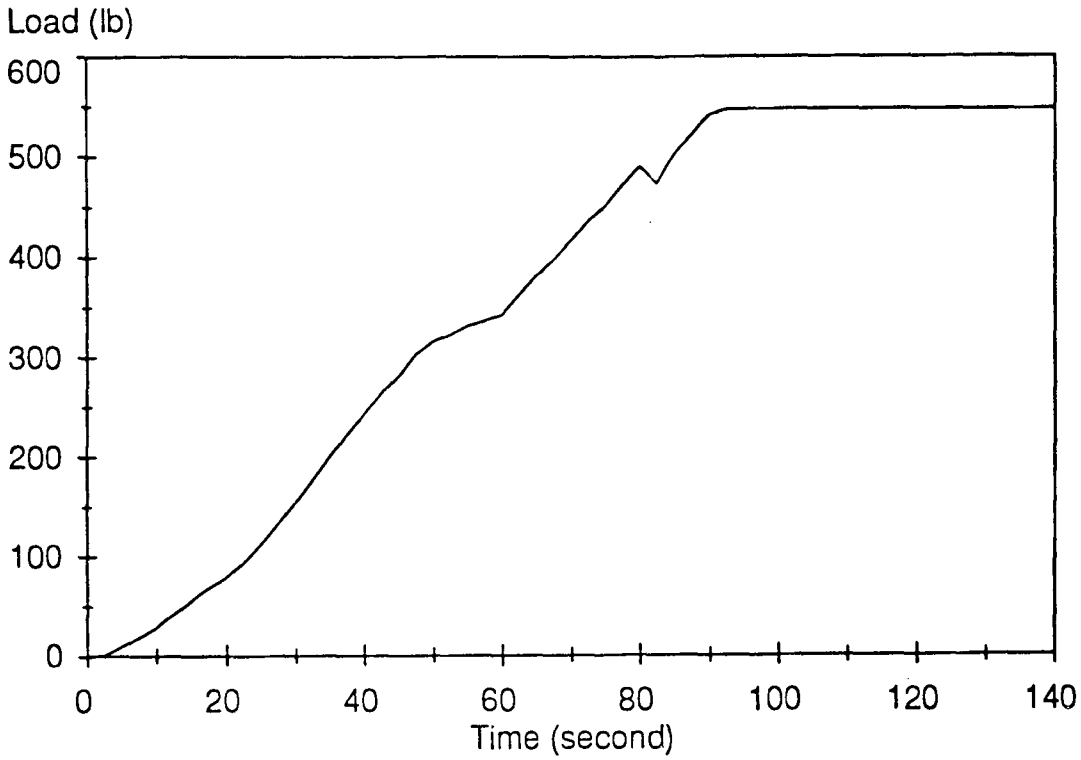

Figure 4.4 Load-time response for HMAR26B.

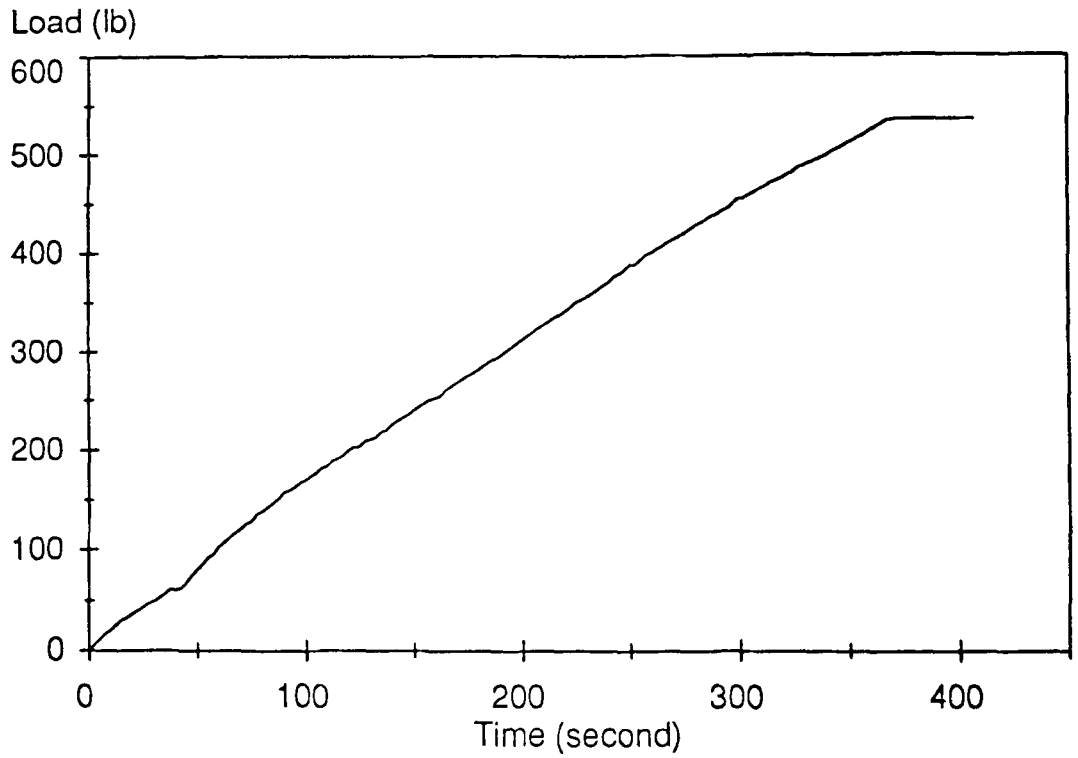

Figure 4.5 Load-time response for HAPR01A.

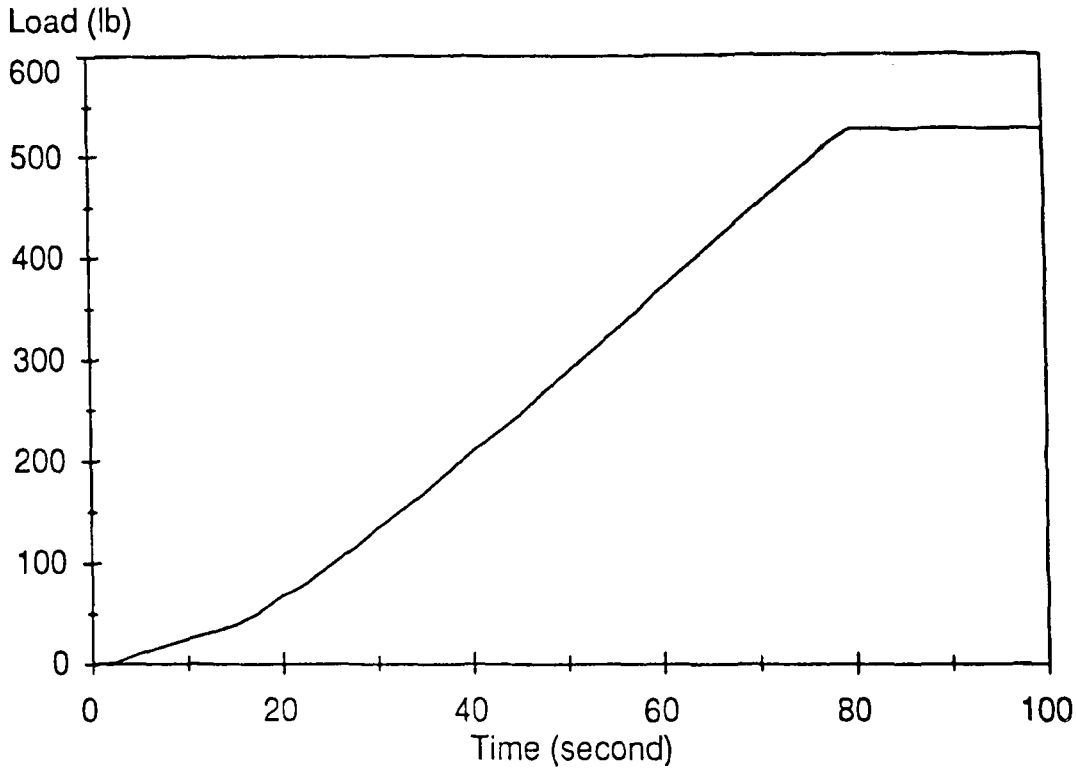

Figure 4.6 Load-time response for HAPR01B.

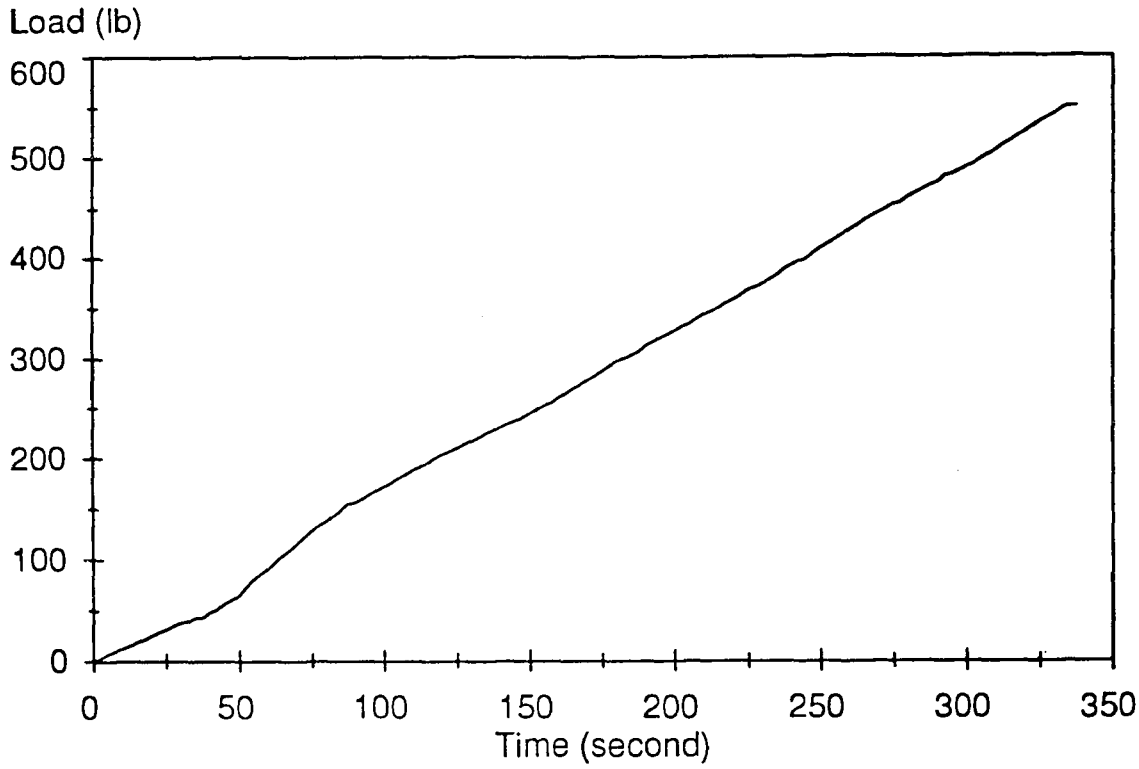

Figure 4.7 Load-time response for HAPR08A.

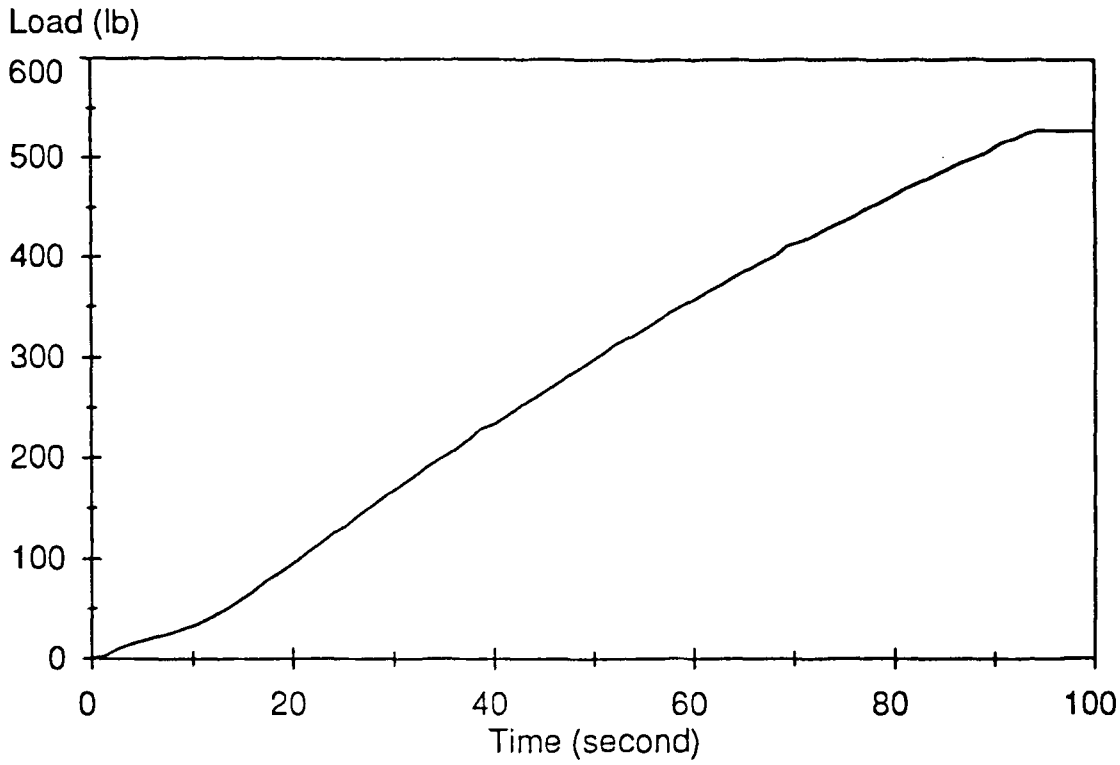

Figure 4.8 Load-time response for HAPR12A.

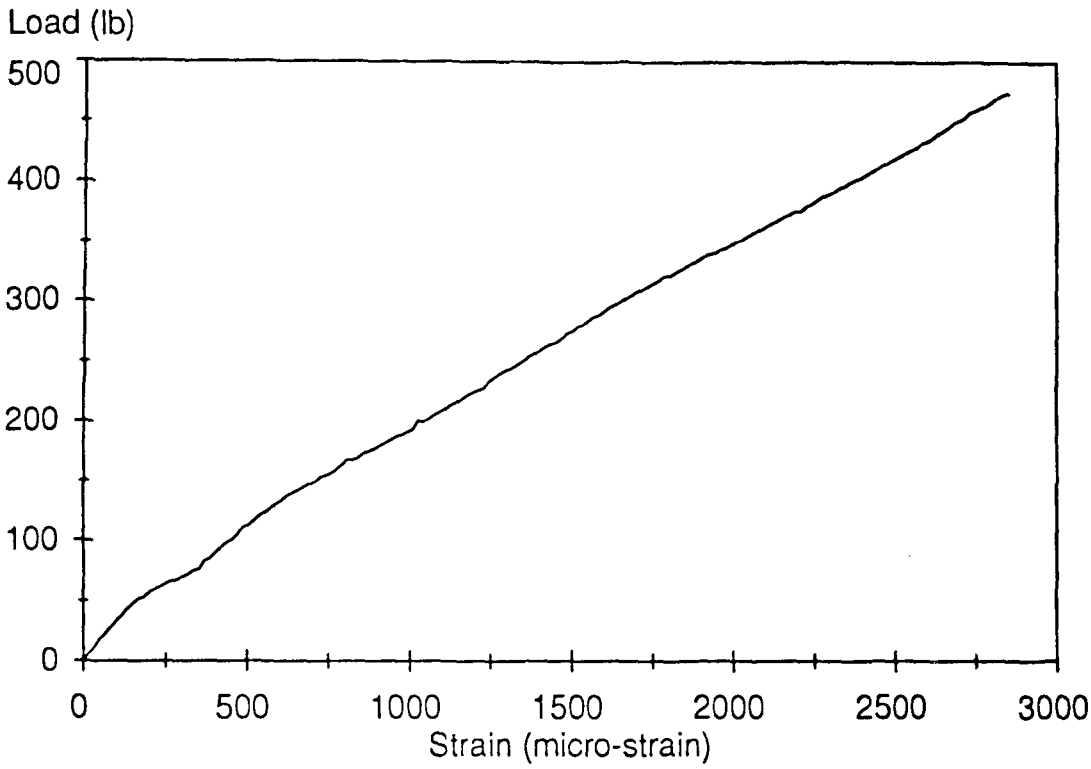

Figure 4.37 HMAR25B load-strain curve.

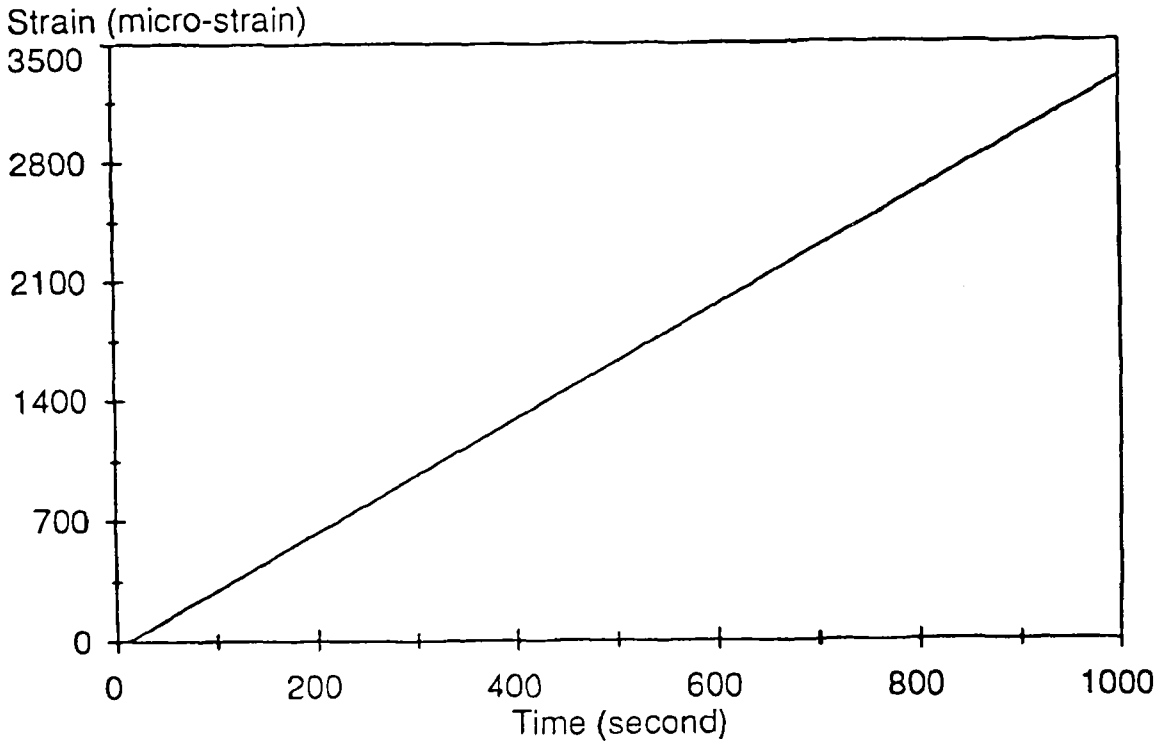

Figure 4.9 Strain-time response for HMAR25A.

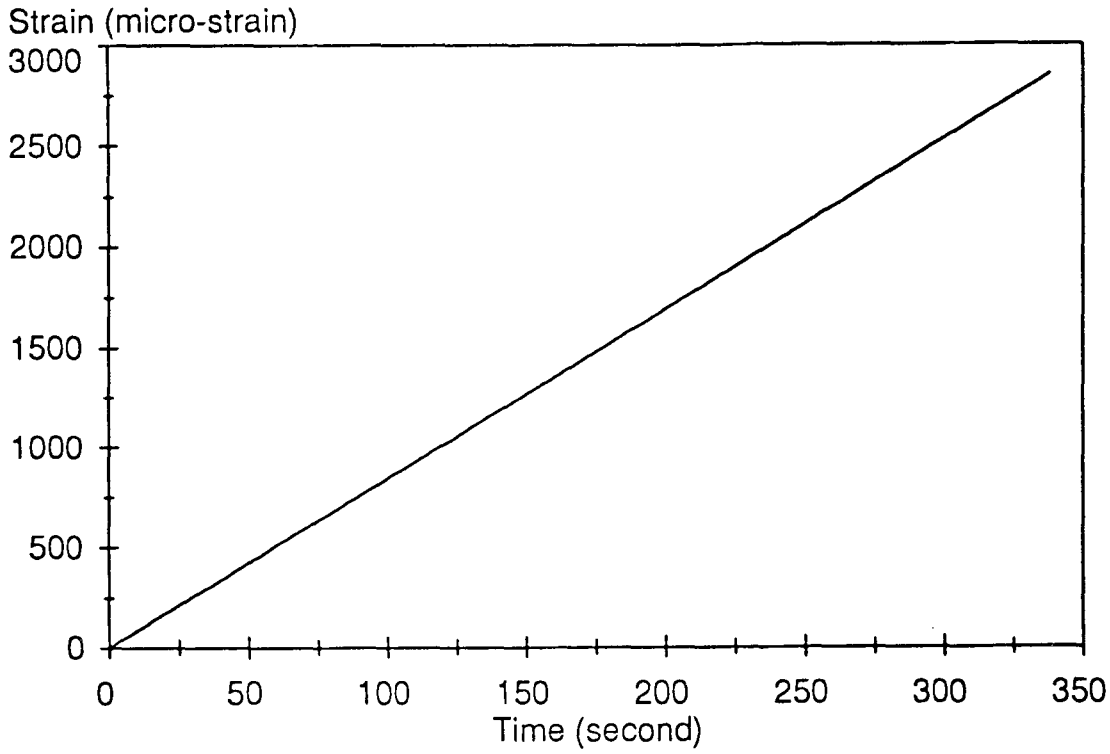

Figure 4.10 Strain-time response for HMAR25B.

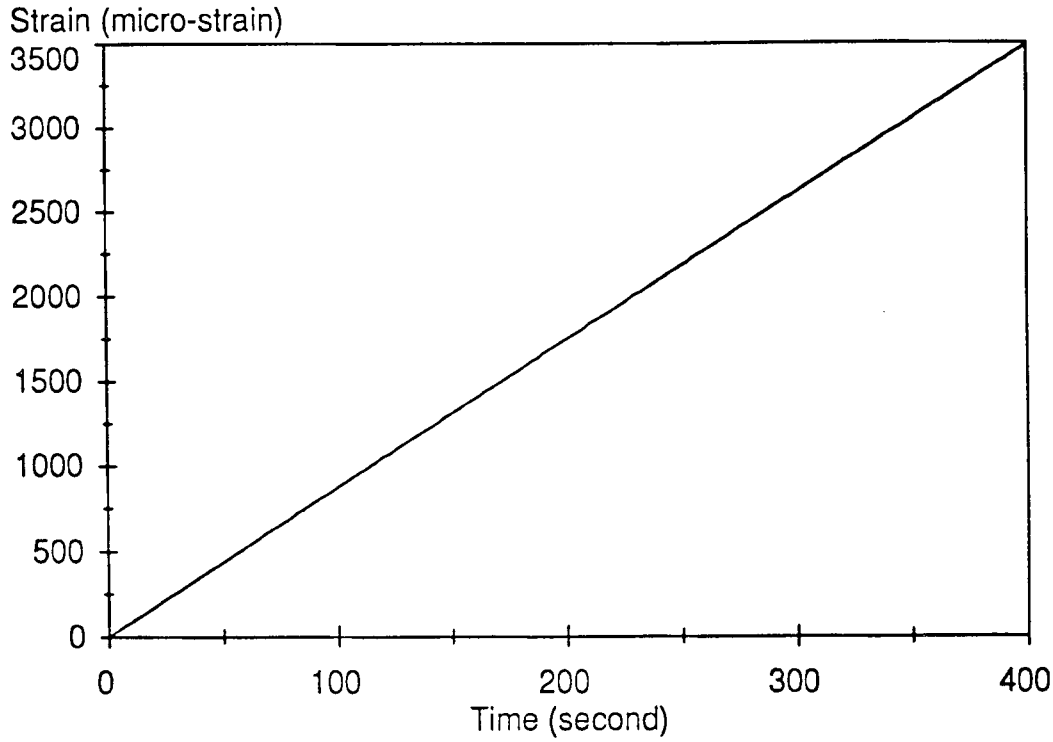

Figure 4.11 Strain-time response for HMAR26A.

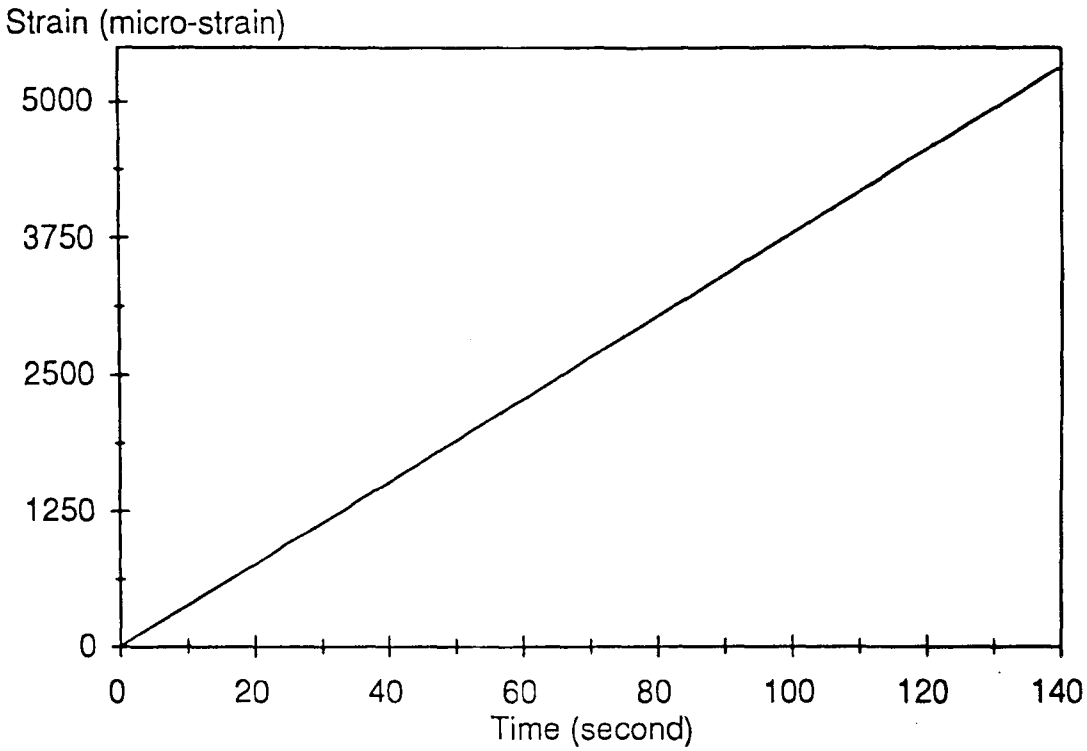

Figure 4.12 Strain-time response for HMAR26B.

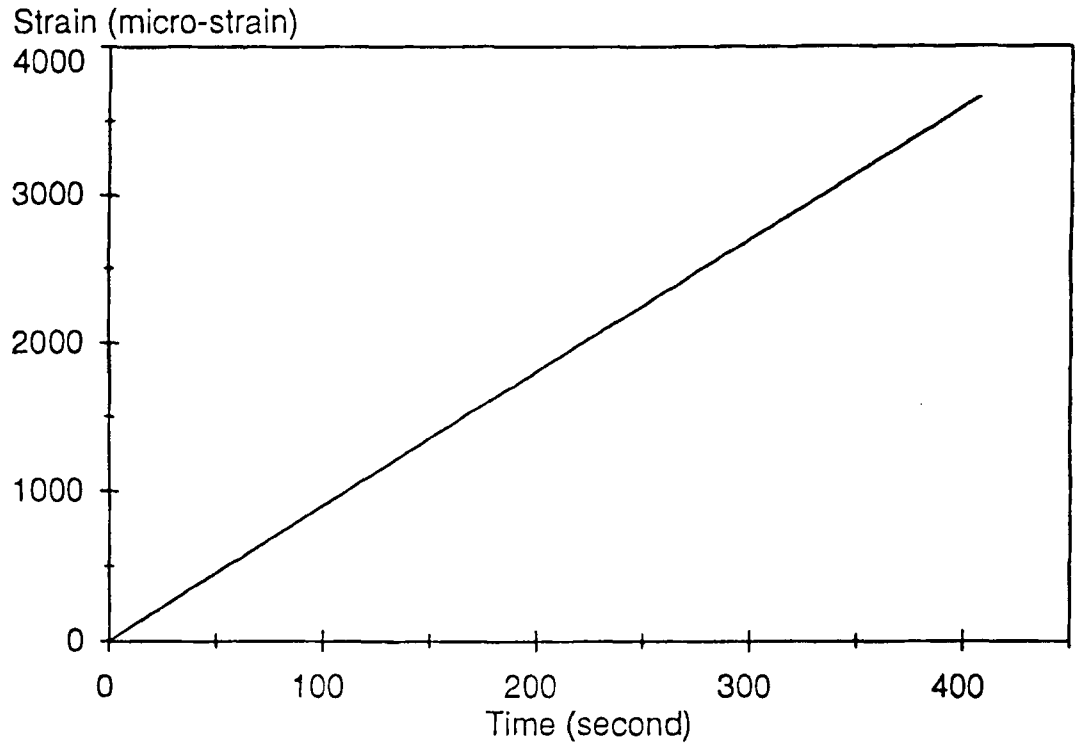

Figure 4.13 Strain-time response for HAPR01A.

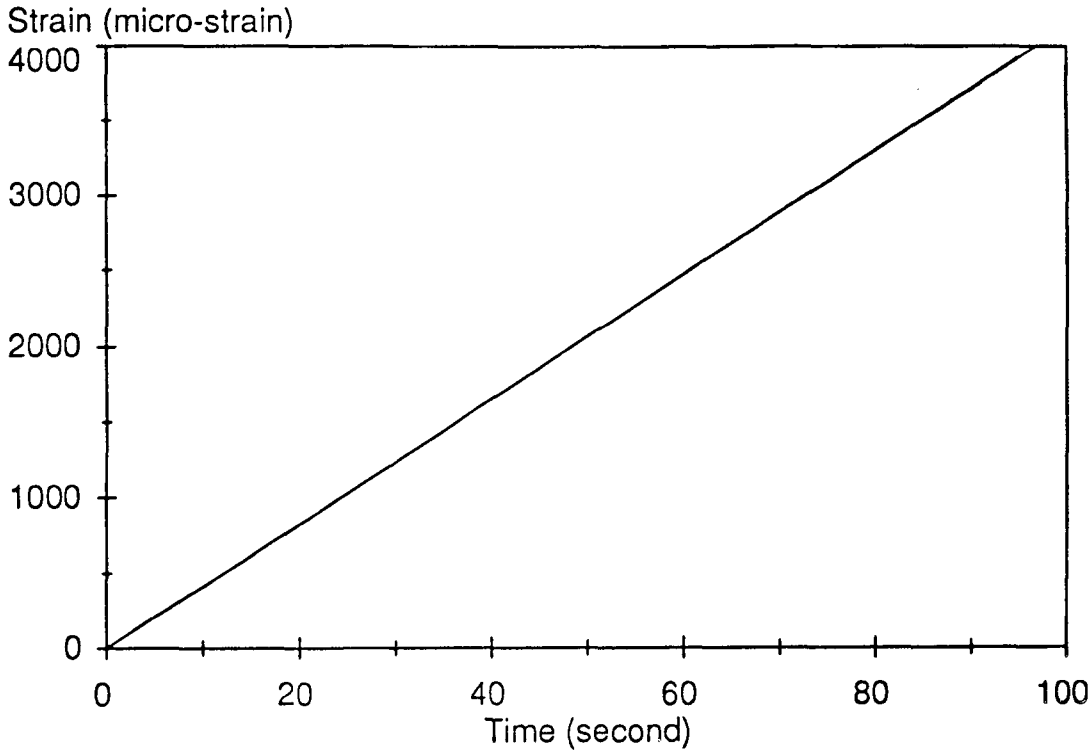

Figure 4.14 Strain-time response for HAPR01B.

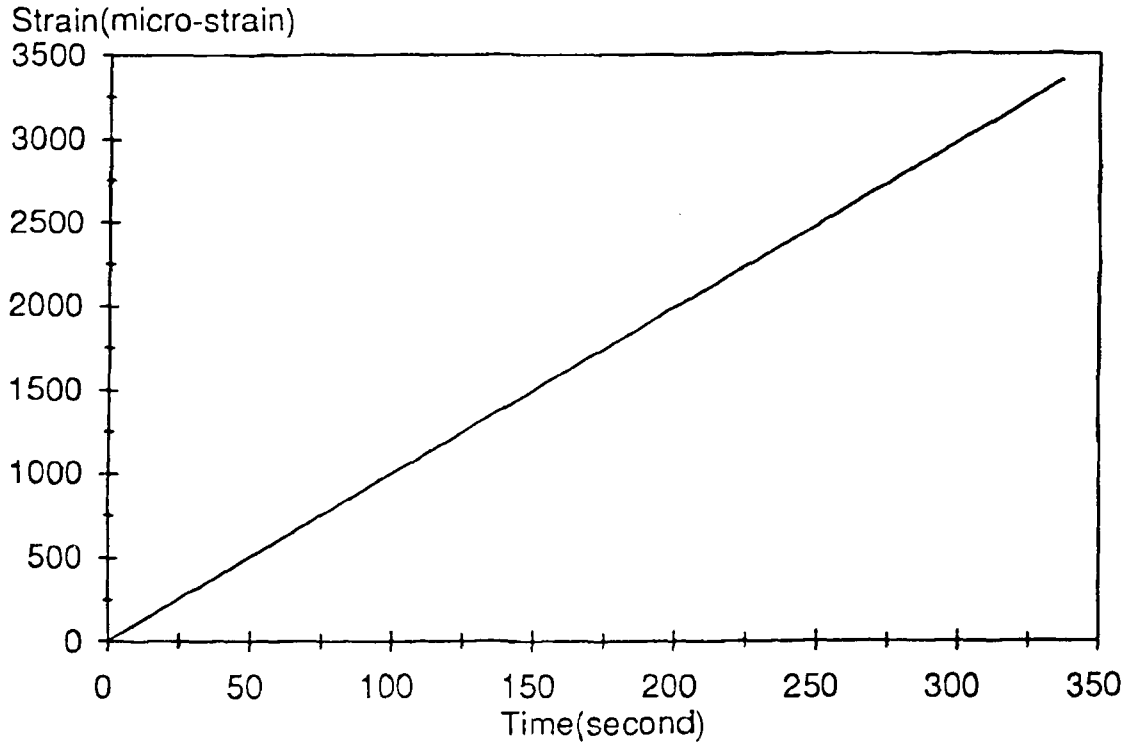

Figure 4.15 Strain-time response for HAPR08A.

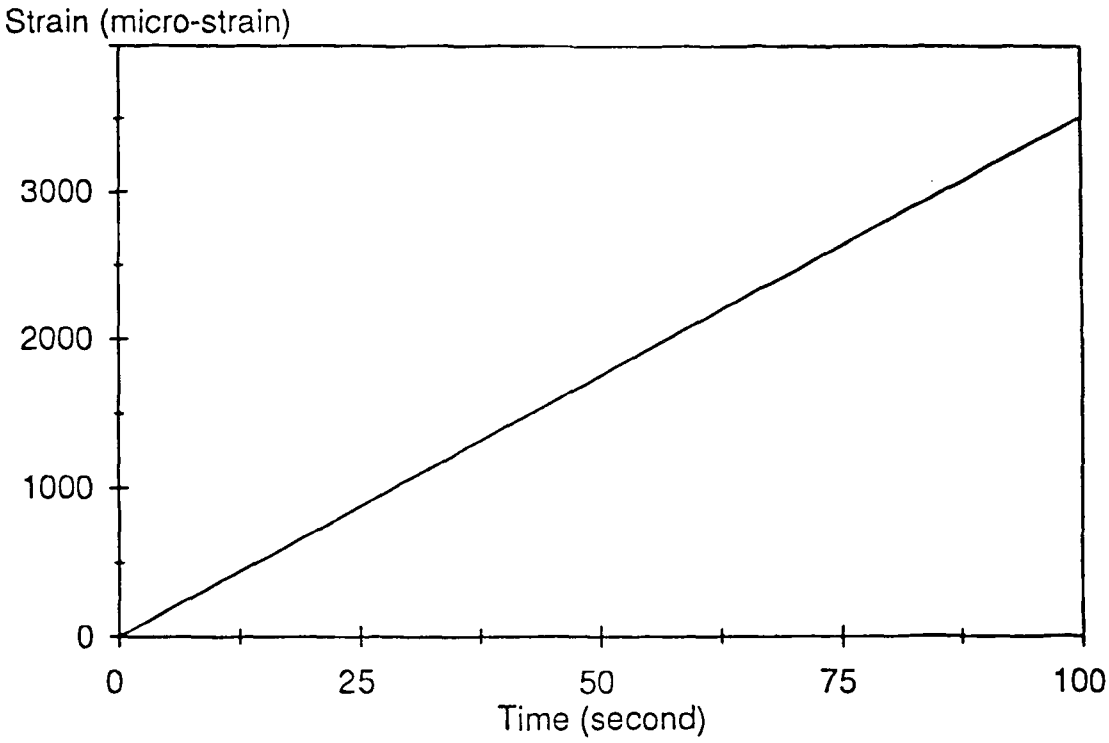

Figure 4.16 Strain-time response for HAPR12A.

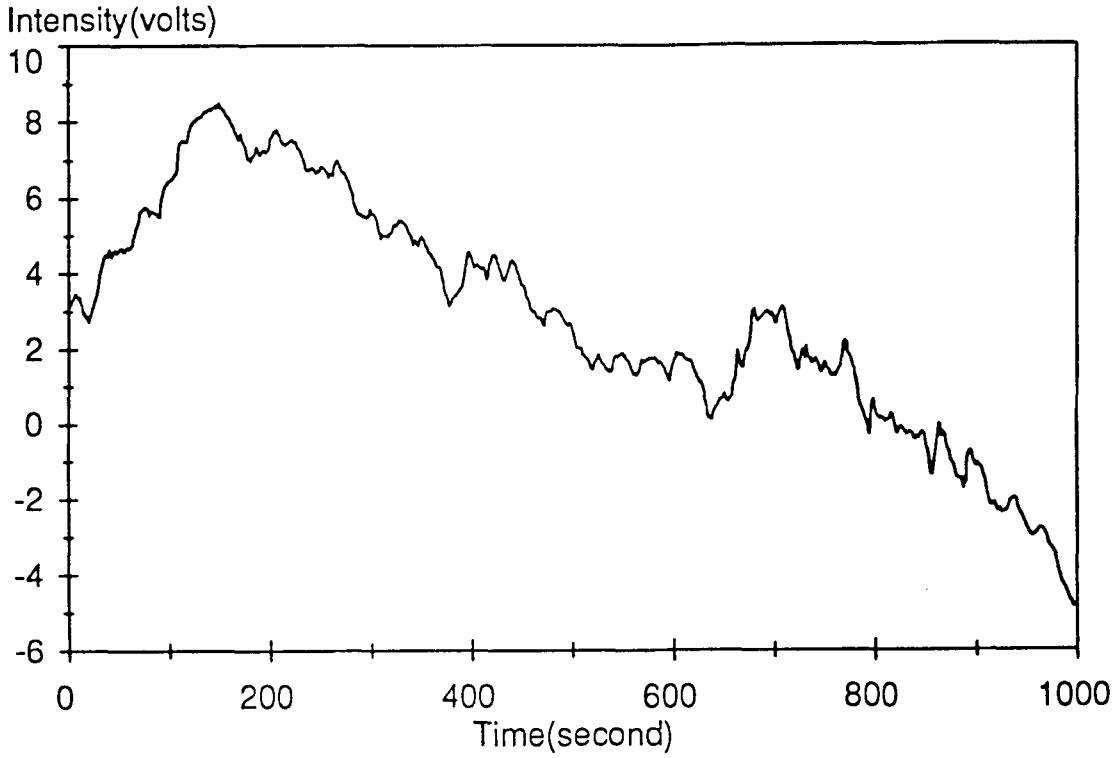

Figure 4.17 Intensity-time response for HMAR25A.

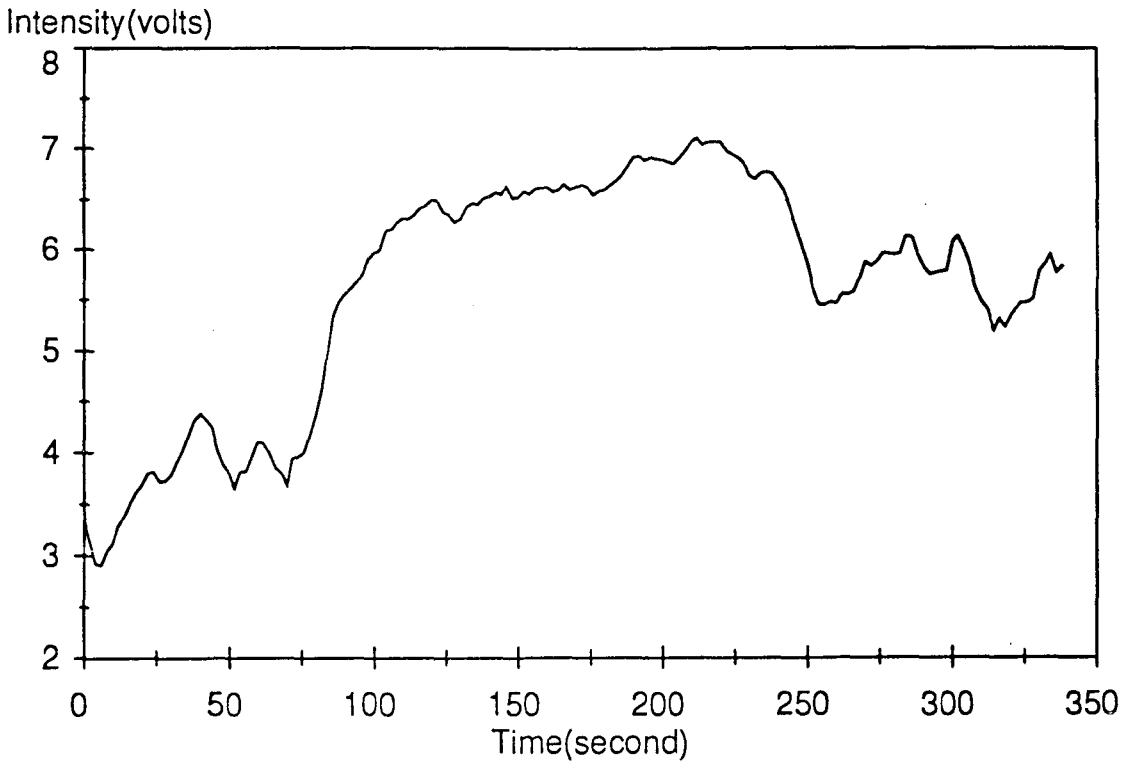

Figure 4.18 Intensity-time response for HMAR25B.

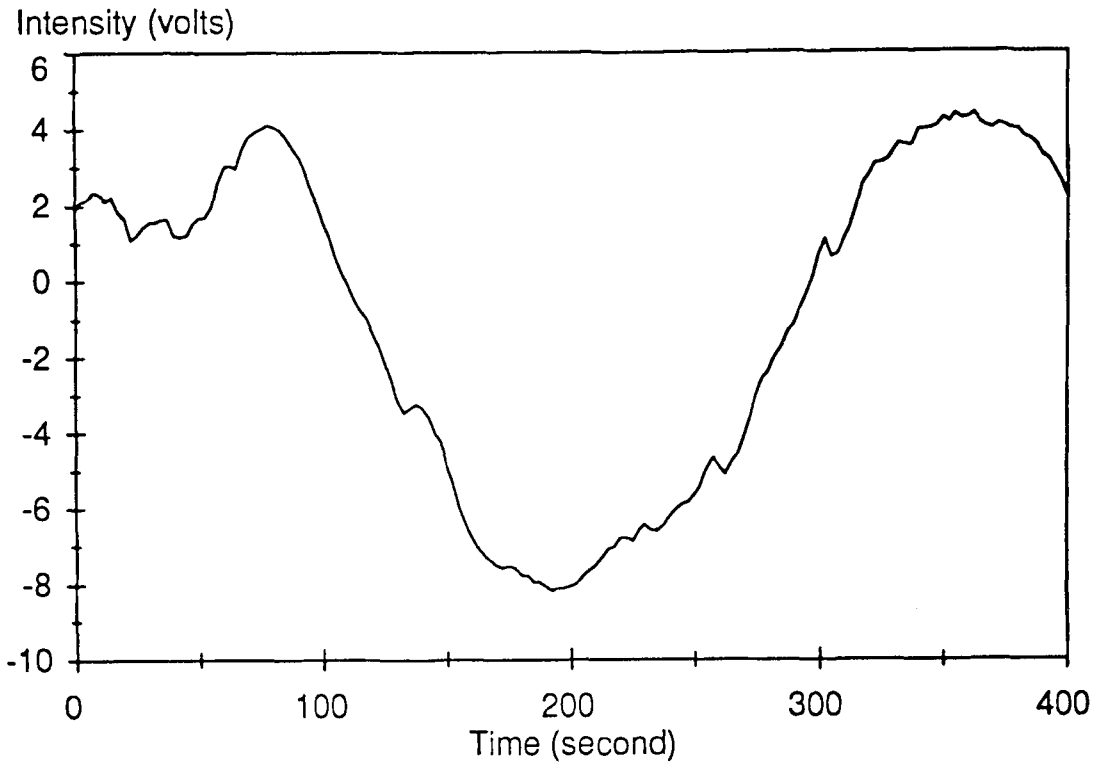

Figure 4.19 Intensity-time response for HMAR26A.

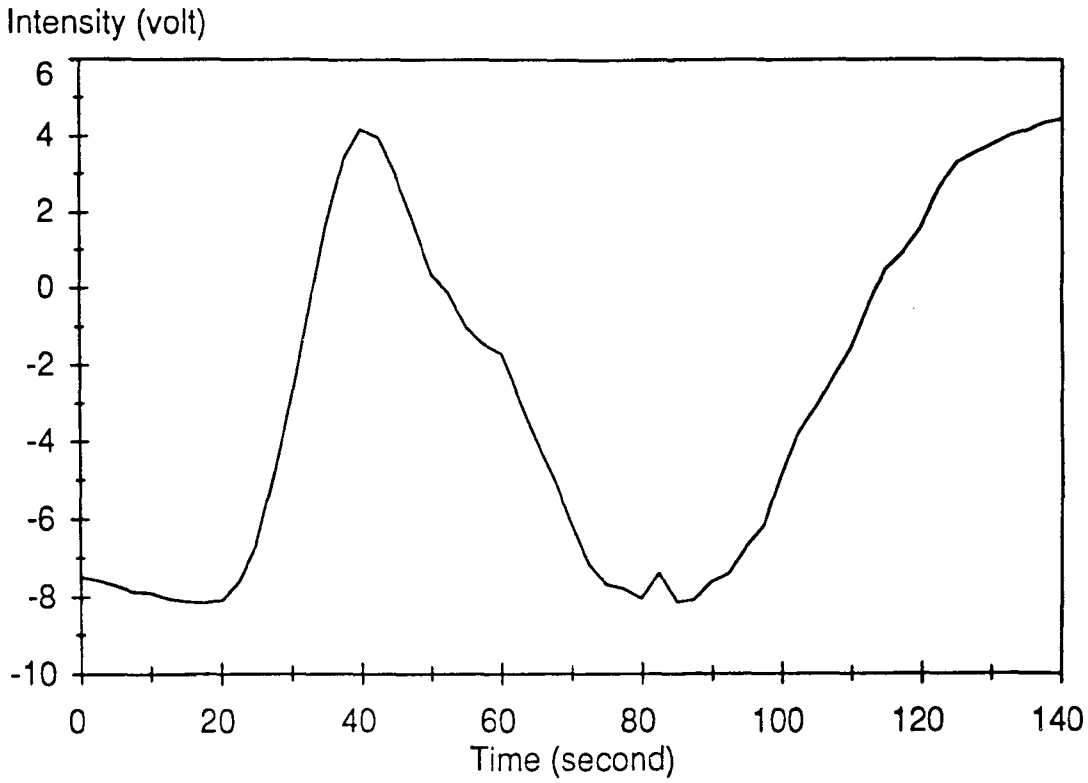

Figure 4.20 Intensity-time response for HMAR26B.

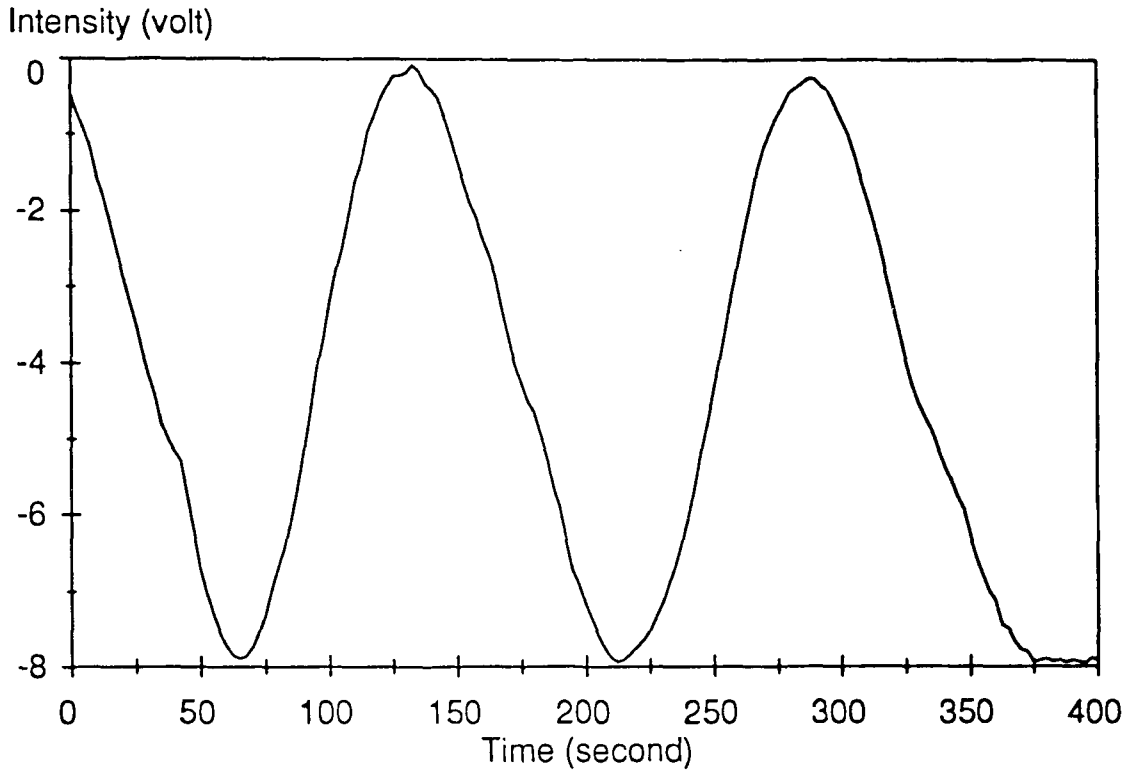

Figure 4.21 Intensity-time response for HAPR01A.

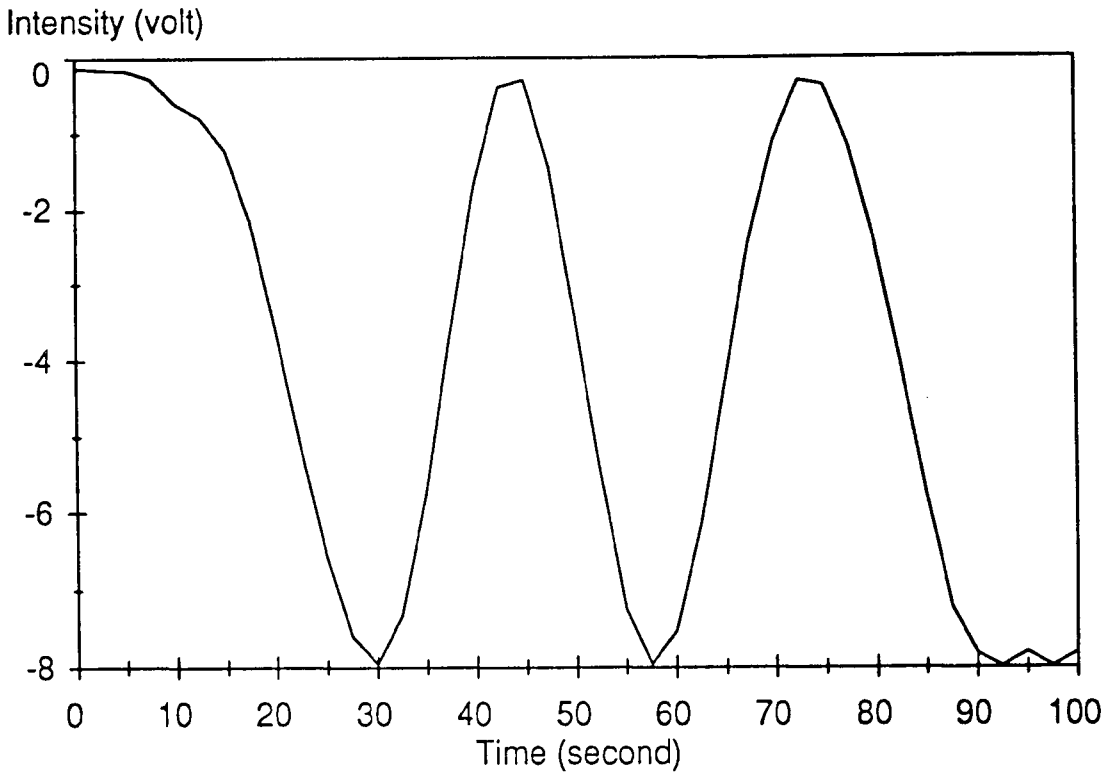

Figure 4.22 Intensity-time response for HAPR01B.

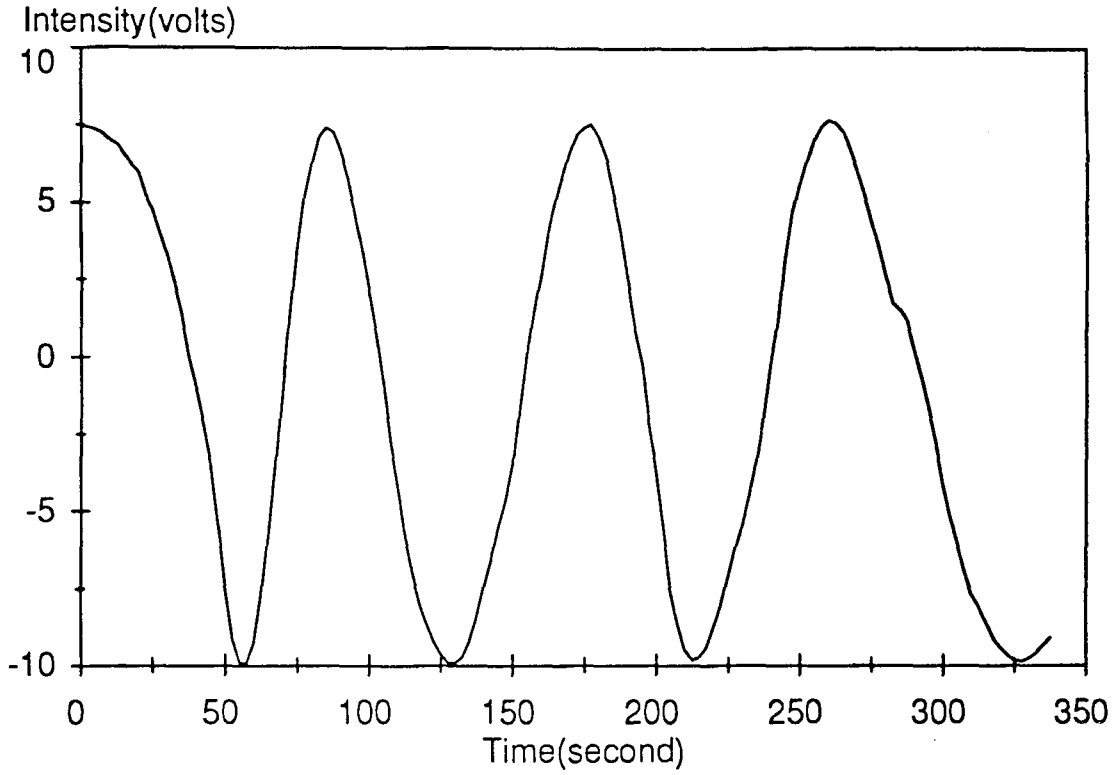

Figure 4.23 Intensity-time response for HAPR08A

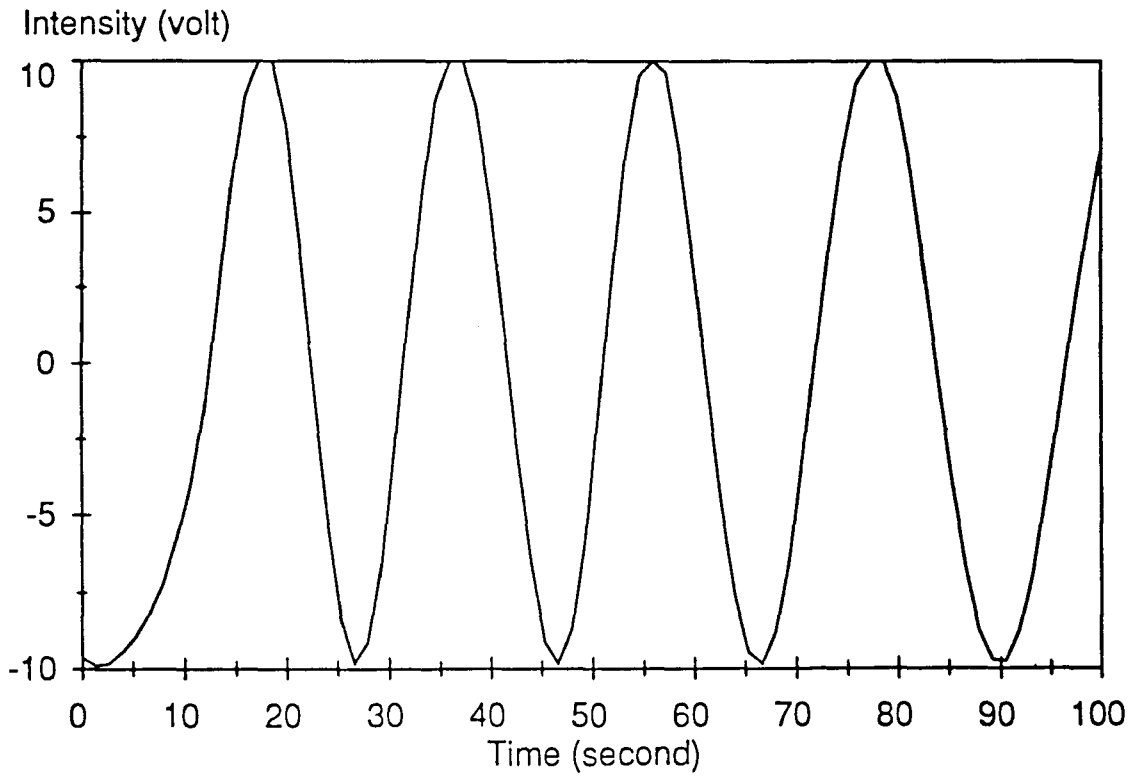

Figure 4.24 Intensity-time response for HAPR12A.

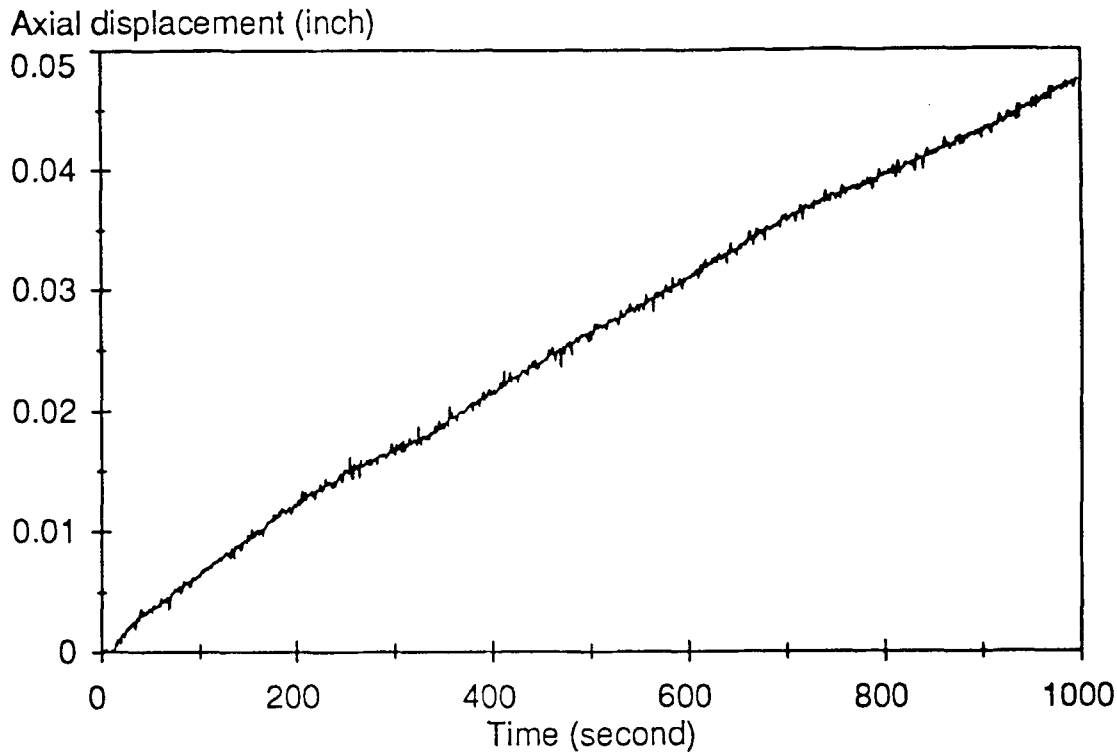

Figure 4.25 Axial displacement-time response for HMAR25A.

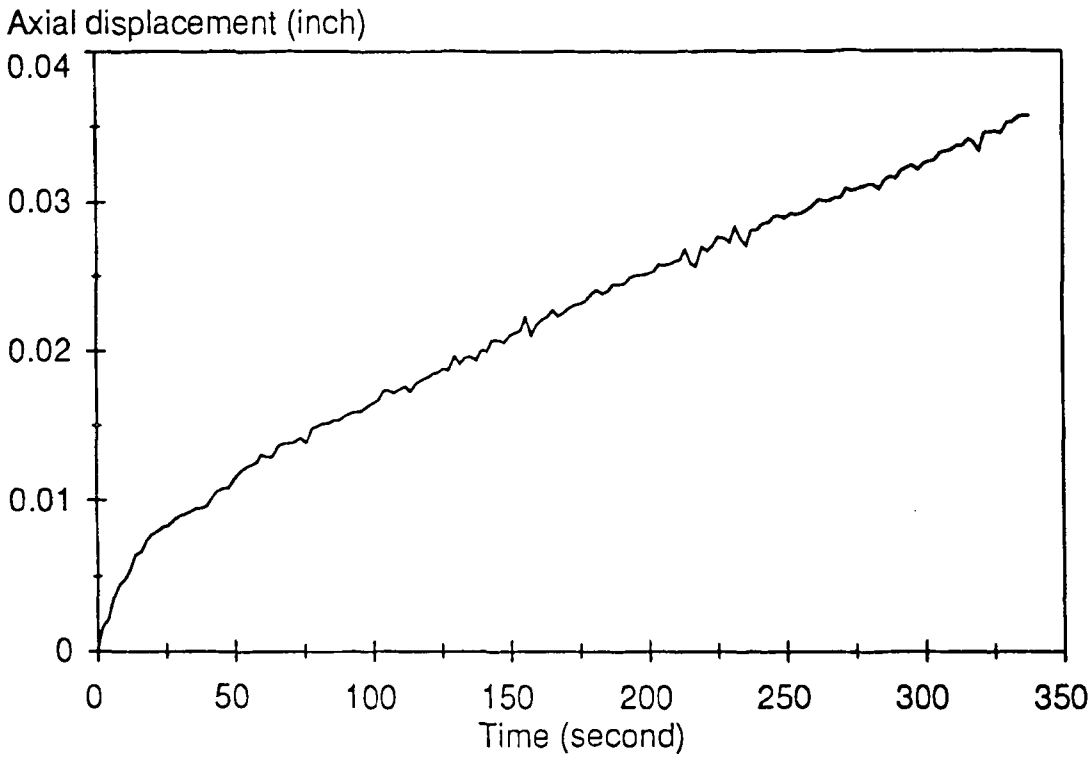

Figure 4.26 Axial displacement-time response for HMAR25B.

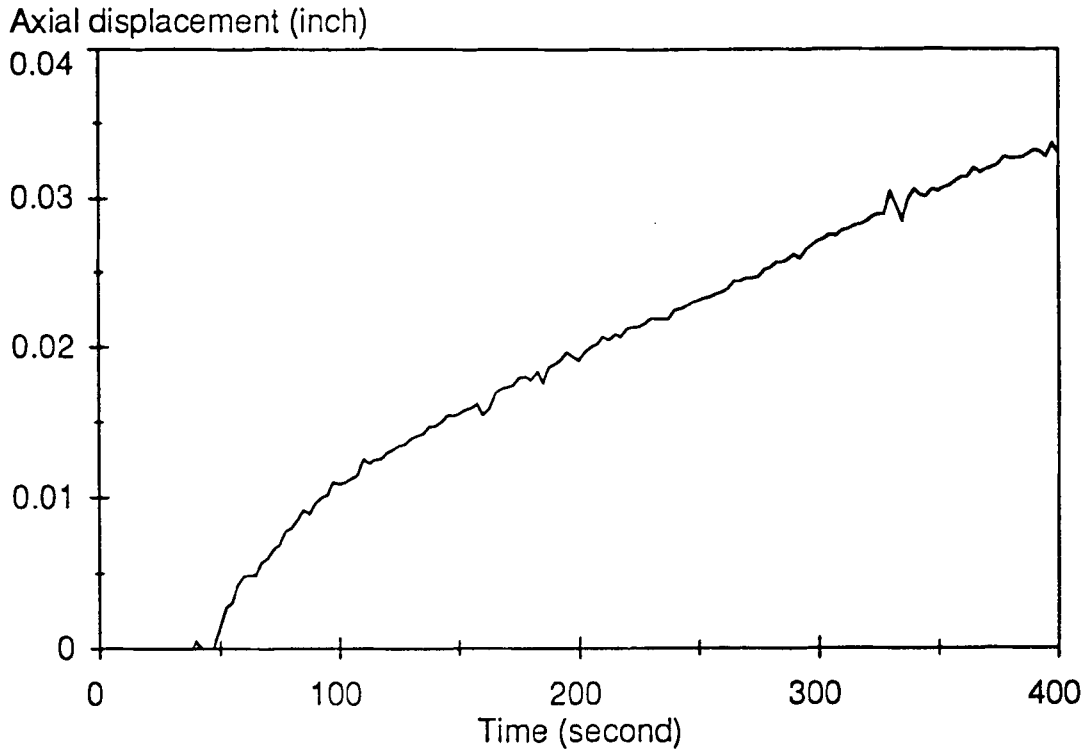

Figure 4.27 Axial displacement-time response for HMAR26A.

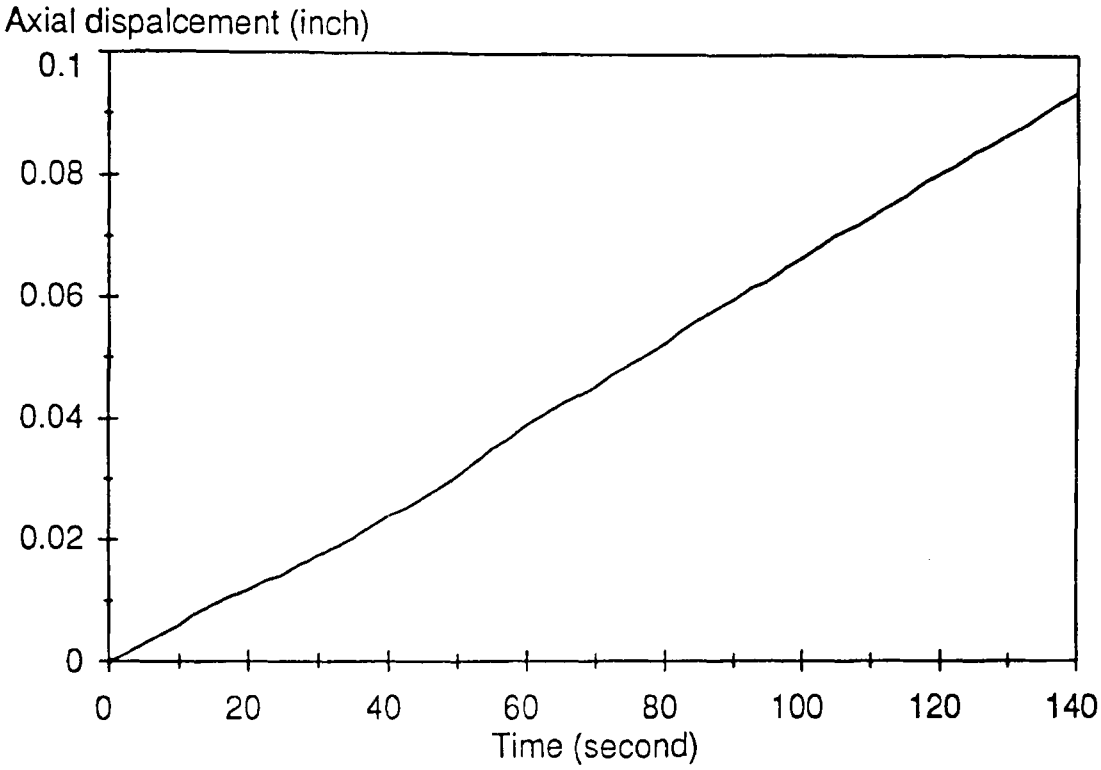

Figure 4.28 Axial displacement-time response for HMAR26B.

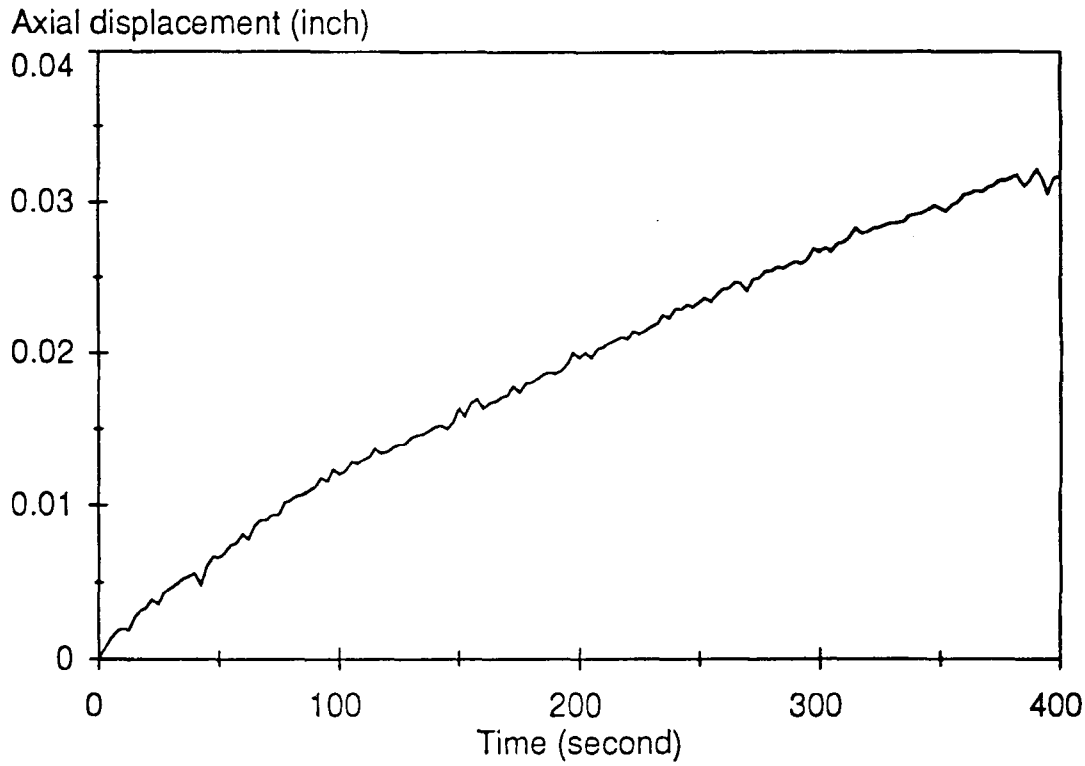

Figure 4.29 Axial displacement-time response for HAPR01A.

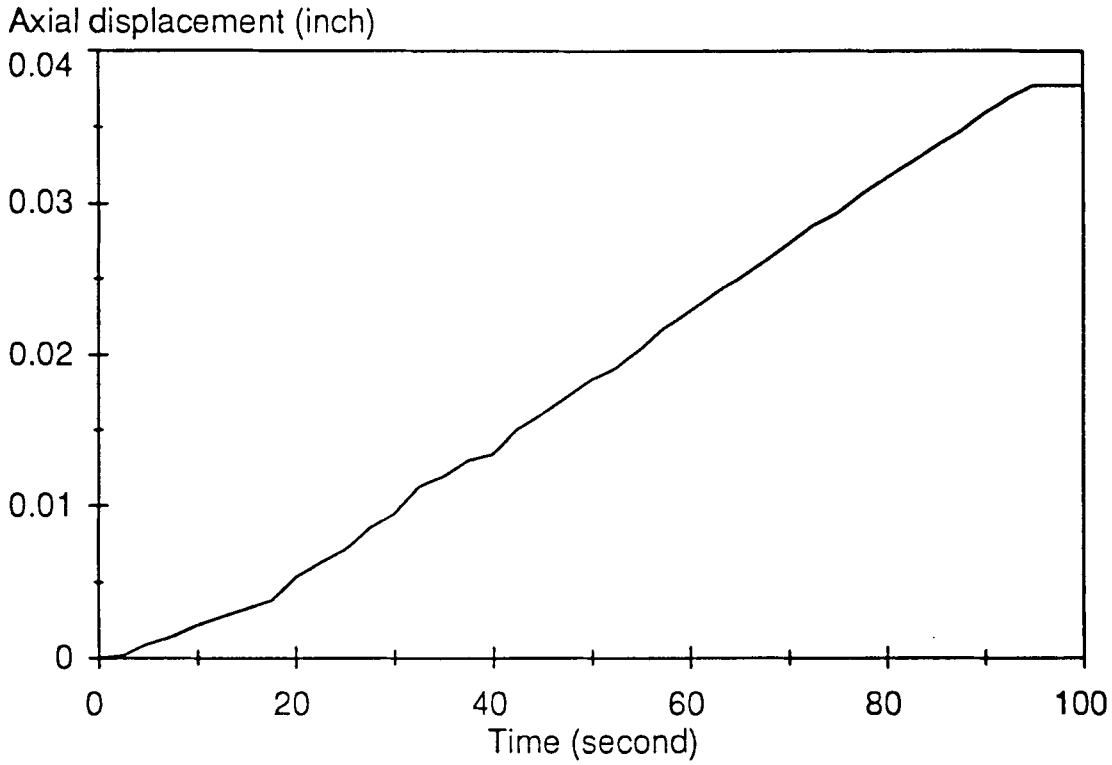

Figure 4.30 Axial displacement-time response for HAPR01B.

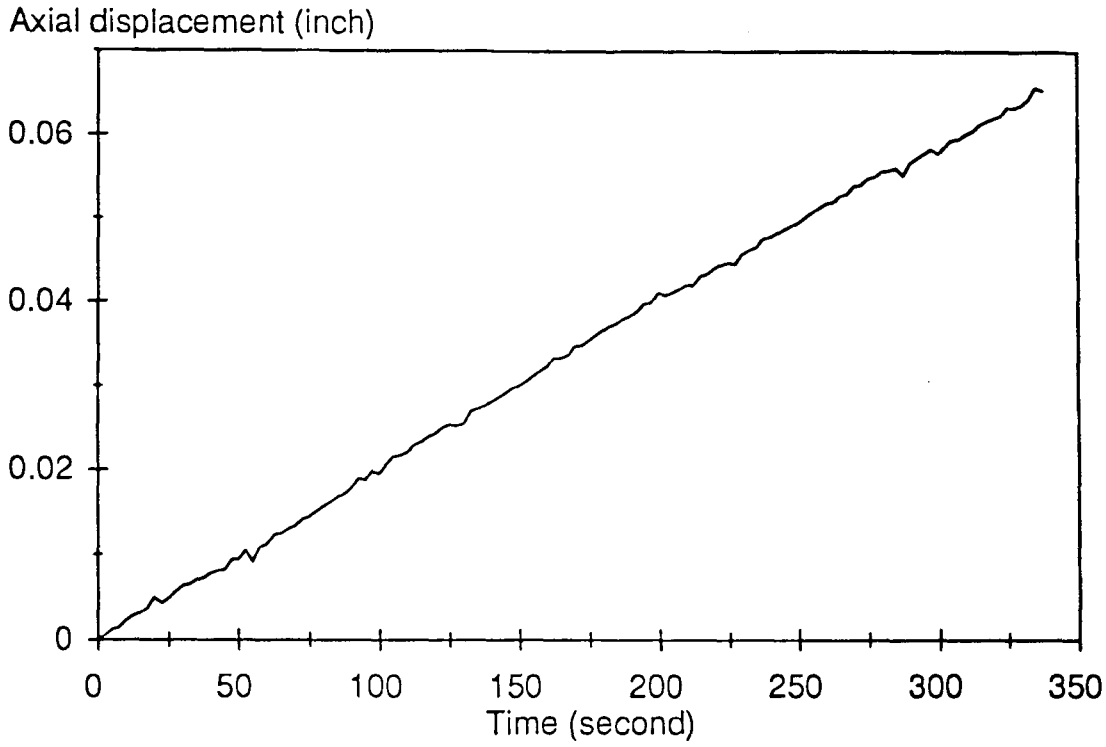

Figure 4.31 Axial displacement-time response for HAPR08A.

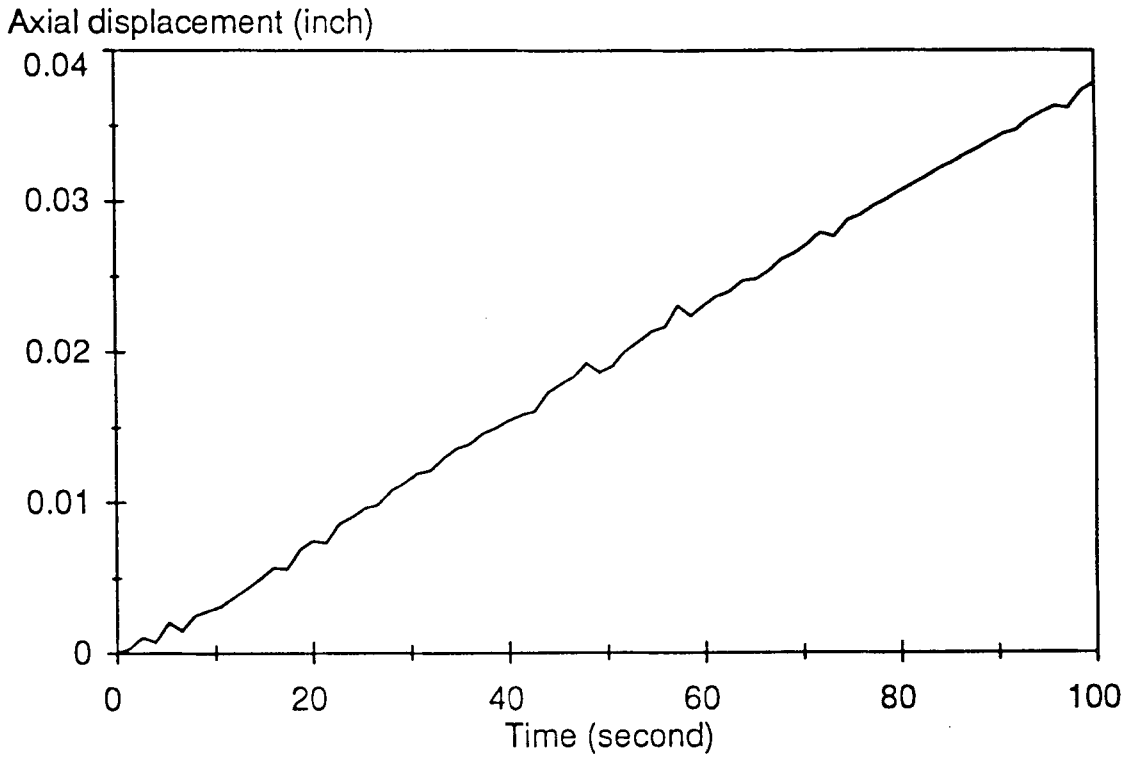

Figure 4.32 Axial displacement-time response for HAPR12A.

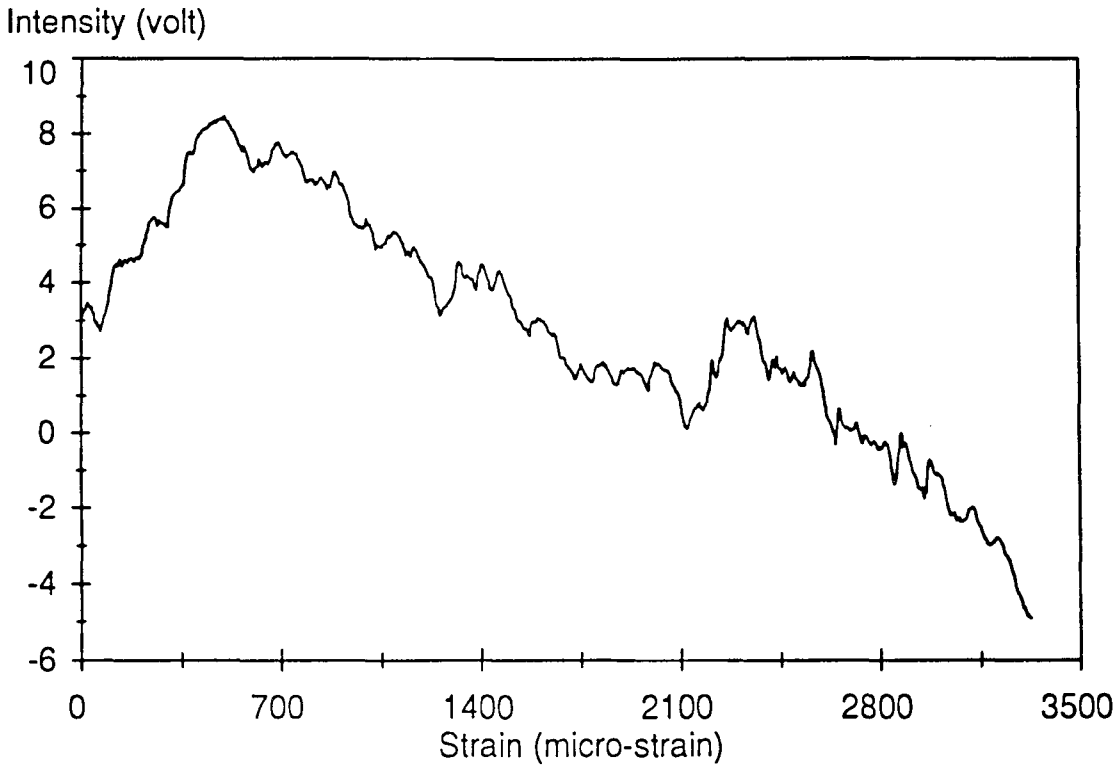

Figure 4.33 Intensity versus tensile strain for HMAR25A.

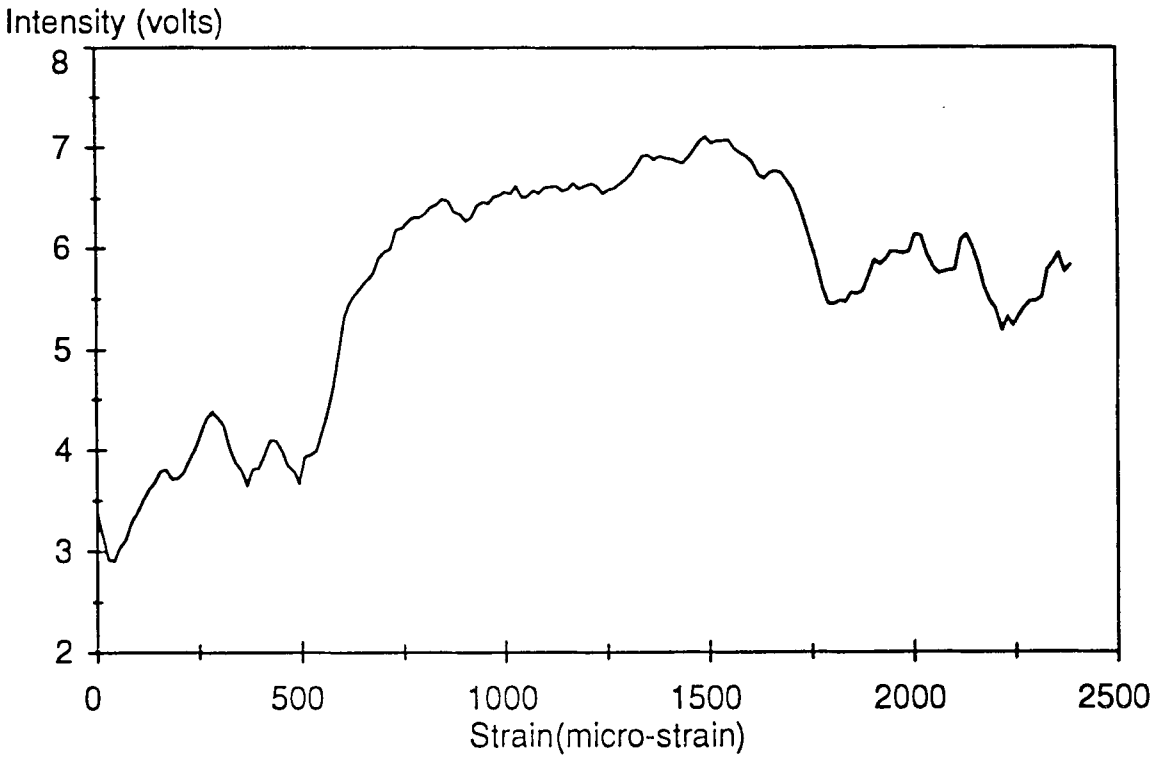

Figure 4.34 Intensity versus tensile strain for HMAR25B.

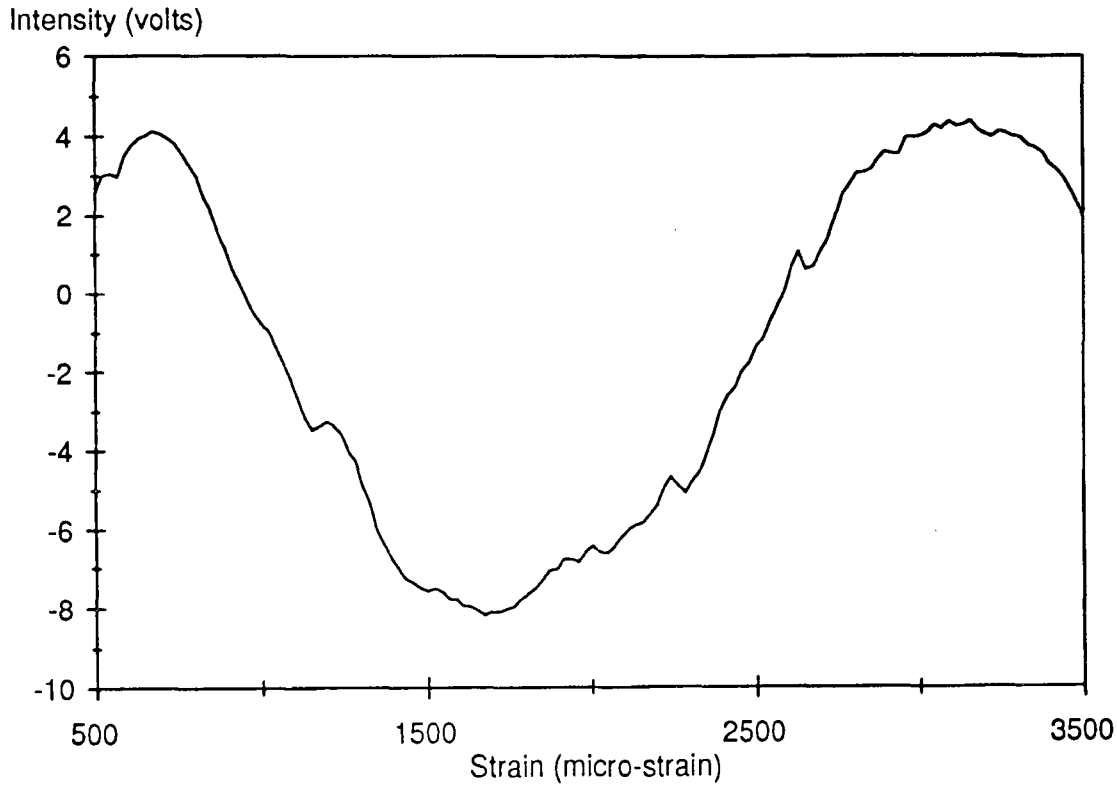

Figure 4.35 Intensity versus tensile strain for HMAR26A.

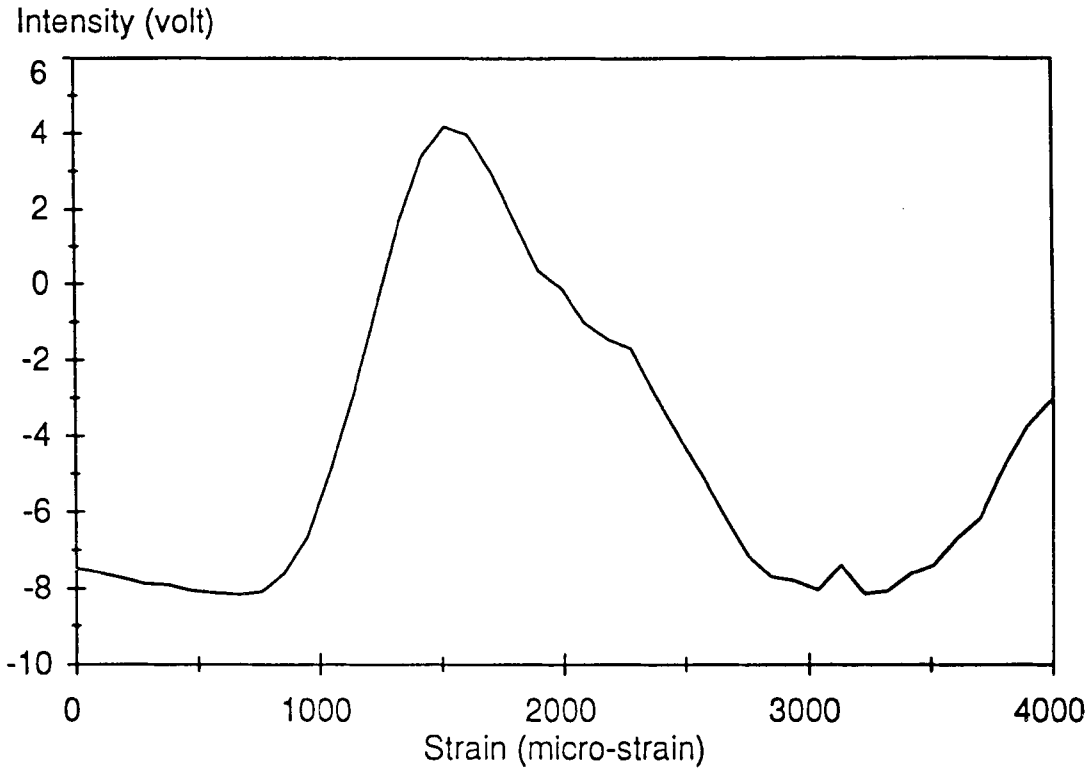

Figure 4.36 Intensity versus tensile strain for HMAR26B.

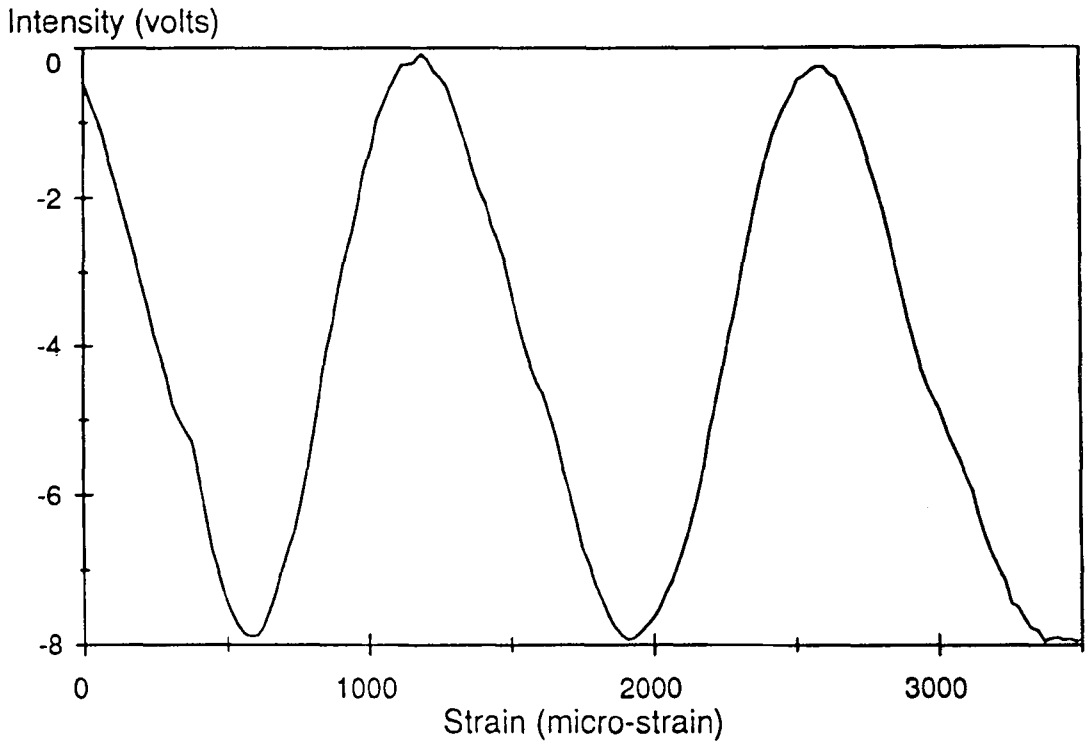

Figure 4.37 Intensity versus tensile strain for HAPR01A.

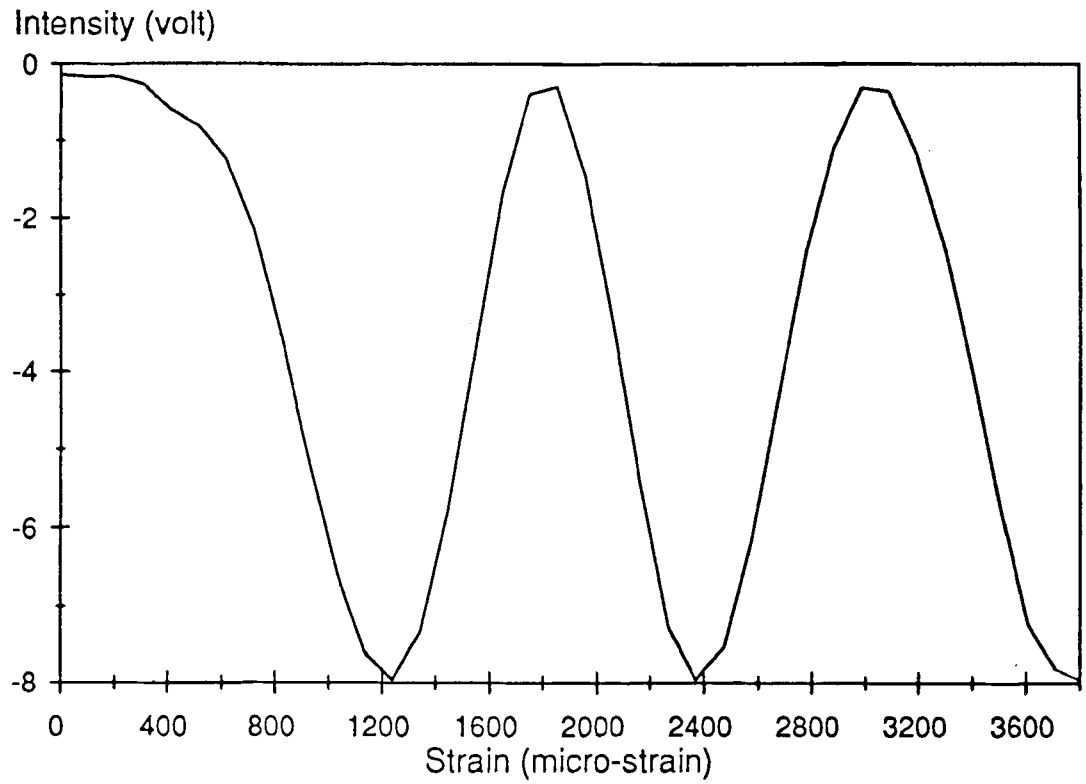

Figure 4.38 Intensity versus tensile strain for HAPR01B.

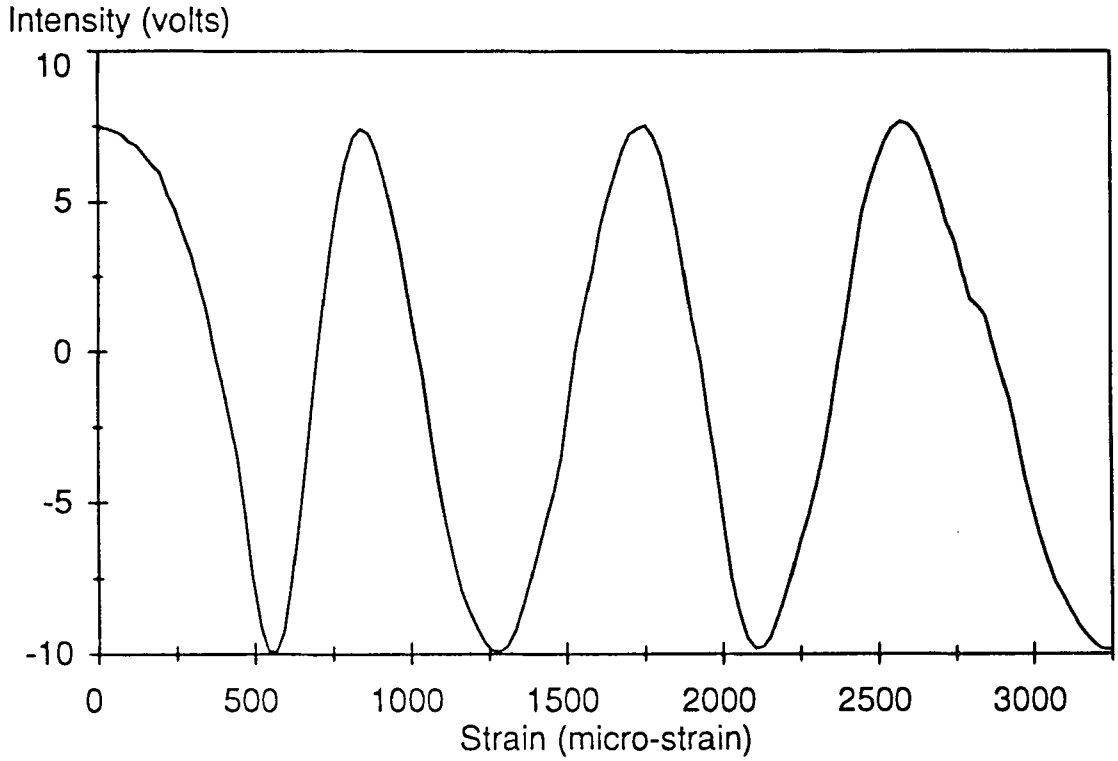

Figure 4.39 Intensity versus tensile strain for HAPR08A.

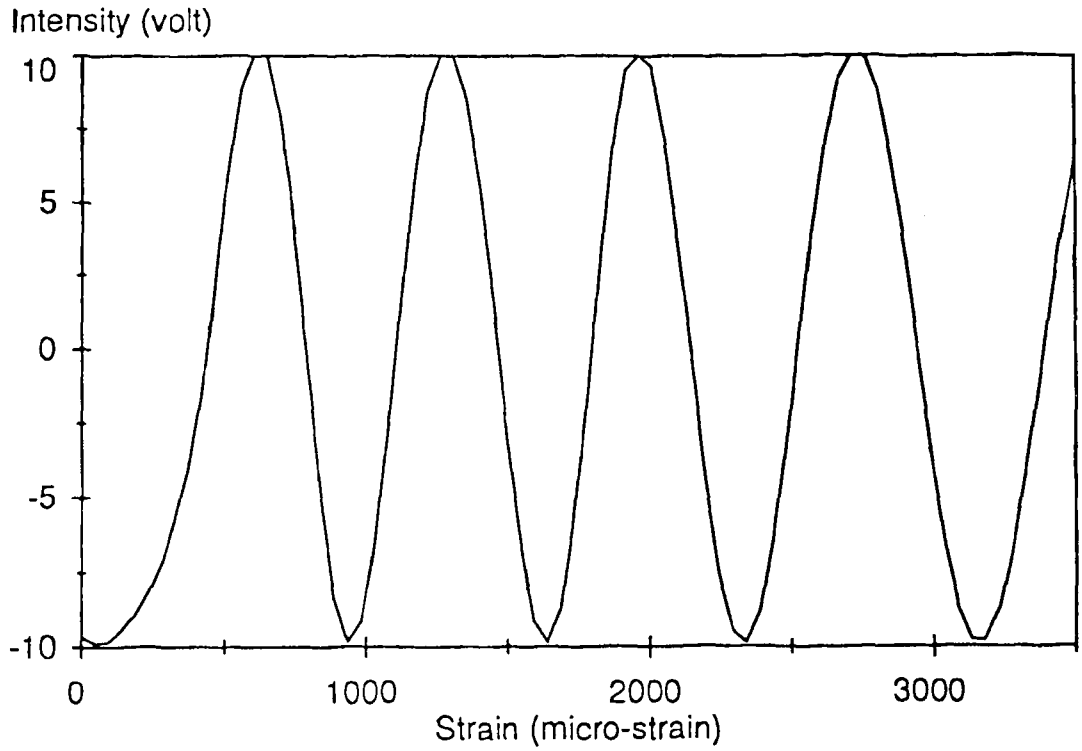

Figure 4.40 Intensity versus tensile strain forHAPR12A.

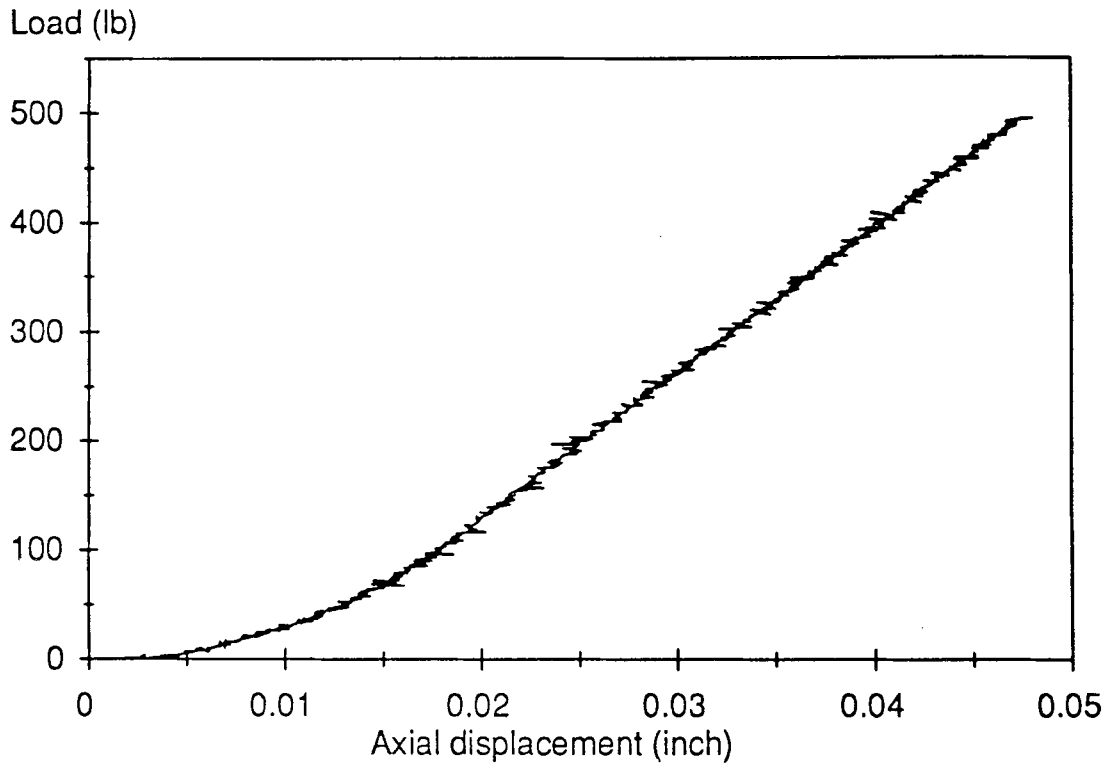

Figure 4.41 Load-axial displacement curve for HMAR25A.

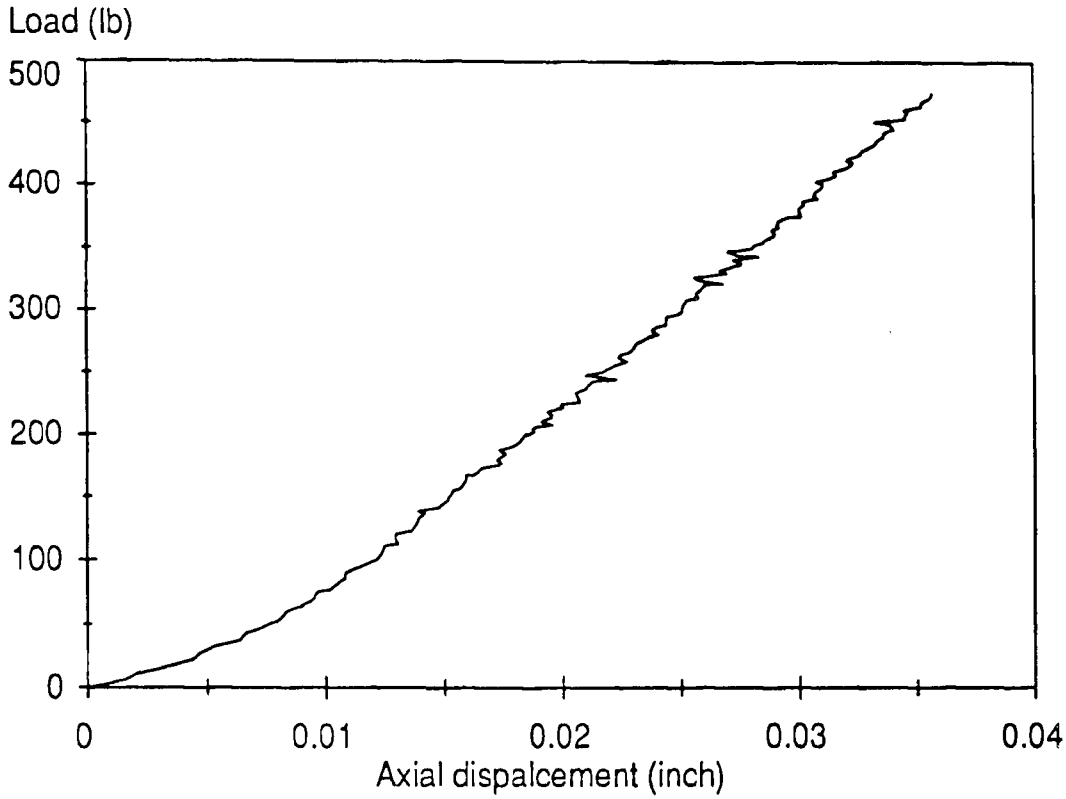

Figure 4.42 Load-axial displacement curve for HMAR25B.

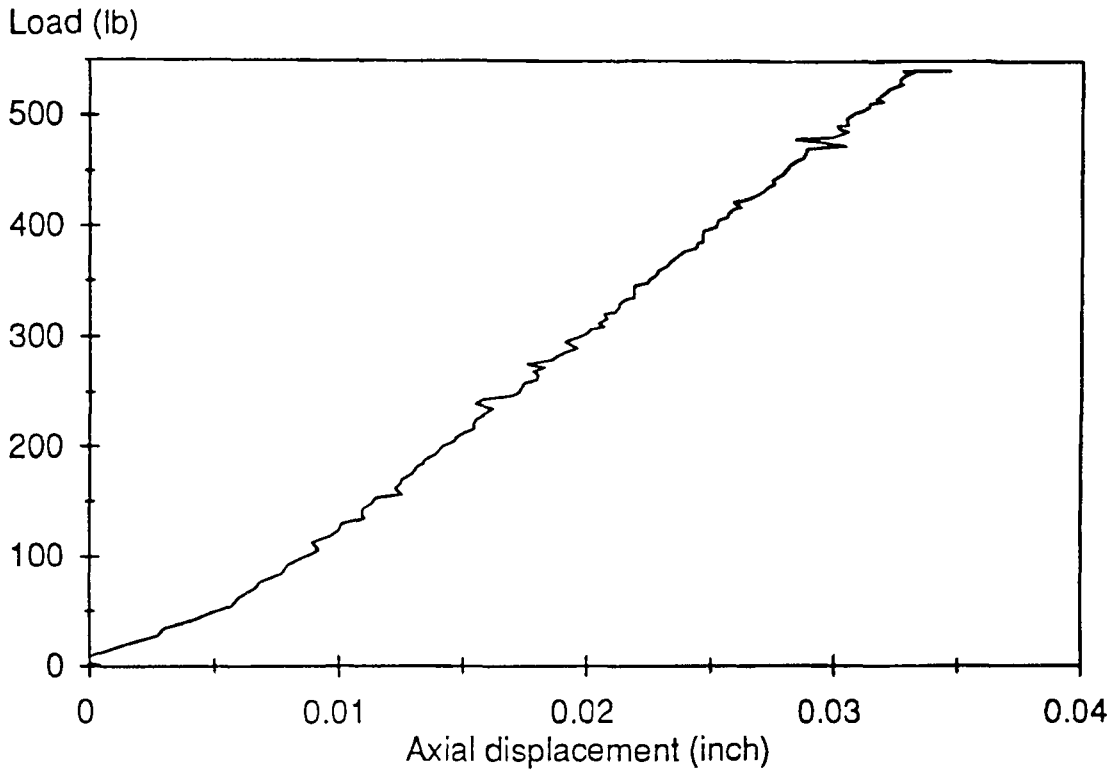

Figure 4.43 Load-axial displacement curve for HMAR26A.

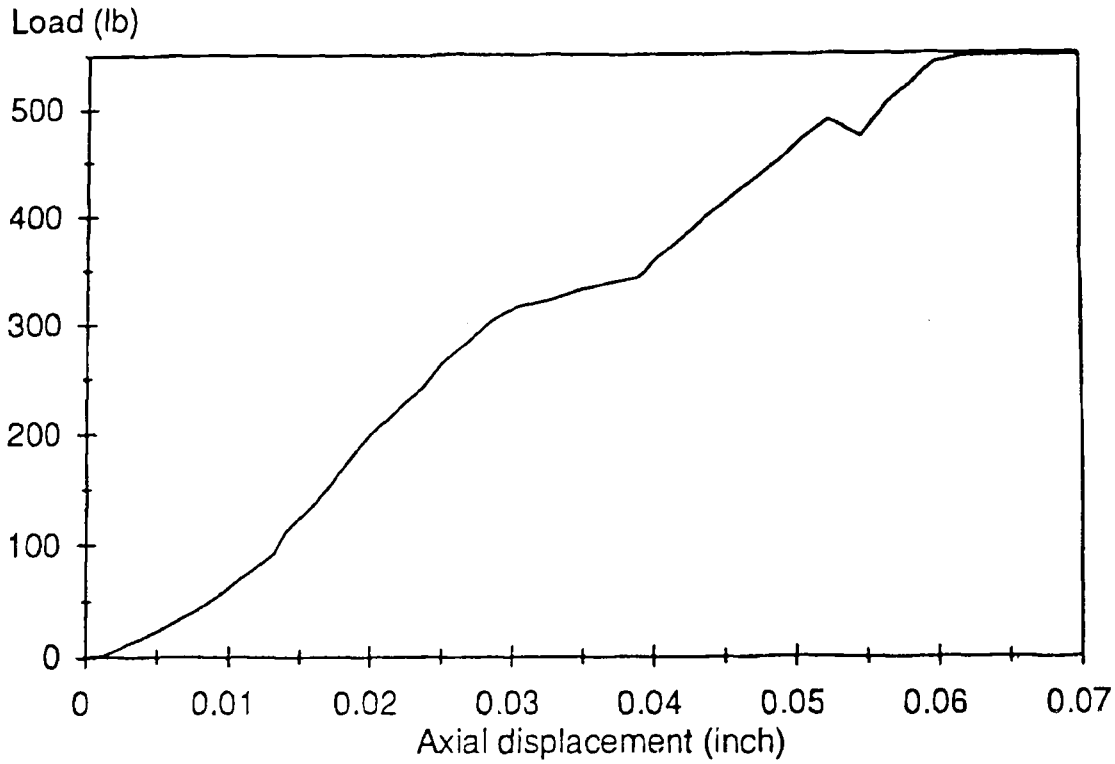

Figure 4.44 Load-axial displacement curve for HMAR26B.

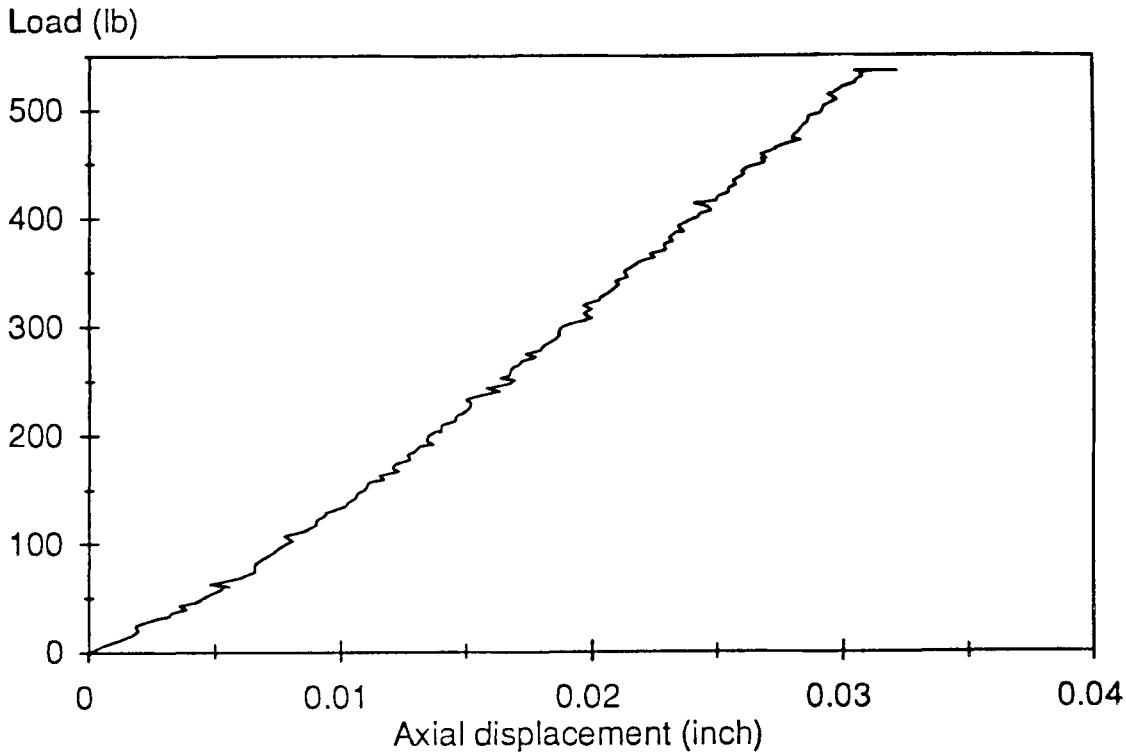

Figure 4.45 Load-axial displacement curve for HAPR01A.

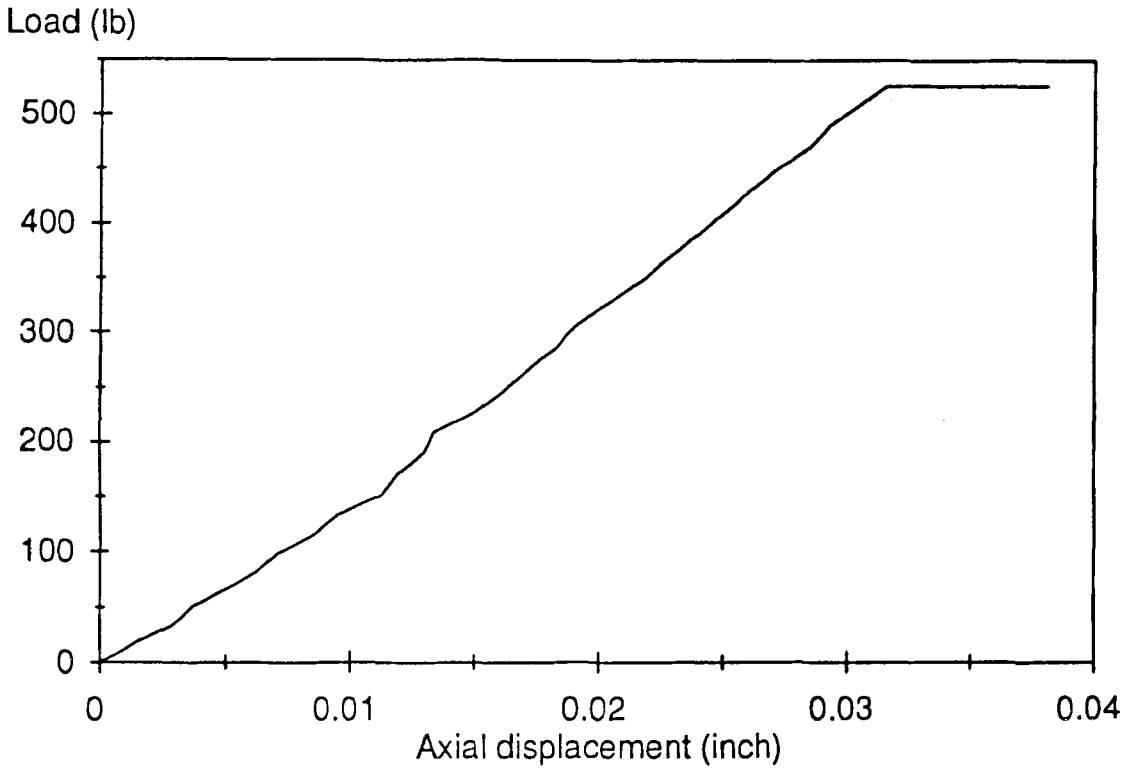

Figure 4.46 Load-axial displacement curve for HAPR01B.

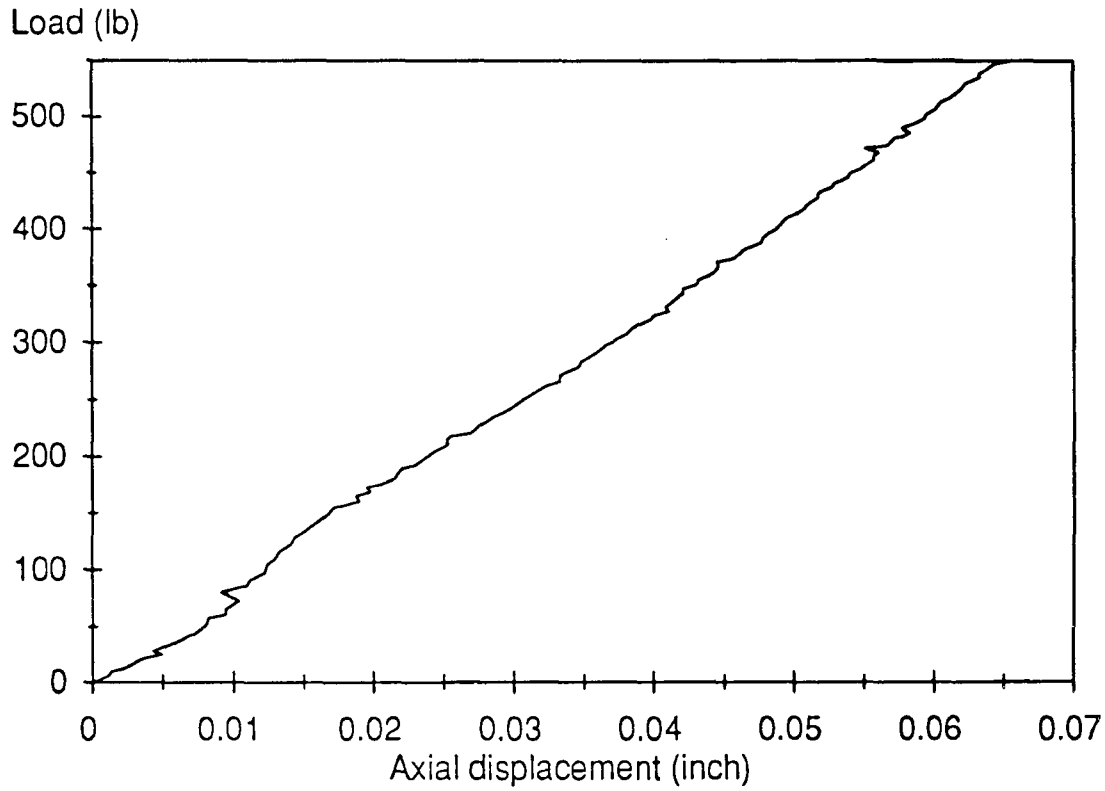

Figure 4.47 Load-axial displacement curve for HAPR08A.

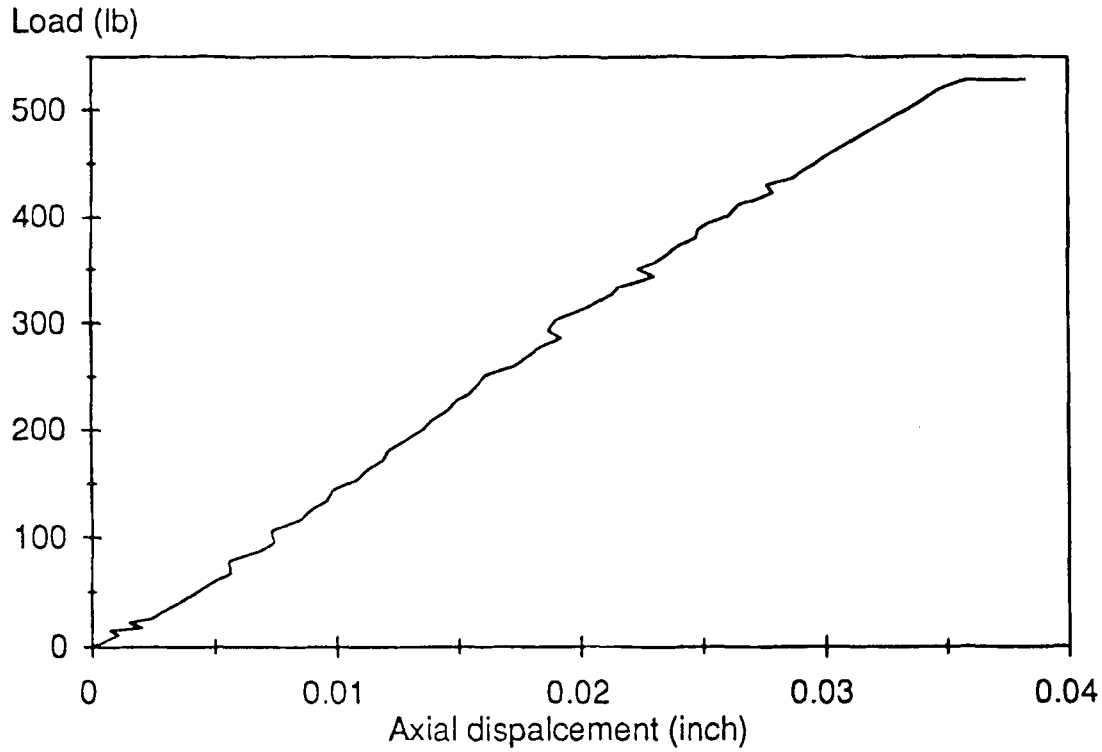

Figure 4.48 Load-axial displacement curve for HAPR12A.

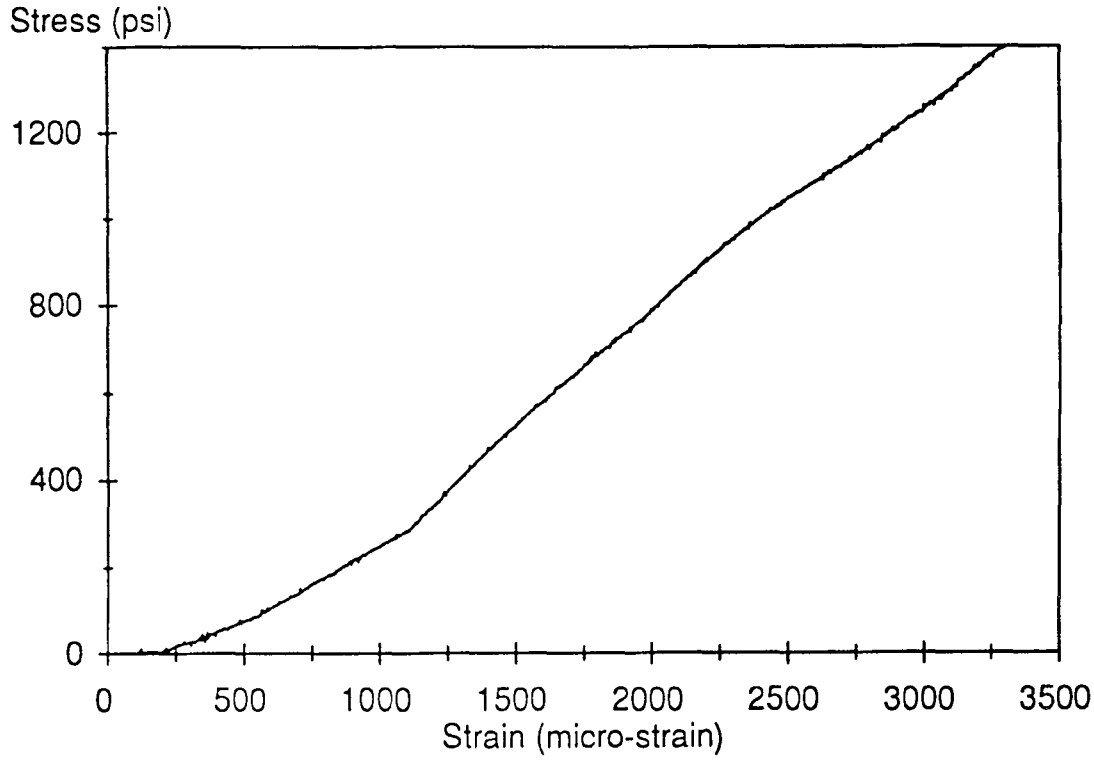

Figure 4.49 Stress-strain curve for HMAR25A.

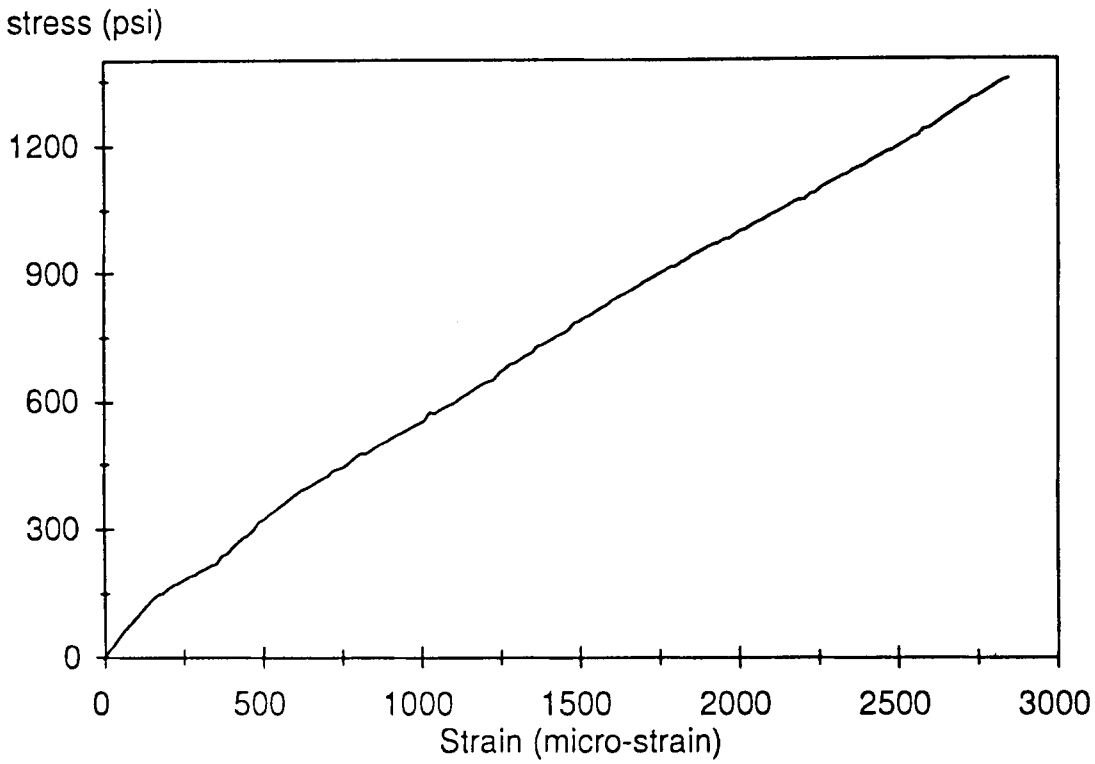

Figure 4.50 Stress-strain curve for HMAR25B.

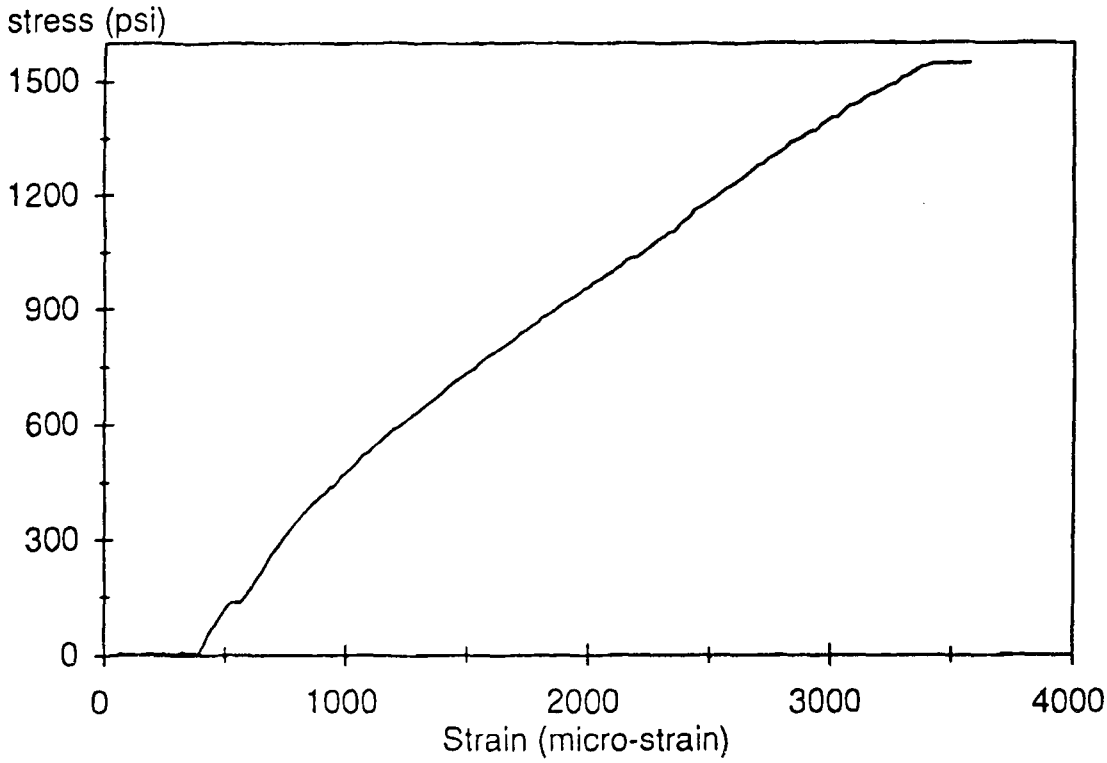

Figure 4.51 Stress-strain curve for HMAR26A.

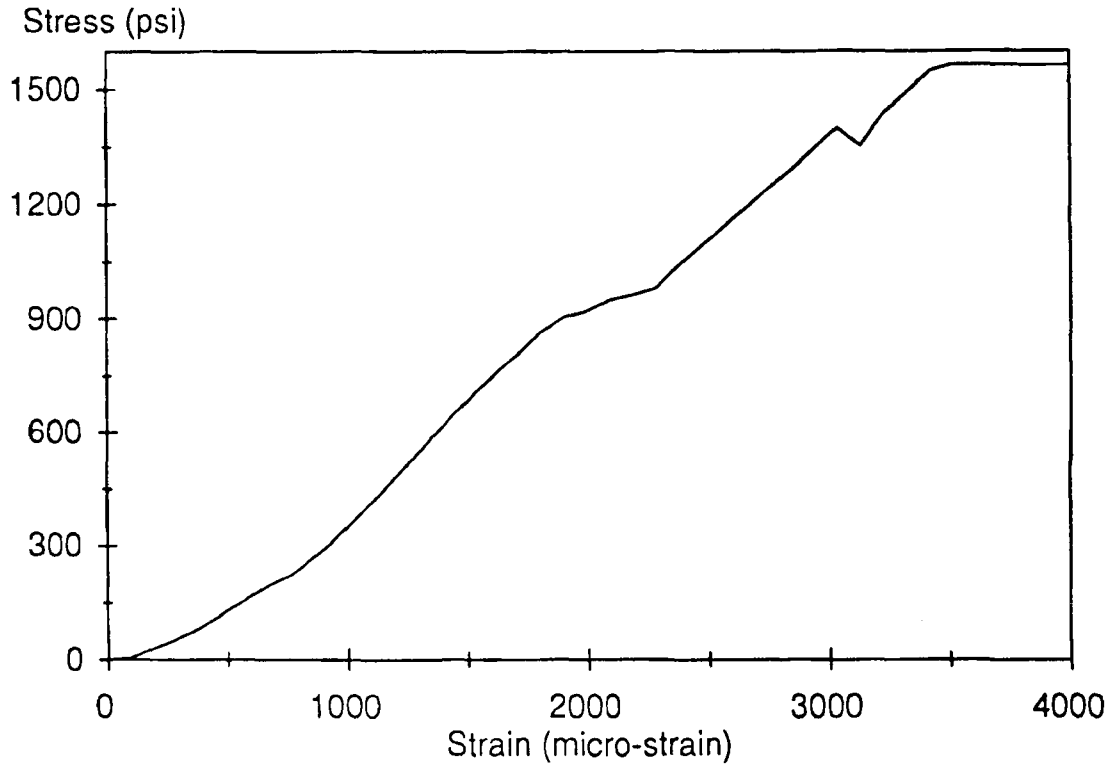

Figure 4.52 Stress-strain curve for HMAR26B.

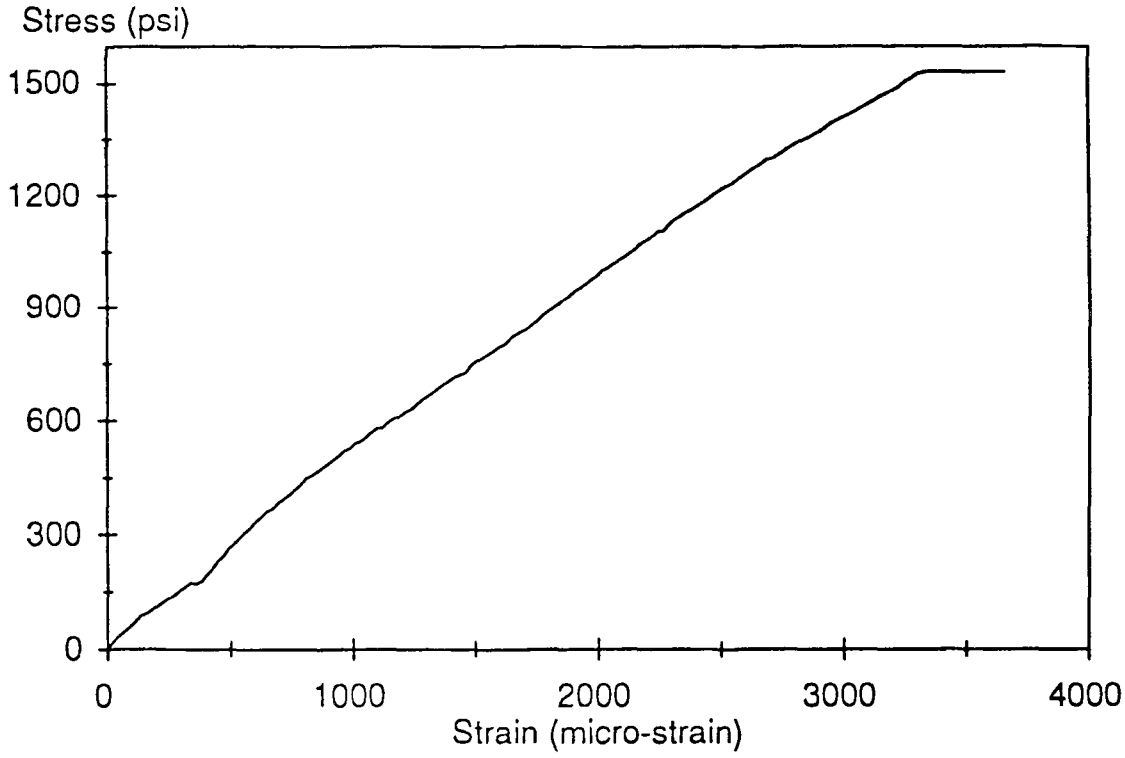

Figure 4.53 Stress-strain curve for HAPR01A.

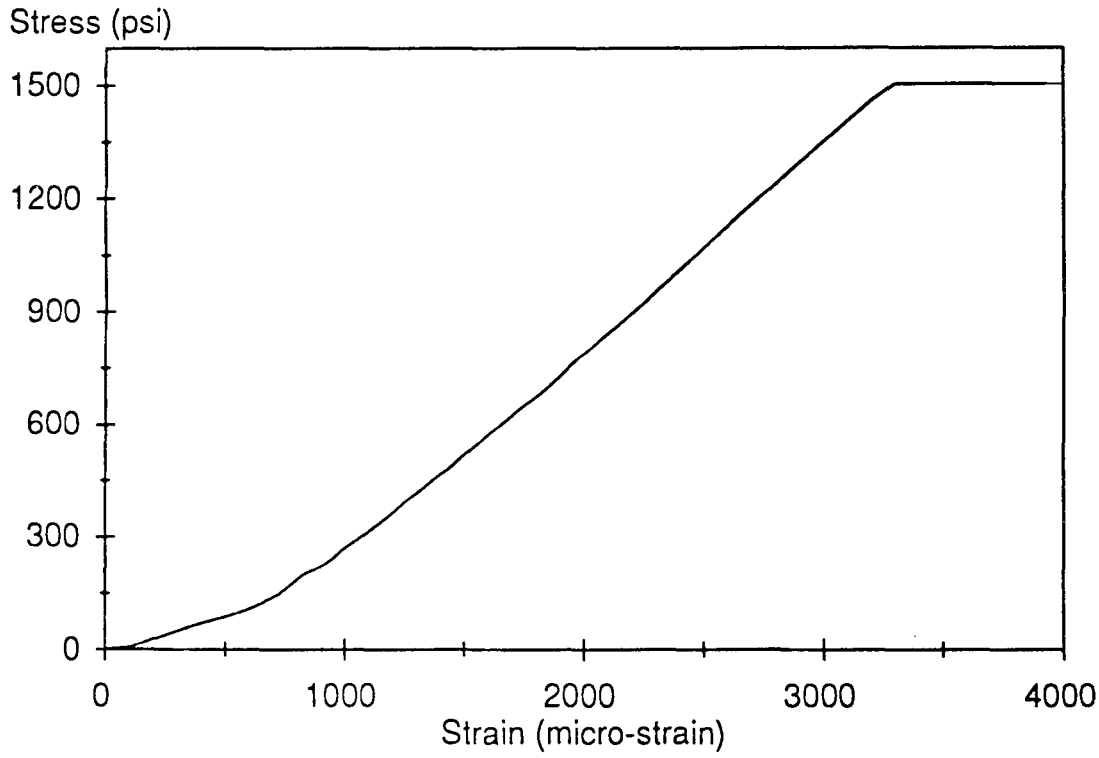

Figure 4.54 Stress-strain curve for HAPR01B.

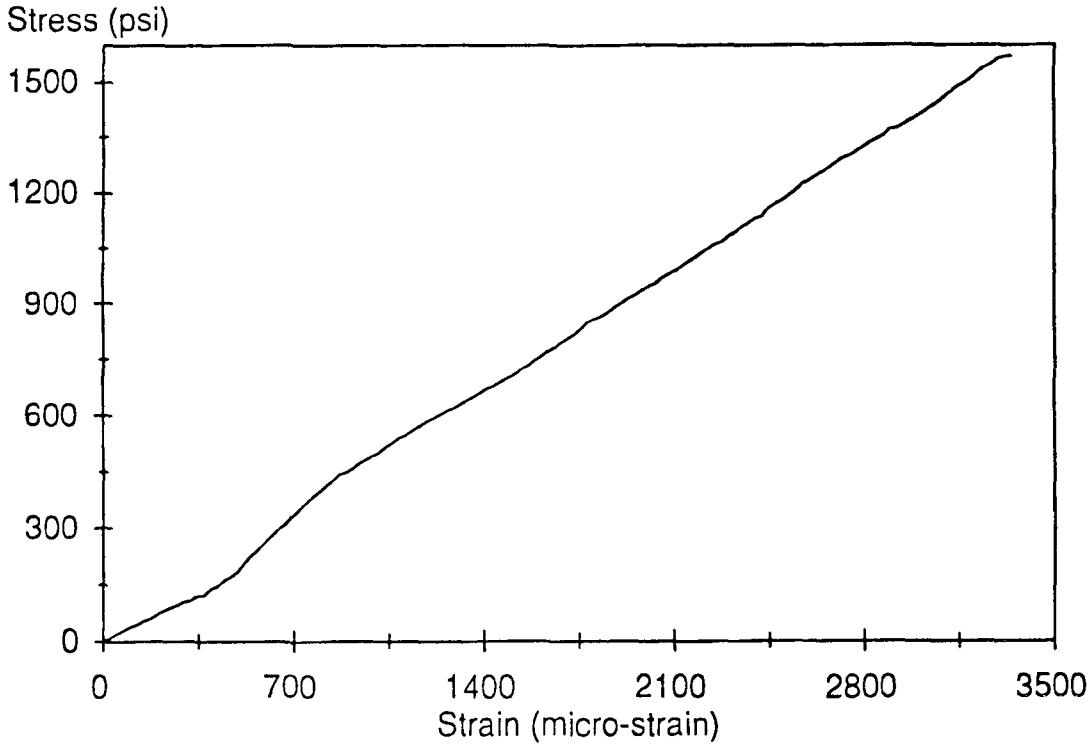

Figure 4.55 Stress-strain curve for HAPR08A.

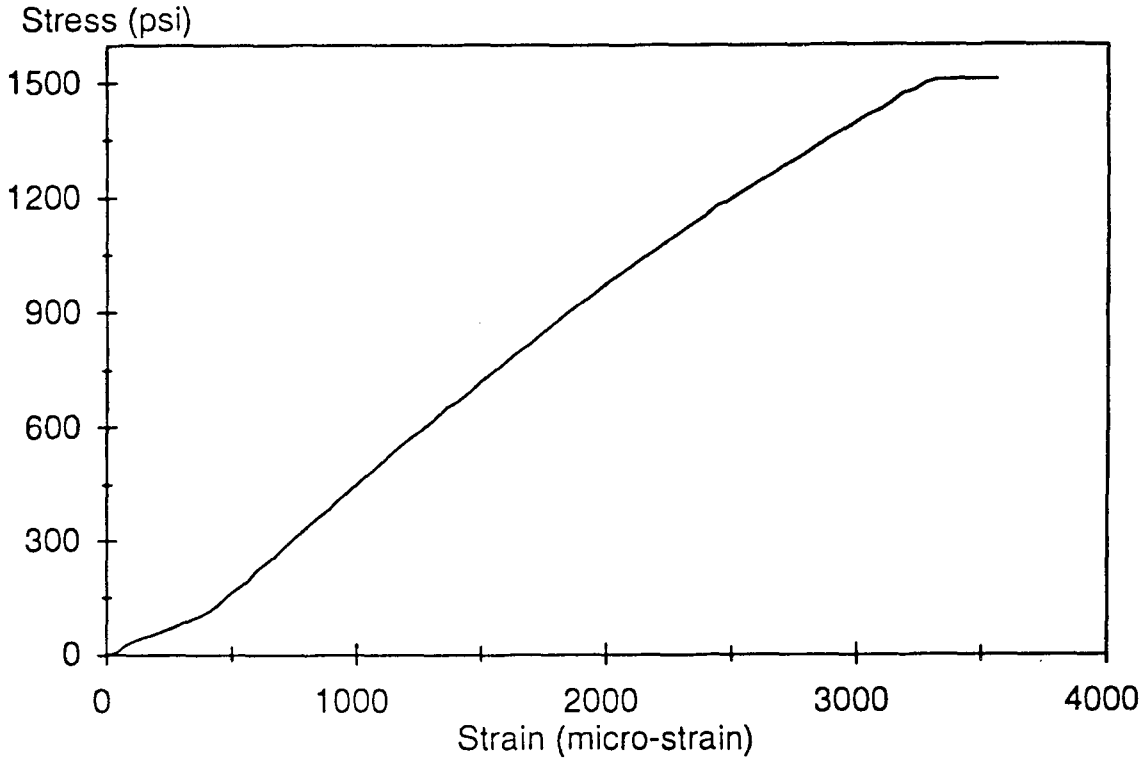

Figure 4.56 Stress-strain curve for HAPR12A.

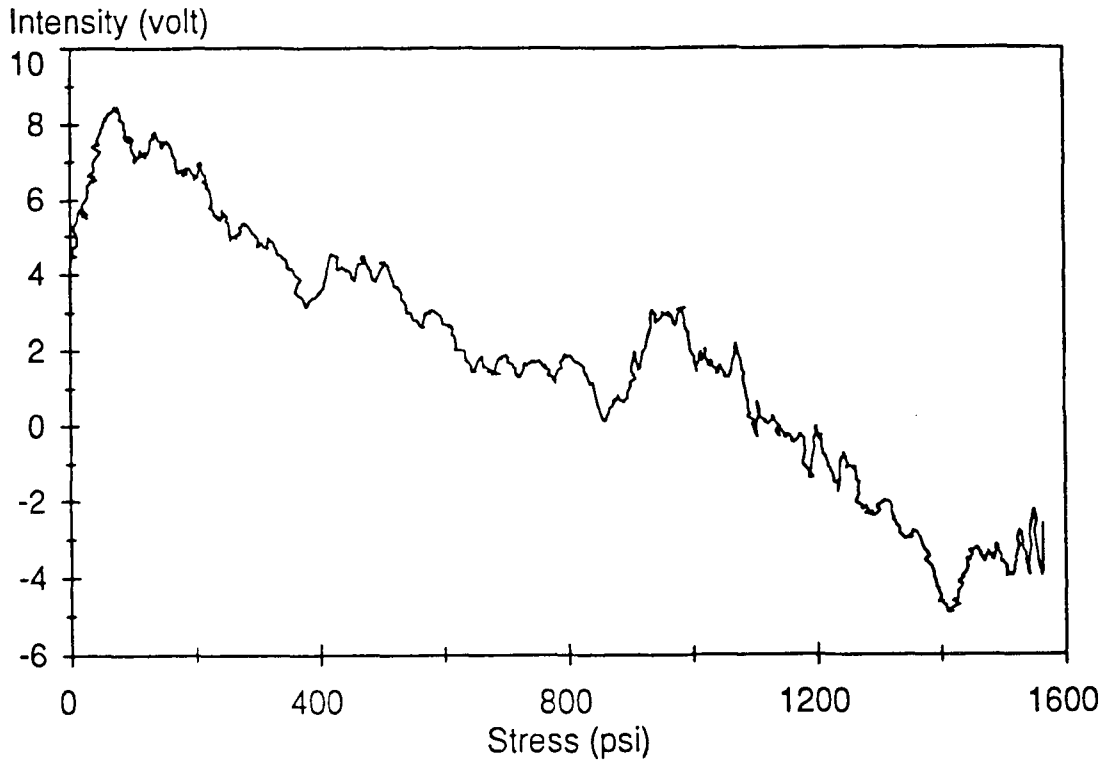

Figure 4.57 Intensity versus tensile stress for HMAR25A.

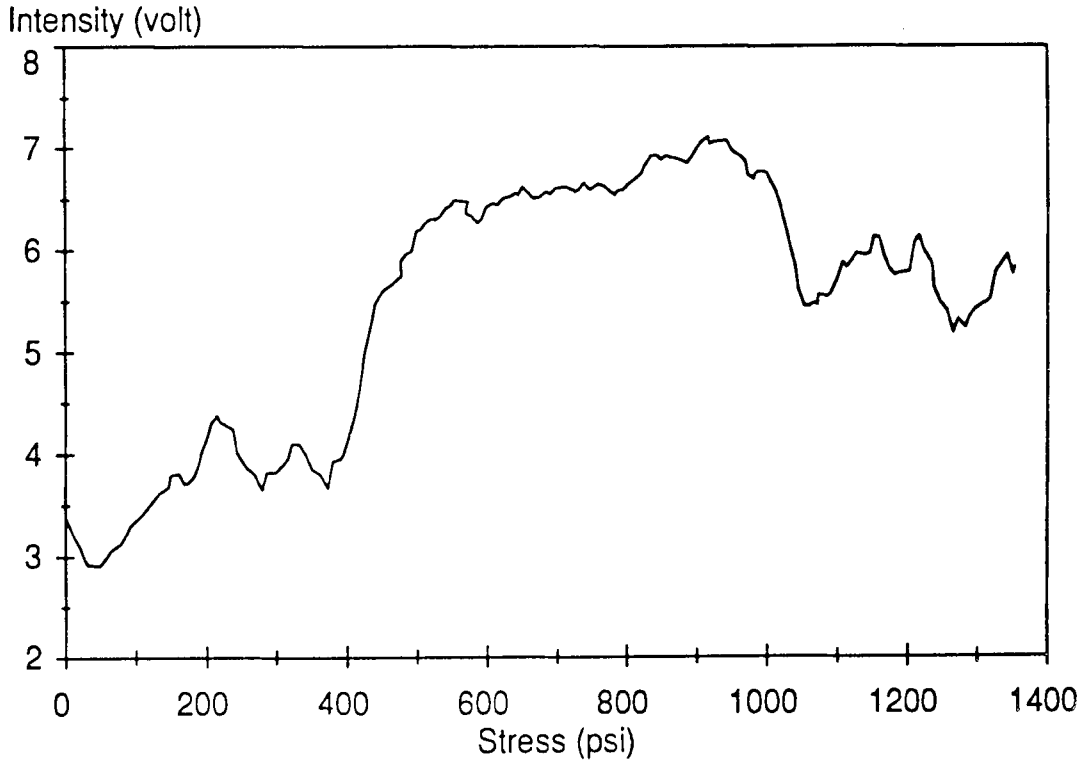

Figure 4.58 Intensity versus tensile stress for HMAR25B.

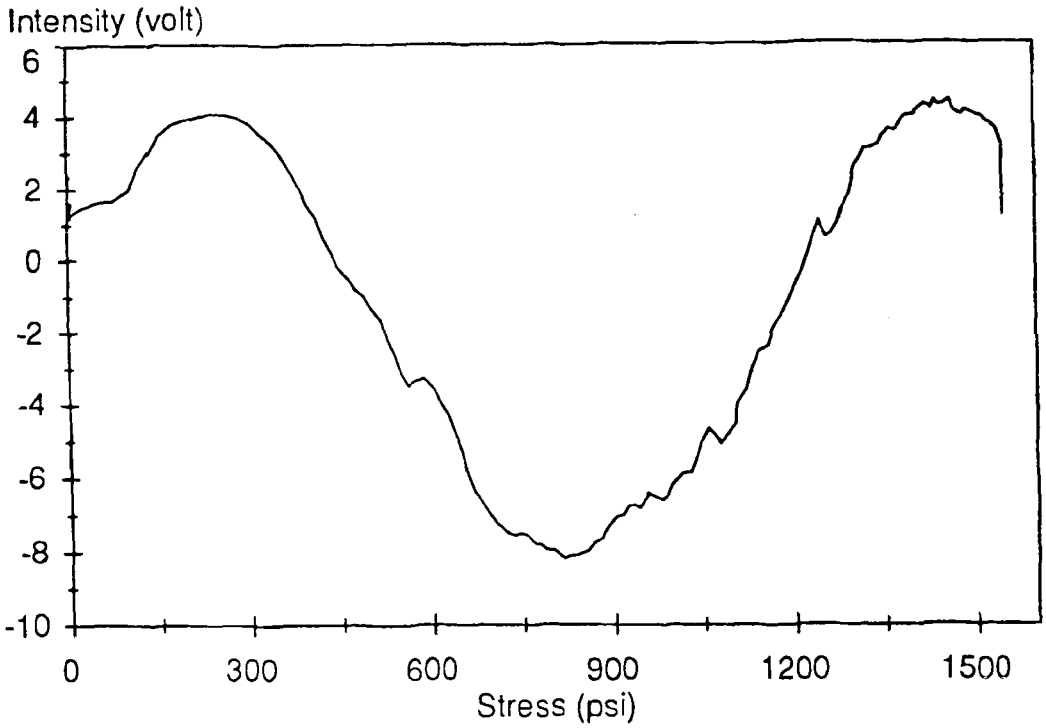

Figure 4.59 Intensity versus tensile stress for HMAR26A.

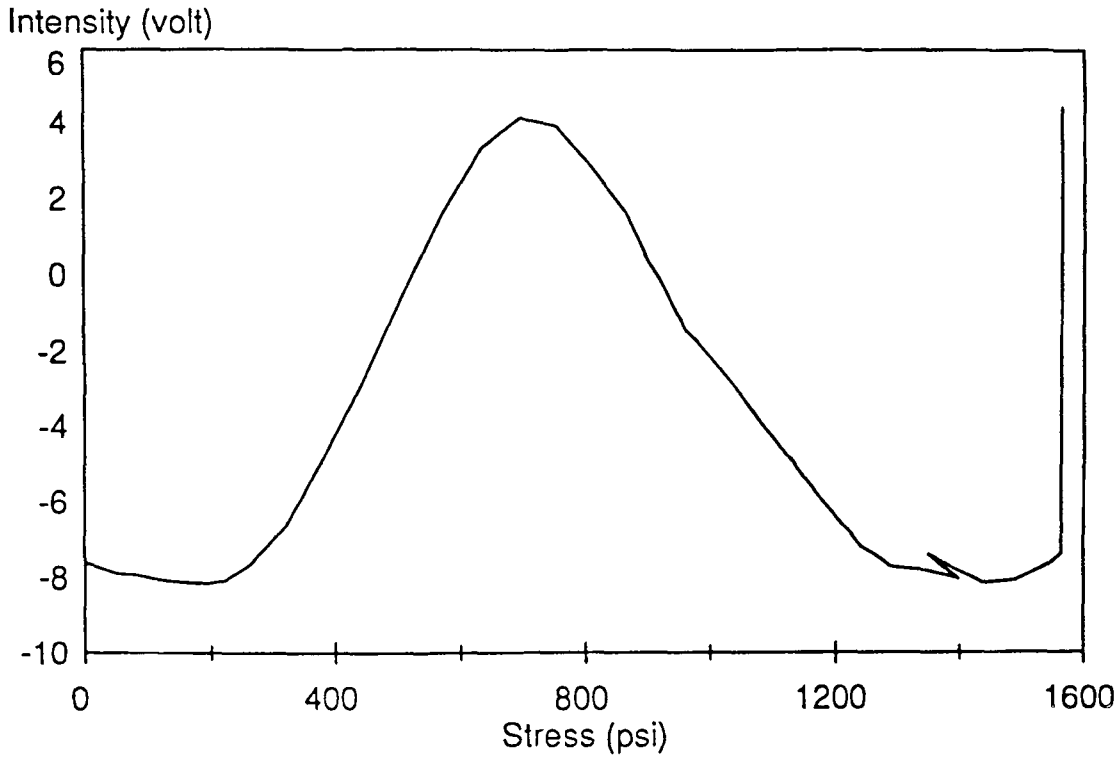

Figure 4.60 Intensity versus tensile stress for HMAR26B.

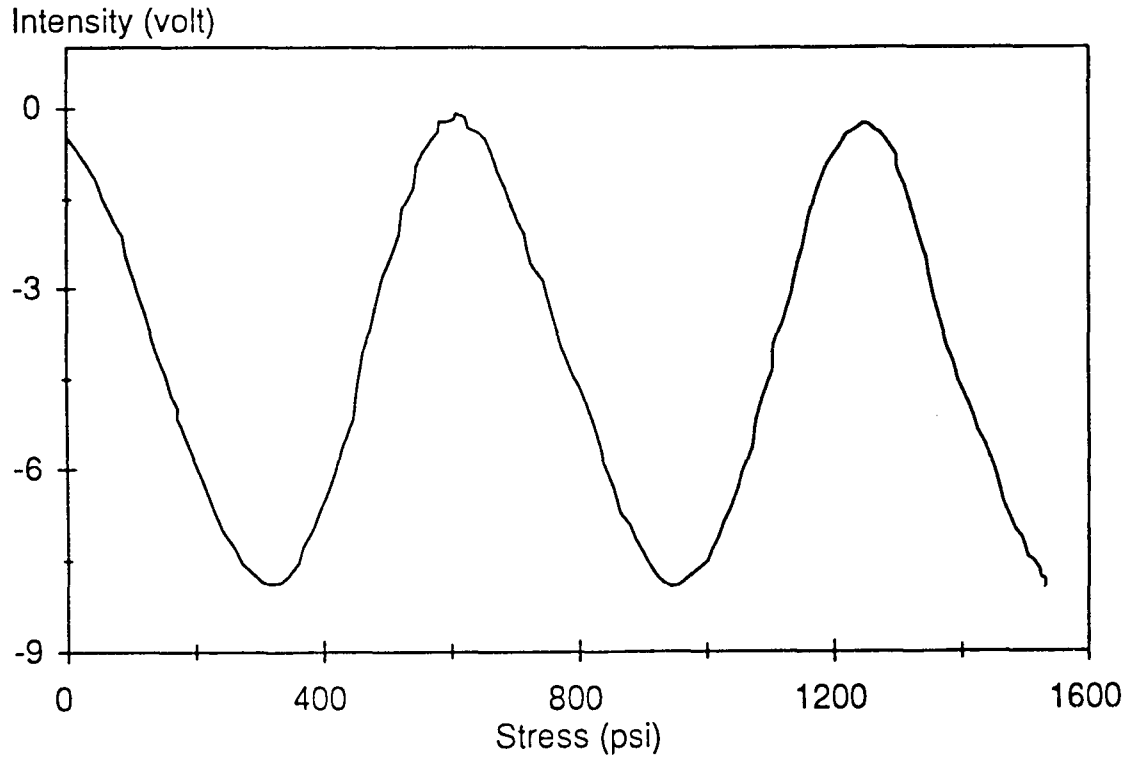

Figure 4.61 Intensity versus tensile stress for HAPR01A.

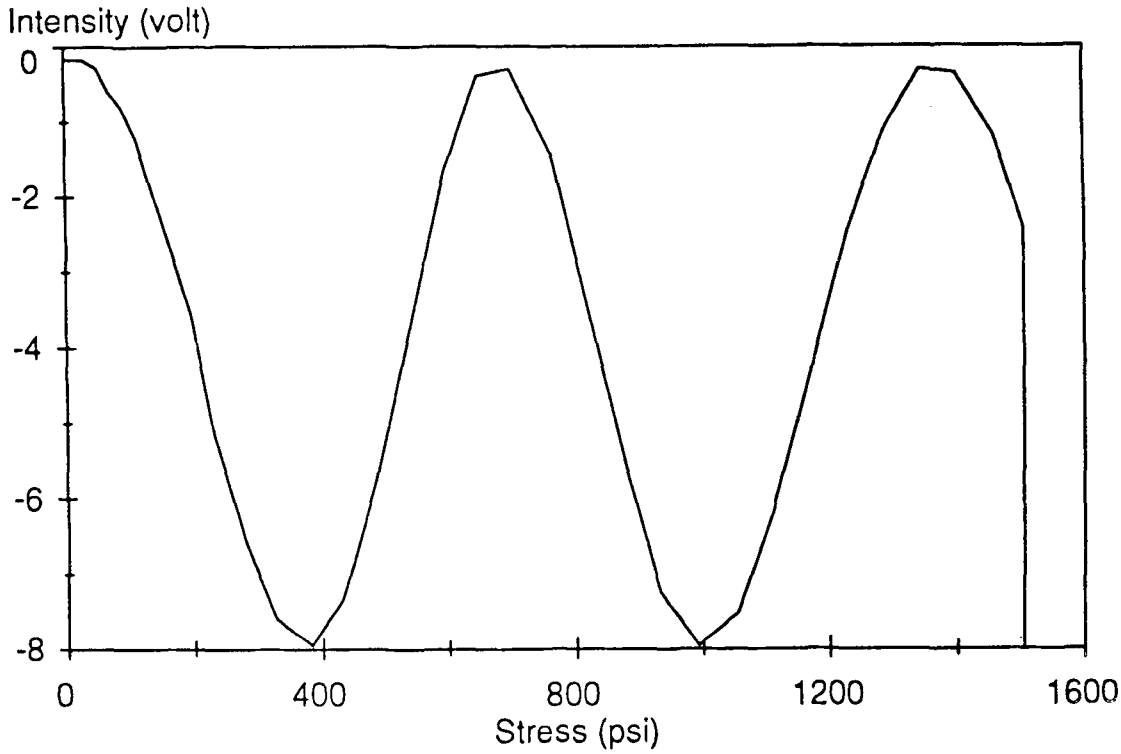

Figure 4.62 Intensity versus tensile stress for HAPR01B.

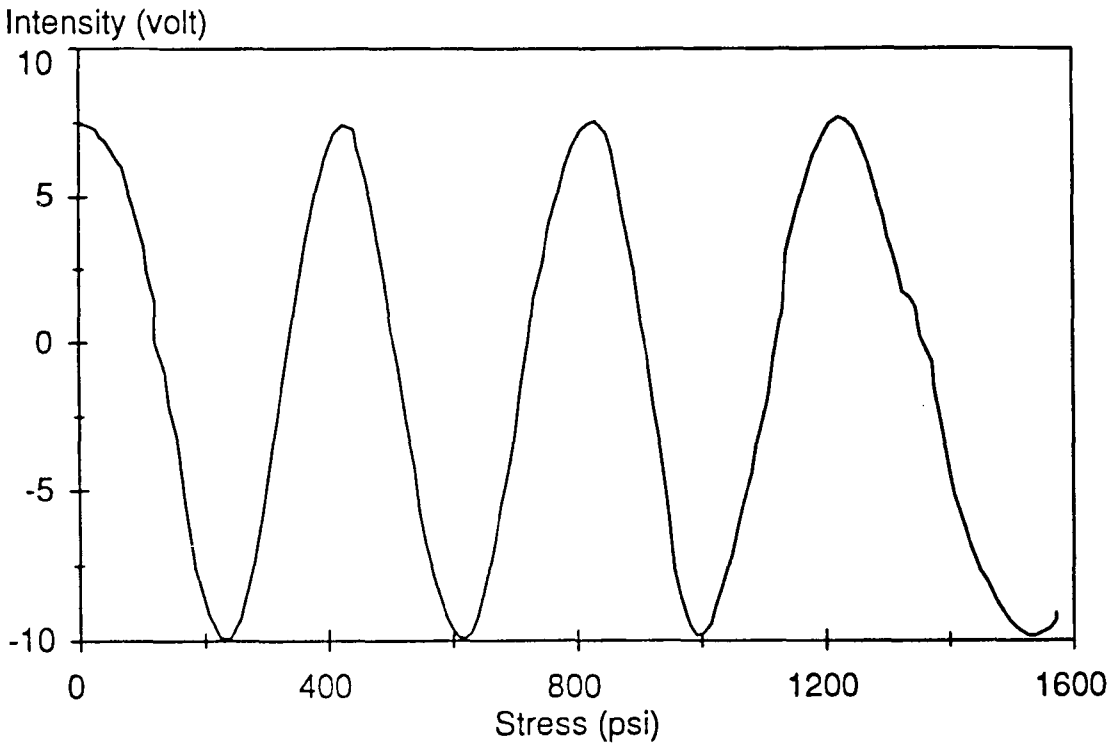

Figure 4.63 Intensity versus tensile stress for HAPR08A.

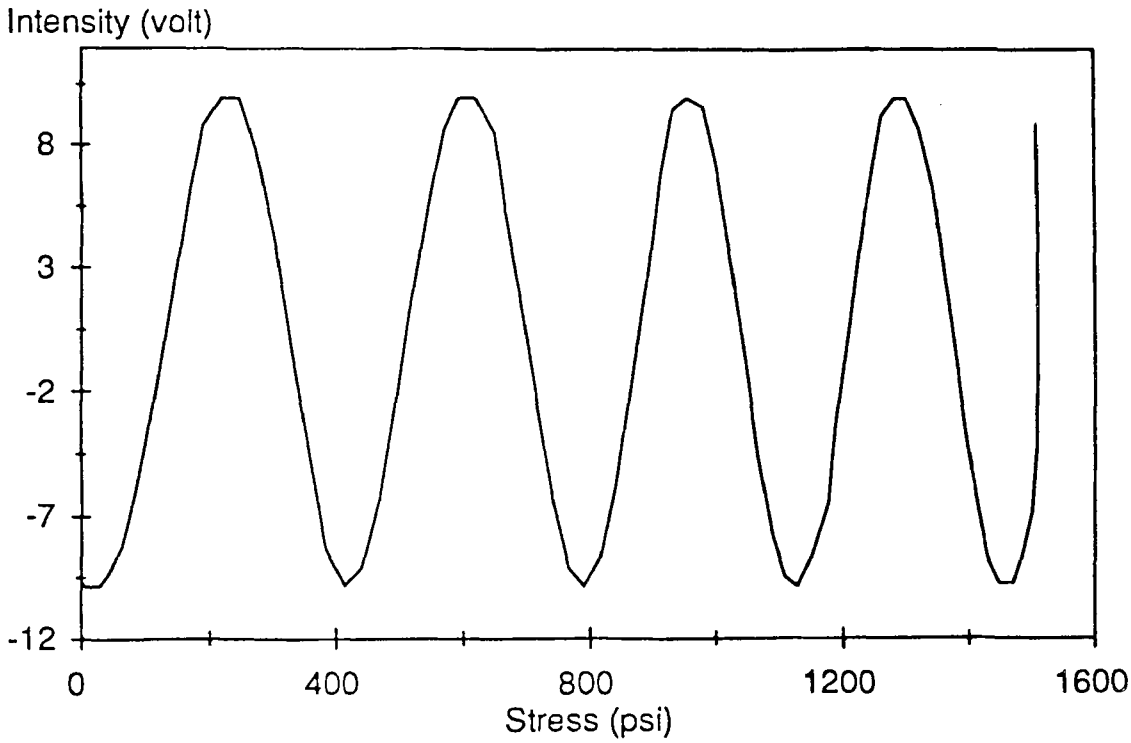

Figure 4.64 Intensity versus tensile stress for HAPR12A.

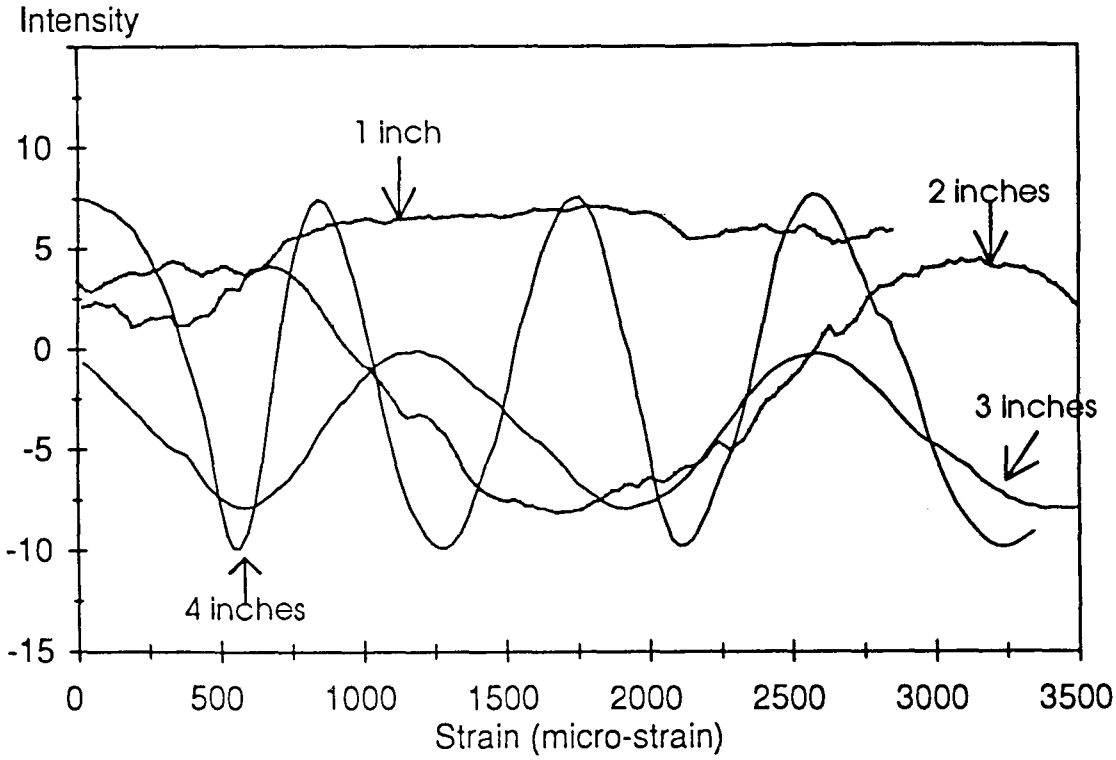

Figure 4.65 Intensity versus strain with different probing length.
Velocity 0.0002 inch/second.

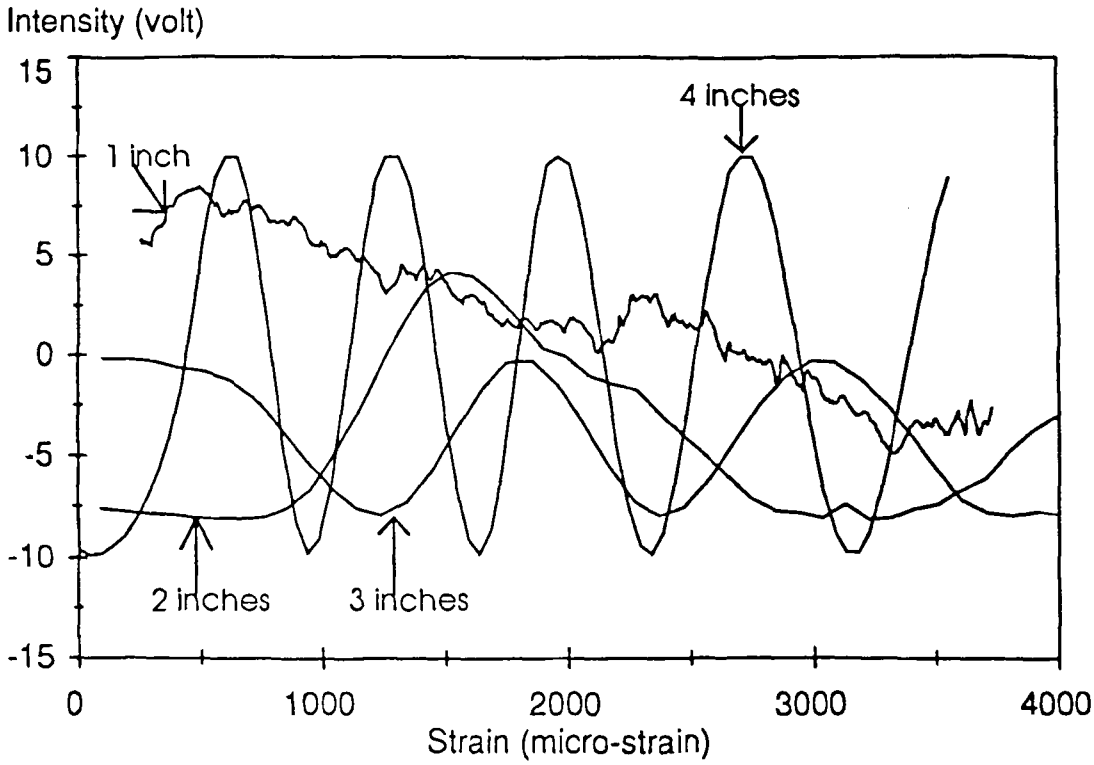

Figure 4.66 Intensity versus strain with different probing length. Velocity 0.0005 inch/second.

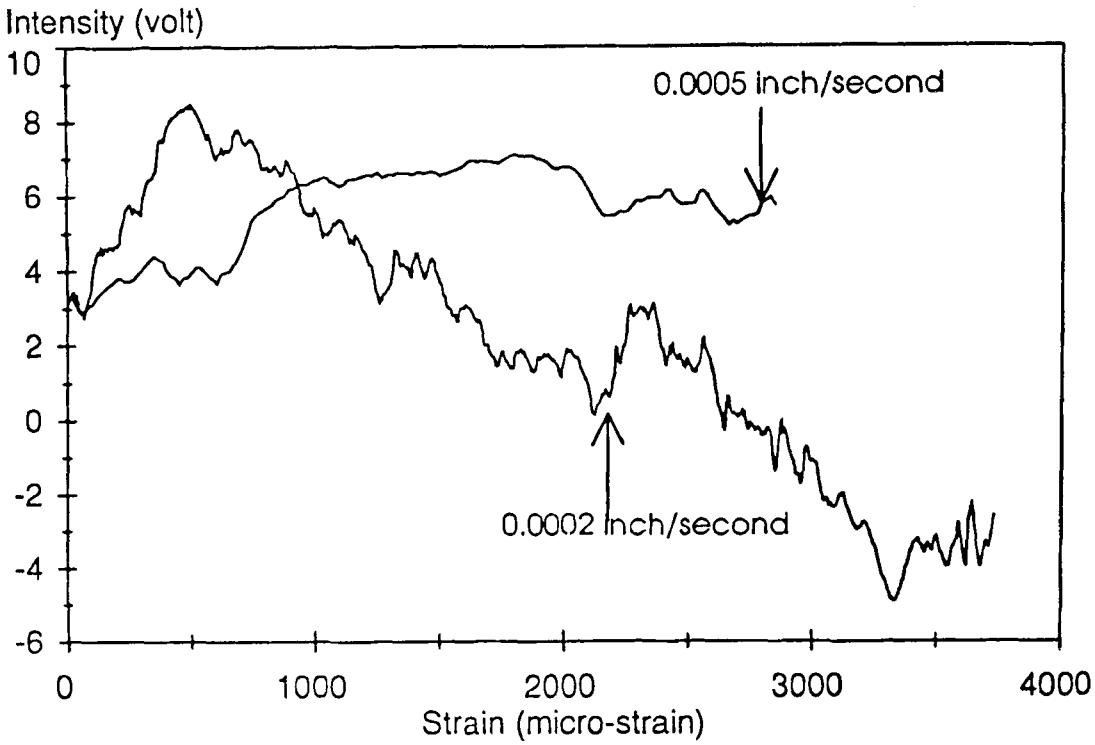

Figure 4.67 Intensity versus strain for probing length of 1 inch.

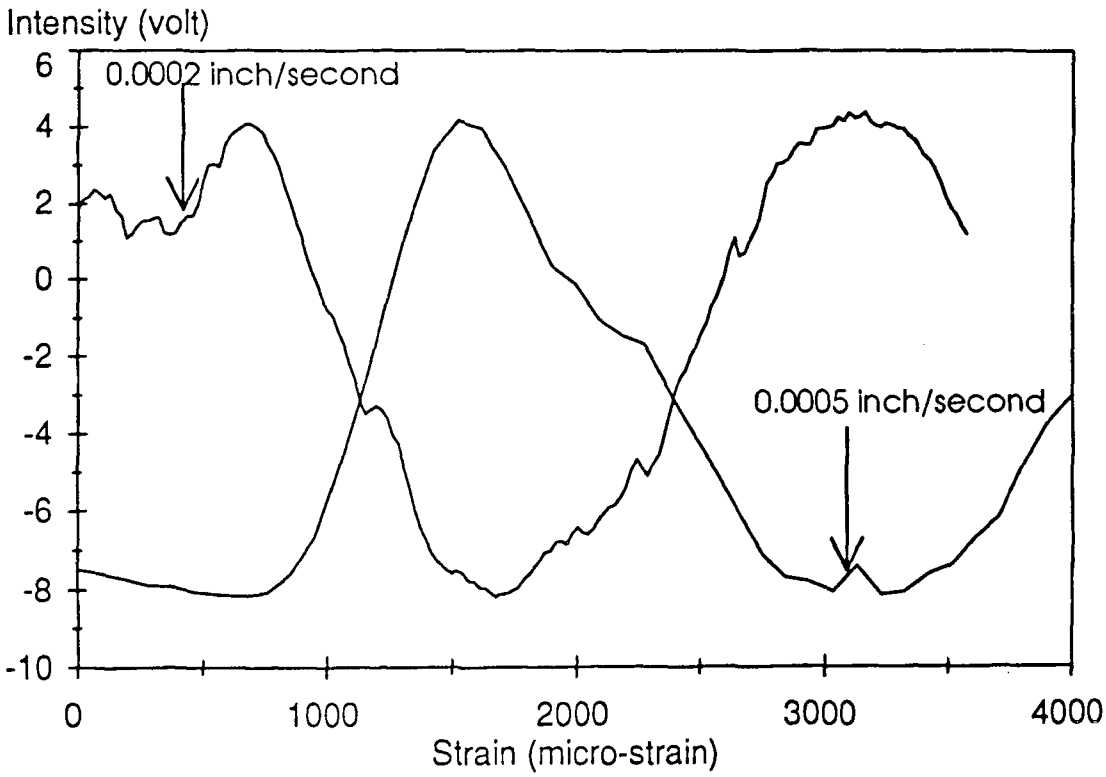

Figure 4.68 Intensity versus strain for probing length of 2 inches.

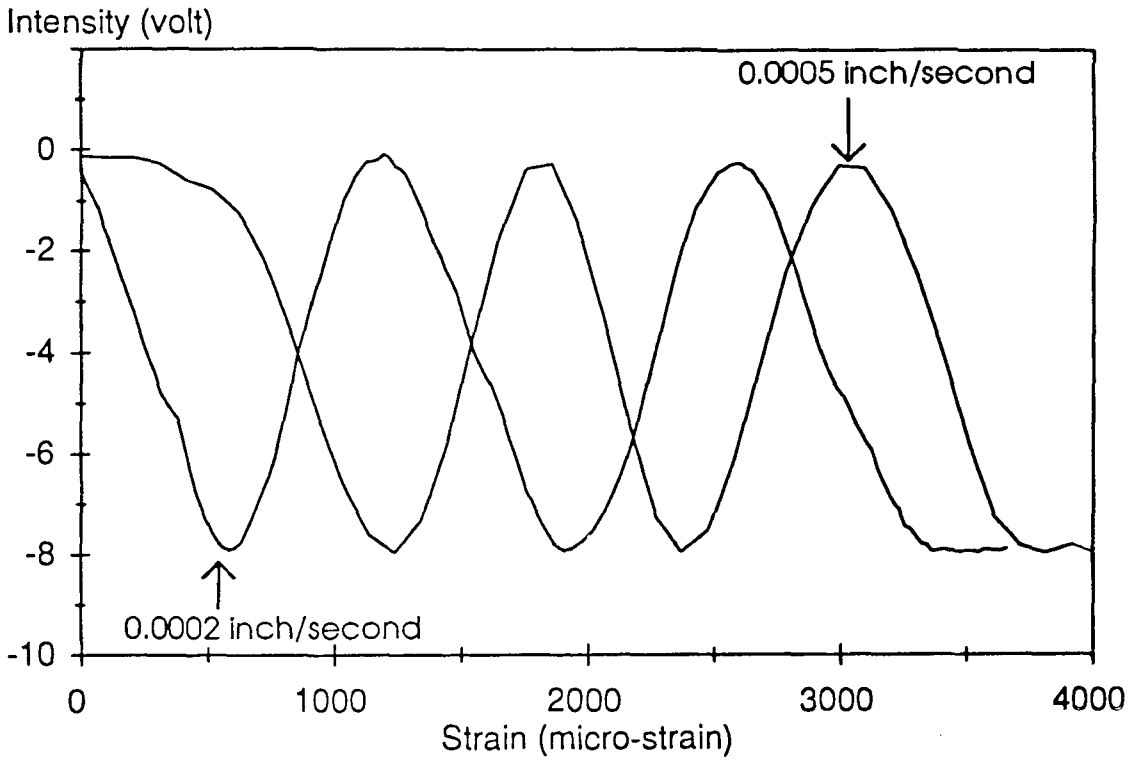

Figure 4.69 Intensity versus strain for probing length of 3 inches.

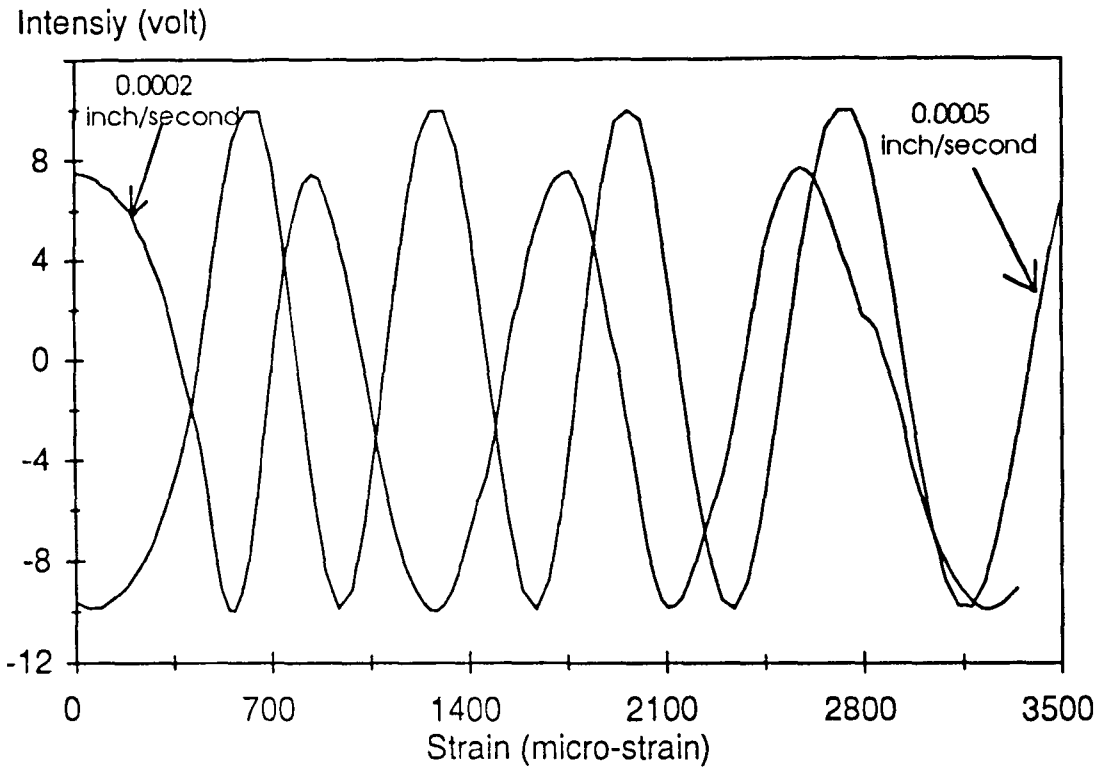

Figure 4.70 Intensity versus strain for probing length of 4 inches

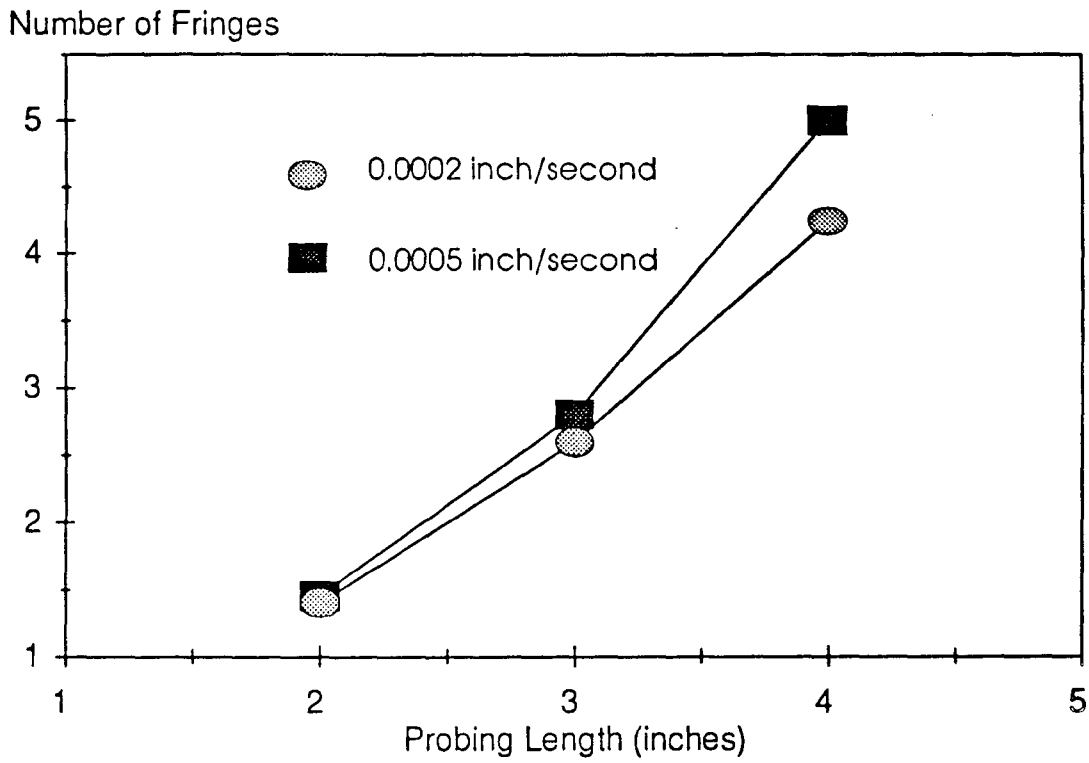

Figure 4.71 Relationship of probing length and number of fringes for 3500 micro-strain for Hi-Birefringence fiber.

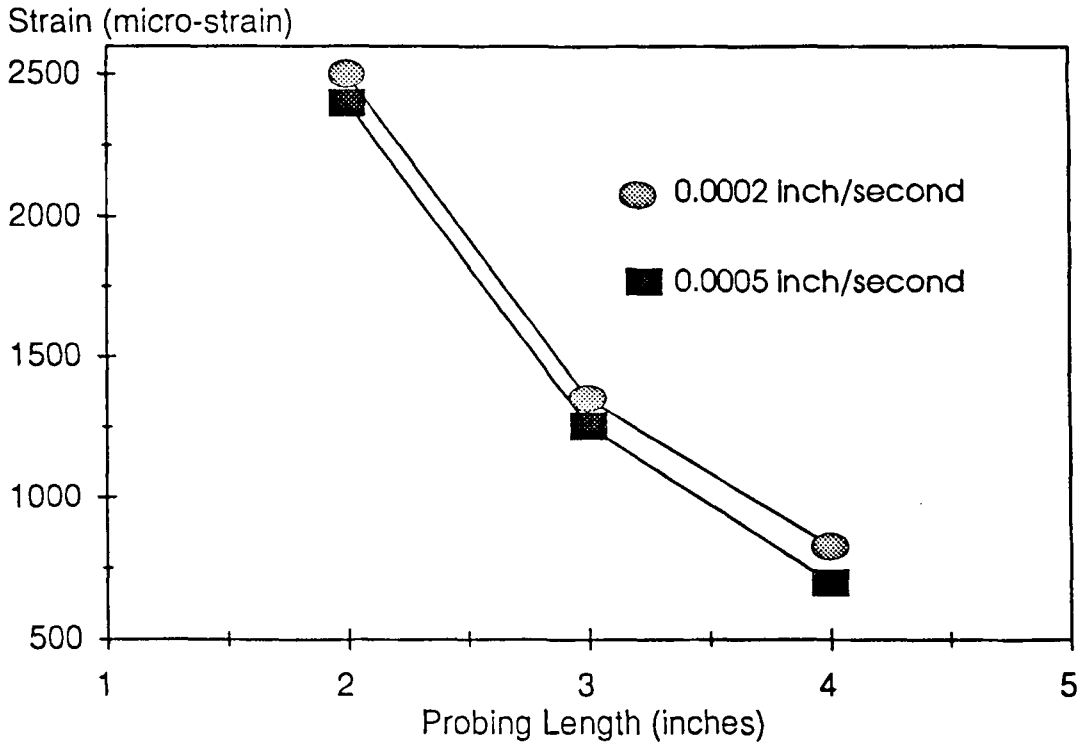

Figure 4.72 Calibration of 1 fringe for different probing lengths for Hi-Birefringence fiber.

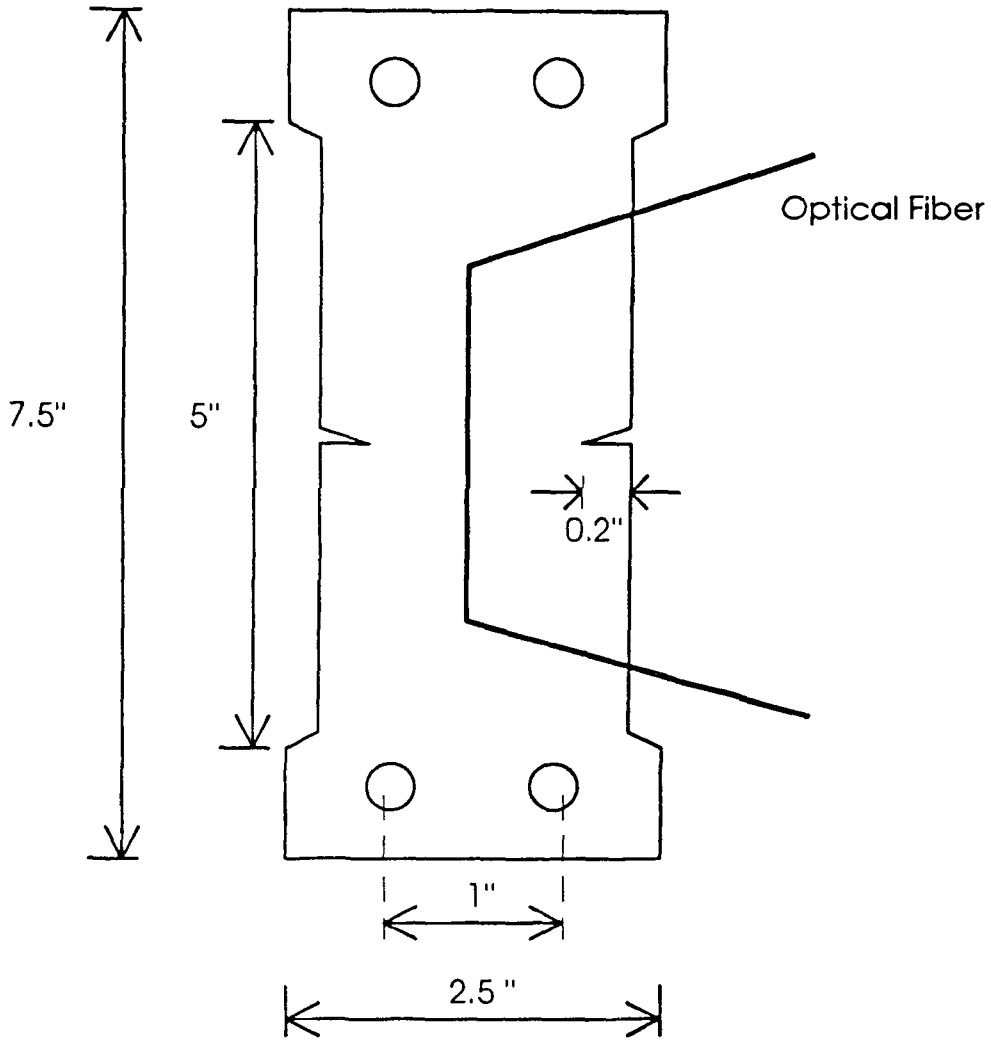

Figure 4.73 Copper specimen for tension test.

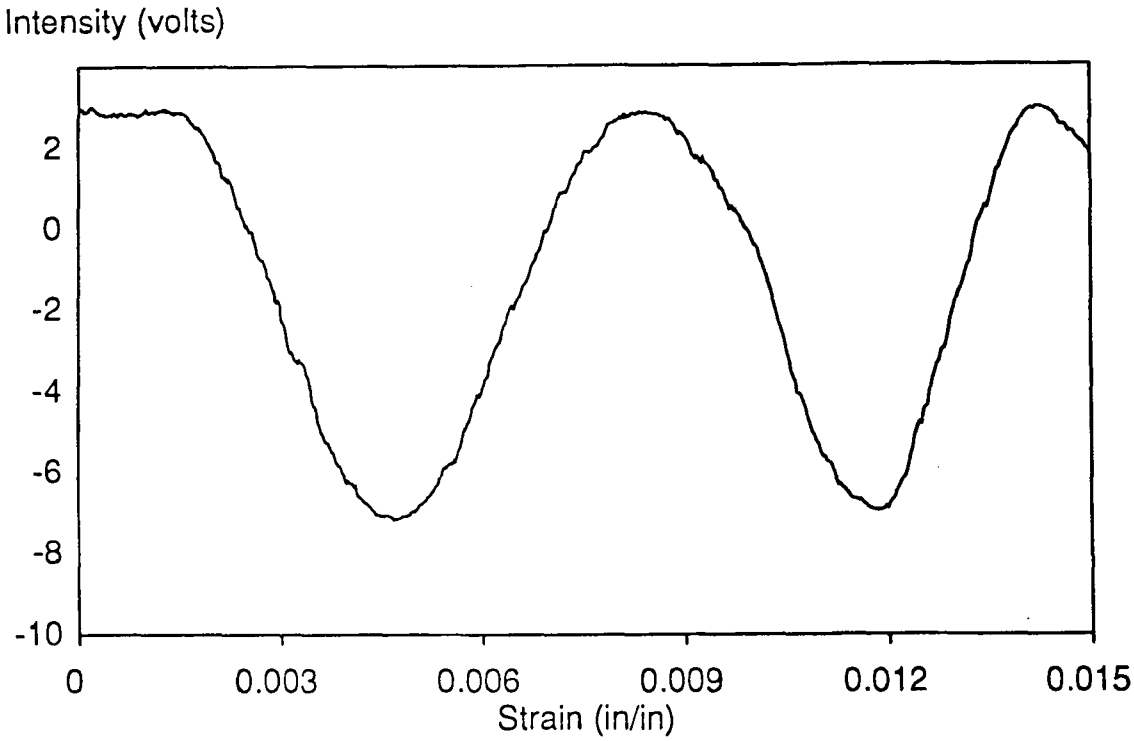

Figure 4.74 Intensity versus tensile strain for LMAR03.

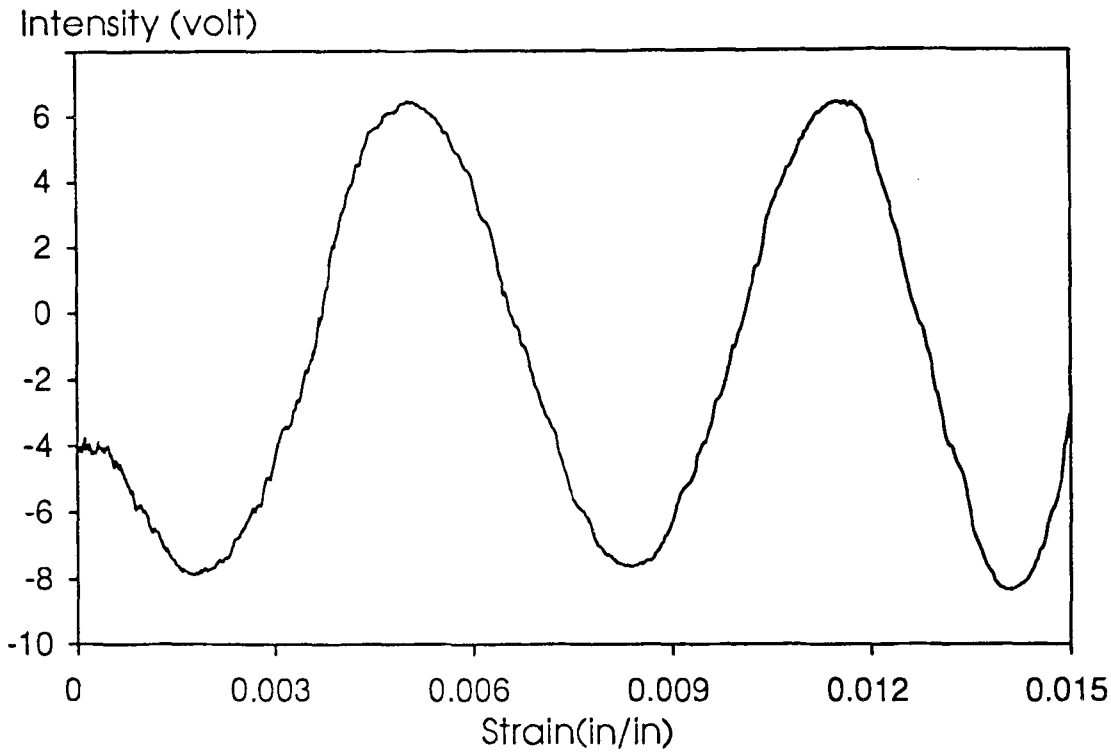

Figure 4.75 Intensity versus tensile strain for LMAR10.

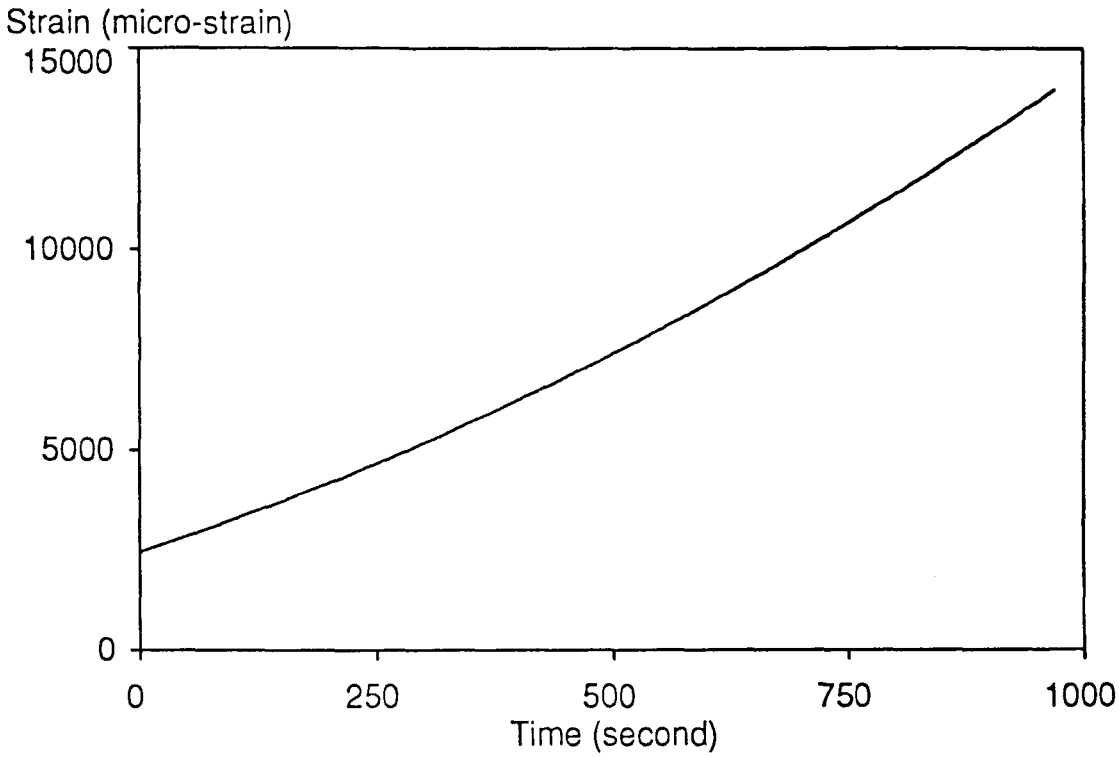

Figure 4.76 Strain-time response for LMAR10 (nonlinear).

CHAPTER 5

CONCLUDING REMARKS

5.1 Conclusions

On the basis of the results obtained in this investigation, the following conclusions can be drawn.

(1) The experimental techniques which were used in this study are new, reliable and worth further usage.

(2) The probing length of the optical fiber sensor has a great effect on the sensitivity. For probing length of 2 inches, the fringe value is 3500 micro-strain/fringe, whereas for the probing length of 4 inches, the fringe value is 750 micro-strain/fringe.

(3) For constant strains the relationship between the probing length and number of fringes is linear.

(4) Calibration tests provided repeatable strain calibration results.

5.2 Future Research

The Polarimetric Fiber Optical Sensor developed in the thesis is new and requires further research. Longer probing lengths and different types of fiber can be employed as testing variables. Possible future research might include the following:

(1) Test with longer specimen in order to completely understand the relationship between probing length and the strain.

(2) Test with cantilever beam. Compare the results with tension test.

(3) A software can be developed to process the data automatically instead of using spreadsheet software (as done in the present work).

(4) Develop a technique for automatic adjustment of the initial phase of the fiber signal. In this way, the experiments will be performed in a more timely manner.

REFERENCES

1. Antonio Nanni, C.C. Yang, and Kun Pan, "Fiber-Optical Sensors for Concrete Strain/Stress Measurement", *ACI Materials Journal*, V. 88, No. 3, May-June 1991.
2. N. Narendran, A. Shukla and S. Letcher, "Optical-Fiber Interferometric Strain Sensor Using a Single Fiber", *Experimental Techniques*, pp. 33-36, November/December 1992.
3. Newport Corporation, *Projects in Fiber Optics*, 1986.
4. Roderick D. Turner, Denis G. Laurin, and R. M. Measures, "Localized dual-wavelength Fiber-Optical Polarimeter for the Measurement of Structural Strain and Orientation", *Applied Optics*, Vol. 31. No. 16 / 1 June 1992.
5. Ashish M. Vengsarkar, W. Craig Michie, Ljilja Jankovic, Brian Culshaw, and Richard O. Claus, "Fiber Optical Sensor for Simultaneous Measurement of Strain and Temperature", *SPIE*, Vol. . 1367 Fiber Optical and Laser Sensors VIII (1990), pp. 249.
6. Shi-Kay Yao and Charles K. Asawa, "Fiber Optical Intensity Sensors", *IEEE Journal on Selected Areas in Communications*, Vol. SAC-1. No. 3. April 1983.
7. Thomas G. Giallorenzi, Joseph A. Bucaro, Anthony Dandridge and G. H. Sigel, "Optical Fiber Sensor Technology", *IEEE Journal of Quantum Electronics*, Vol. QE-18, No. 4, April 1982.
8. Luc B. Jeunhomme, *Single-Mode Fiber Optics Principles and Applications*, pp. 166, 1983.

9. James W. Dally and William F. Riley, *Experimental Stress Analysis*, 1978.

10. Shang-Yuan Huang, James N. Blake, and Byoung Yoon Kim, "Perturbation Effects on Mode Propagation in Highly Elliptical Core Two-Mode Fibers", *Journal of Lightwave Technology*, Vol. 8, No. 1, January 1990.

11. T. H. Chua and Chin-Lin Chen, "Fiber Polarimetric Stress Sensors", *Applied Optics*, Vol. 28, No. 15, August 1989.

12. Ashish M. Vengsarkar, W. Craig Michhie, Ljilja Jankovic, Brian Culshaw, and Richard O. Claus, "Fiber optic sensor for simultaneous measurement of strain and temperature", *SPIE-The International Society for Optical Engineering, Fiber Optic and Laser Sensors VIII (1990)*, pp.249-260.